Università degli studi del Piemonte Orientale

“Amedeo Avogadro”

UNIVERSITÀ DEL PIEMONTE ORIENTALE

Department of Health Sciences

PhD Program in Food, Health and Longevity

XXXVII cycle

Double-Edge Sword of Ketogenic Diet: Hepatic Improvement at the Expense of Musculoskeletal Health

SSD MED/49

PhD coordinator:

Prof. Antonia Follenzi

PhD supervisor:

Prof. Flavia Prodam

PhD candidate:

Alessandro Antonioli

Academic years: 2021-2025

To PhD Coordinator

DECLARATION AND AUTHORISATION TO ANTIPLAGIARISM DETECTION

The undersigned ANTONIOLI ALESSANDRO…….. student of ……
……FOOD, HEALTH and LONGEVITY ……. PhD course, ……XXXVII…… Ciclo

DECLARES

- to be aware that the University has adopted a web-based service to detect plagiarism through a software system called "Turnit.in",

- his/her Ph.D. thesis was submitted to Turnit.in scan and reasonably it resulted an original document, which correctly cites the literature;

ACKNOWLEDGES

- his/her Ph.D. thesis can be verified by his/her Ph.D. tutor and/or Ph.D Coordinator in order to confirm its originality.

……NOVARA, 18/06/2025……
(Place, date)

……
(signature)

TABLE OF CONTENTS

Summary

The Western diet (WD), marked by elevated levels of sugars and saturated fats, significantly contributes to obesity and its related health complications. Its influence on insulin resistance and inflammation has been associated with several conditions, such as type 2 diabetes (T2D), cardiovascular diseases (CVDs), metabolic dysfunction-associated steatotic liver disease (MASLD).

Ketogenic diets (KDs) represent dietary approaches characterized by minimal carbohydrate intake, high fat, and adequate protein levels. Energy is sourced from ketone bodies (KBs), derived primarily from fat oxidation. Given the increasing evidence supporting the effectiveness of KDs in reducing inflammation, oxidative stress, and improving mitochondrial function, we hypothesized that KDs could hold promise in addressing obesity-related conditions. To test this hypothesis, we subjected mice to a Western diet (WD) for 16 weeks, followed by a transition to an *ad libitum* KD, or continued adherence to WD for an additional 2, 4 or 8 weeks.

Our finding demonstrated that the switch from WD to KD elicited opposite effects on liver, muscle, and bone. On one hand, it markedly improved hepatic outcomes, significantly reducing liver weight, inflammation, fibrosis, and expression of steatotic and fibrogenic genes. On the other hand, KD did not produce positive effects within muscle and bone. Indeed, KD further exacerbated muscle wasting and myofiber size reduction, concomitantly with lower branched chain amino acids (BCAAs) levels and an elevation of genes associate with atrophy and protein degradation. *In vitro* we examined various doses of palmitate (PA) and butyrate (BU) on C2C12-derived myotubes to further investigate the impact of fatty acids and KBs on muscle cells. PA significantly reduced myotube diameter in a dose-dependent manner but also induced ROS production, and mitochondrial membrane depolarization. In contrast, low doses of BU protected against PA-induced atrophy in myotubes, while high doses appear to be ineffective or may even contribute to atrophy. Similarly, bone assessments revealed that short-term KD after WD feeding did not improve bone microarchitecture and was associated with reduced trabecular thickness and volume, increased osteoclast activity, and decreased osteoblast number, indicating enhanced bone resorption and defective mineralization.

Our findings suggest that KD could exert different actions on several tissues, suggesting that if it favors a rapid weight loss, eliciting an improvement in glucose metabolism and liver function, some detrimental effects could be present on other organs. Optimization of dietary timing, duration, and nutrient composition tailored doses of KBs should be taken into account in future studies. Notably, these outcomes further underscore the need for a carefully monitored, specialized, and tailored dietary approach.

Sommario

La dieta occidentale (WD), caratterizzata da elevati livelli di zuccheri e grassi saturi, contribuisce significativamente all'obesità e alle relative complicazioni per la salute. La sua influenza sulla resistenza all'insulina e sull'infiammazione è stata associata a diverse condizioni, come il diabete di tipo 2 (T2D), le malattie cardiovascolari (CVD) e la steatosi epatica associata a disfunzione metabolica (MASLD).

Le diete chetogeniche (KD) rappresentano approcci dietetici caratterizzati da un apporto minimo di carboidrati, un elevato apporto di grassi e livelli proteici adeguati. L'energia proviene dai corpi chetonici (KB), derivati principalmente dall'ossidazione dei grassi. Date le crescenti prove a supporto dell'efficacia delle KD nel ridurre l'infiammazione, lo stress ossidativo e il miglioramento della funzione mitocondriale, abbiamo ipotizzato che le KD potessero essere promettenti nel trattamento delle condizioni correlate all'obesità. Per verificare questa ipotesi, abbiamo sottoposto i topi a una dieta occidentale (WD) per 16 settimane, seguita da una transizione a una KD *ad libitum* o da un continuo consumo di WD per ulteriori 2, 4 o 8 settimane. I nostri risultati hanno dimostrato come il passaggio da WD a KD ha prodotto effetti opposti su fegato, muscoli e ossa. Da un lato, ha migliorato significativamente gli esiti epatici, riducendo significativamente il peso del fegato, l'infiammazione, la fibrosi e l'espressione dei geni steatotici e fibrogenici. Dall'altro, la KD non ha prodotto effetti positivi su muscoli e ossa. Anzi, la KD ha ulteriormente esacerbato l'atrofia muscolare e la riduzione delle dimensioni delle miofibre, contemporaneamente a una riduzione dei livelli di aminoacidi ramificati (BCAA) e a un aumento dei geni associati all'atrofia e alla degradazione proteica. In vitro abbiamo esaminato diverse dosi di palmitato (PA) e butirrato (BU) su miotubi derivati da C2C12 per indagare ulteriormente l'impatto degli acidi grassi e dei chetoni sulle cellule muscolari. Il PA ha ridotto significativamente il diametro dei miotubi in modo dose-dipendente, ma ha anche indotto la produzione di

ROS e la depolarizzazione della membrana mitocondriale. Al contrario, basse dosi di BU hanno protetto dall'atrofia indotta da PA nei miotubi, mentre dosi elevate sembrano essere inefficaci o potrebbero persino contribuire all'atrofia. Analogamente, le valutazioni ossee hanno rivelato che la dieta chetogenica a breve termine dopo l'alimentazione con WD non ha migliorato la microarchitettura ossea ed è stata associata a una riduzione dello spessore e del volume trabecolare, a un aumento dell'attività degli osteoclasti e a una diminuzione del numero di osteoblasti, indicando un aumento del riassorbimento osseo e una mineralizzazione difettosa.

I nostri risultati suggeriscono che la dieta chetogenica potrebbe esercitare azioni diverse su diversi tessuti, suggerendo che nonostante favorisce una rapida perdita di peso, inducendo un miglioramento del metabolismo del glucosio e della funzionalità epatica, alcuni effetti negativi potrebbero essere presenti su altri organi. L'ottimizzazione dei tempi, della durata e della composizione nutrizionale della dieta e delle dosi personalizzate di KB dovrebbero essere prese in considerazione in studi futuri. In particolare, questi risultati sottolineano ulteriormente la necessità di un approccio dietetico attentamente monitorato, specializzato e personalizzato.

1. Obesity Pandemic and Its Metabolic Consequences

Nowadays, more than 500 million people worldwide are overweight or obese and obesity is considered to be the fifth leading risk for death globally. World Health Organization (WHO) defines overweight as a body mass index (BMI; calculated as weight [kg] divided by height squared [m2]) equal to or greater than 25 kg/m^2 and obese as a BMI equal to or greater than 30 kg/m^2. From 1990 to 2022, the rates of overweight and obesity boosted exponentially and continue to grow in both adults and children. In 2022 WHO considered overweight or with obesity 2.5 billion of adults, which corresponds to the 43% of the world population. Meanwhile, the prevalence among children and adolescents aged 5-19 has risen dramatically from just 8% in 1990 to 20% in 2022, including 390 million of individuals [1–3].

Recently, the European Association for the Study of Obesity (EASO) recommend using BMI in association with other factors, including waist-to-height ratio (WtHR), emphasising that BMI alone is insufficient as diagnostic criterion. The new framework comprehends people with lower BMI (≥25–30 kg/m2), but increased abdominal fat accumulation and the presence of complication in the context of obesity, which consist in medical, functional, psychological impairments. Moreover, in the diagnosis waist-to-height ratio replaced waist circumference measure due to its majority as a cardiometabolic disease risk marker [4].

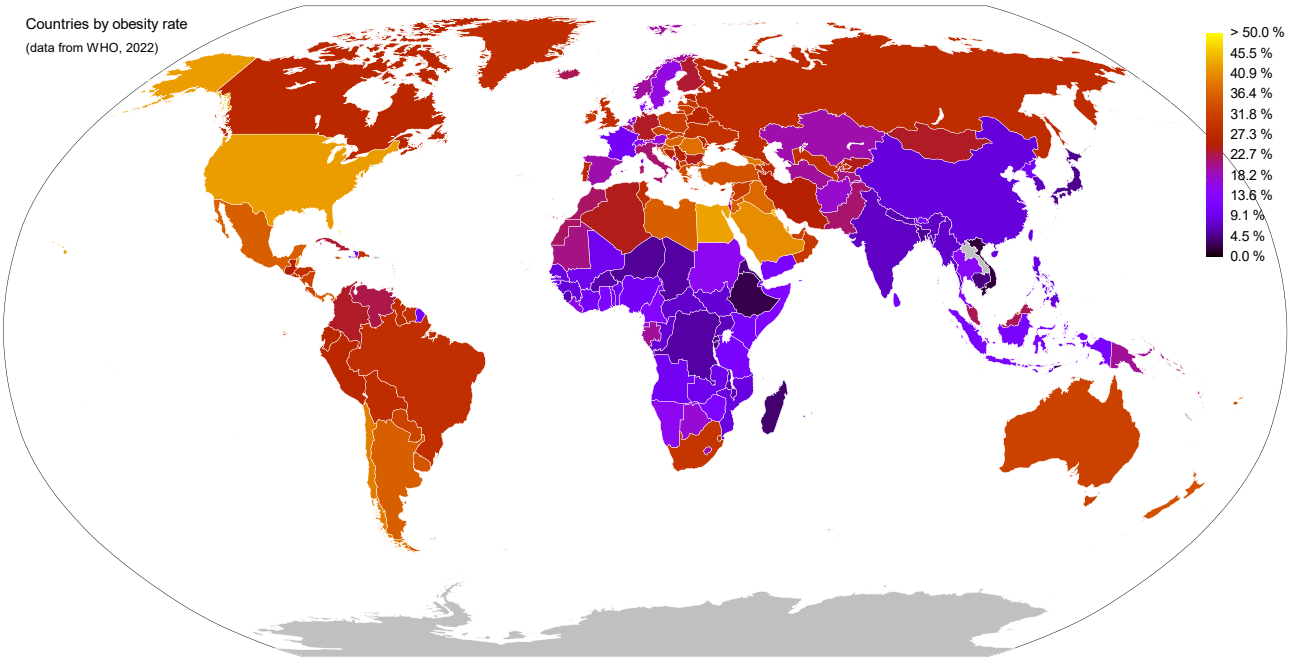

Figure 1: Worldwide obesity incidence (WHO, 2022)

Obesity is defined as abnormal or excessive fat accumulation in the adipose tissue (AT) and other ectopic tissues resulting from a long-term energy imbalance, in which energy intake is greater than energy expenditure [5,6]. It is a complex, multifactorial condition influenced by multiple risk factors, such as genetics, maternal and perinatal environment, gender, aging, energy-dense diets, gut microbiota, and sedentary lifestyle [2,7,8]. However, obesity is the result of several metabolic deregulated processes that not only trigger weight gain, but also other health complications, such as insulin resistance, type 2 diabetes (T2D), cardiovascular diseases (CVDs), metabolic-associated fatty liver diseases or metabolic dysfunction-associated steatotic liver disease (MAFLD/MASLD), arthritis, Alzheimer disease, cancer, and recent studies suggested its crucial role in the development of both microbial and viral infections [9–12].

Obesity is characterized by an overabundance of AT deposition and adipocyte expansion in both subcutaneous, and visceral regions, and in non-adipose organs, a phenomenon called ectopic lipid

accumulation. When the storage capacity of adipocytes is saturated, AT in obese individuals firstly undergoes several remodelling alterations to adapt to excessive food intake, including hyperplasia and hypertrophy, secondly overtakes its oxygen diffusion limit, thereby leading hypoxia, endoplasmic reticulum (ER) stress, cell death, and enhancing circulating free-fatty acids (FFA) and triglycerides (TG) accumulation in ectopic sites [2,13]. The resulted obesity-related lipotoxic environment triggers the recruitment and the activation of immune cells, such as macrophages, which infiltrate adipose tissue and start to secrete pro-inflammatory cytokines such as TNFα, interleukin-1β (IL-1β) and interleukin-6 (IL-6). This paracrine action activates serine kinases in adipocytes including IκB kinase β (IKKβ), c-Jun N-terminal kinase (JNK), P70S6K and mTOR [14]. Moreover, these kinases carry out inhibitory serine/threonine phosphorylation of IRS1, causing insulin resistance in adipocytes. Consistent with this, activation of inflammatory pathways can impair glucose metabolism and cause systemic insulin resistance, and T2D. Additionally, mitochondrial dysfunctions in adipocytes and other metabolic tissues play a crucial role in obesity-related insulin resistance [15]. Furthermore, impaired mitochondrial function leads to excessive production of reactive oxygen species (ROS) due to inefficient electron transfer in the electron transfer chain (ETC), overwhelm cellular antioxidant defences and further exacerbate oxidative stress and inflammation [16,17].

In parallel to such a dysfunctional AT leads to ectopic fat accumulation, both activated adipocytes and immune cells release pro-inflammatory factors active locally and in distant metabolically active organs such as liver and muscle [18–20].

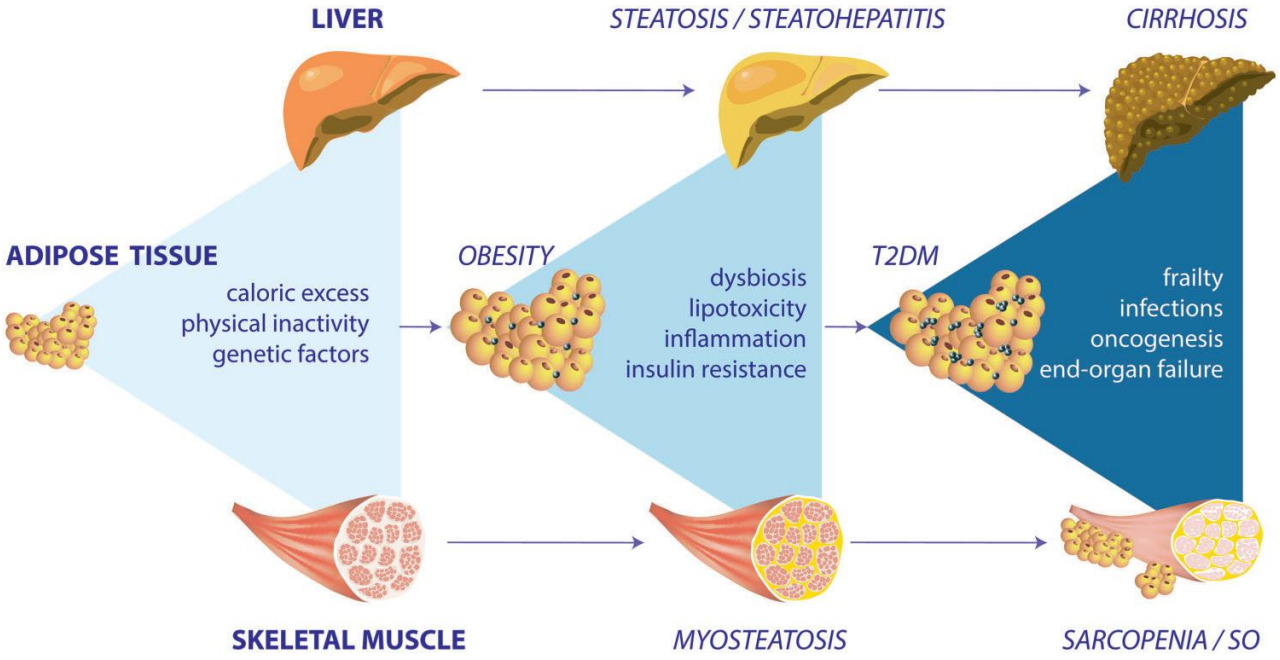

Figure 2: Ectopic fat accumulation in liver and muscle leads to health complications, thereby may triggering progression to cirrhosis and sarcopenia/sarcopenic obesity [21].

Despite obesity being one of the most extensively researched global health issues, an effective global treatment or a prevention strategy has yet to be clearly defined or identified. To address this growing epidemic, ongoing medical supervision, multidisciplinary care teams, and a broad range of interventions have been proposed since it is well known that obesity results from a complex interplay of various factors. The common final goal is to improve obesity-associated risk factors, reduce fat mass, and the overall improvement of quality of life. Non-surgical and non-pharmacological therapies primarily focus on lifestyle and behavioural strategies that aim to reduce energy intake while increasing energy expenditure [7,17]. Indeed, among all the non-pharmacological strategies to prevent obesity, dietary regimen intervention is one of the most studied in the field of obesity-related health complications, particularly MASLD and T2DM.

1.1. The impact of obesity on liver dysfunctions

Given its central and critical role in regulating human physiology, maintaining hepatic homeostasis and preventing liver-related diseases is essential for overall health. However, substantial evidences highlight that the prevalence of liver dysfunctions, such as MASLD and its progression to metabolic dysfunction-associated steatohepatitis (MASH), has increased exponentially in recent years, mirroring obesity evolution, due to bad lifestyle habits, characterized by over- and malnutrition associated with insufficient physical activity [22,23]. The term MAFLD was proposed for the first time in 2020 to overcome the issues related to the previous non-alcoholic fatty liver disease (NAFLD) terminology. The shift from NAFLD to MAFLD nomenclature highlights the pivotal role of metabolic dysfunction in liver disease [22]. MAFLD is the most frequent form of hepatic steatosis, affecting worldwide 30-40% of men and 15-20% of women [24]. It might remain benign, or it can develop MASH with injury, inflammation, and fibrosis; furthermore, MASH can progress a more severe form, if left untreated: cirrhosis and hepatocellular carcinoma (HCC) [22,23,25]. The diagnosis of MAFLD consists in the presence of hepatic steatosis and at least one among these three conditions: T2D, obesity, and metabolic dysregulation [22]. Steatosis is confirmed both biochemically, when lipid content exceeds 5-10% of total liver weight, and histopathologically, when more than 5% of hepatocytes exhibit lipid droplet accumulation [26]. Nowadays, MAFLD is replaced by MASLD as the overarching term to encompass the various causes of steatosis, which includes patients with concomitantly hepatis steatosis and at least one of five cardiometabolic risk factors [27].

Its pathophysiology is complex and multifactorial, and consists in oxidative stress and inflammation promoted by hepatic fat accumulation, mainly triacyclglycerols (TAGs) within hepatocytes.

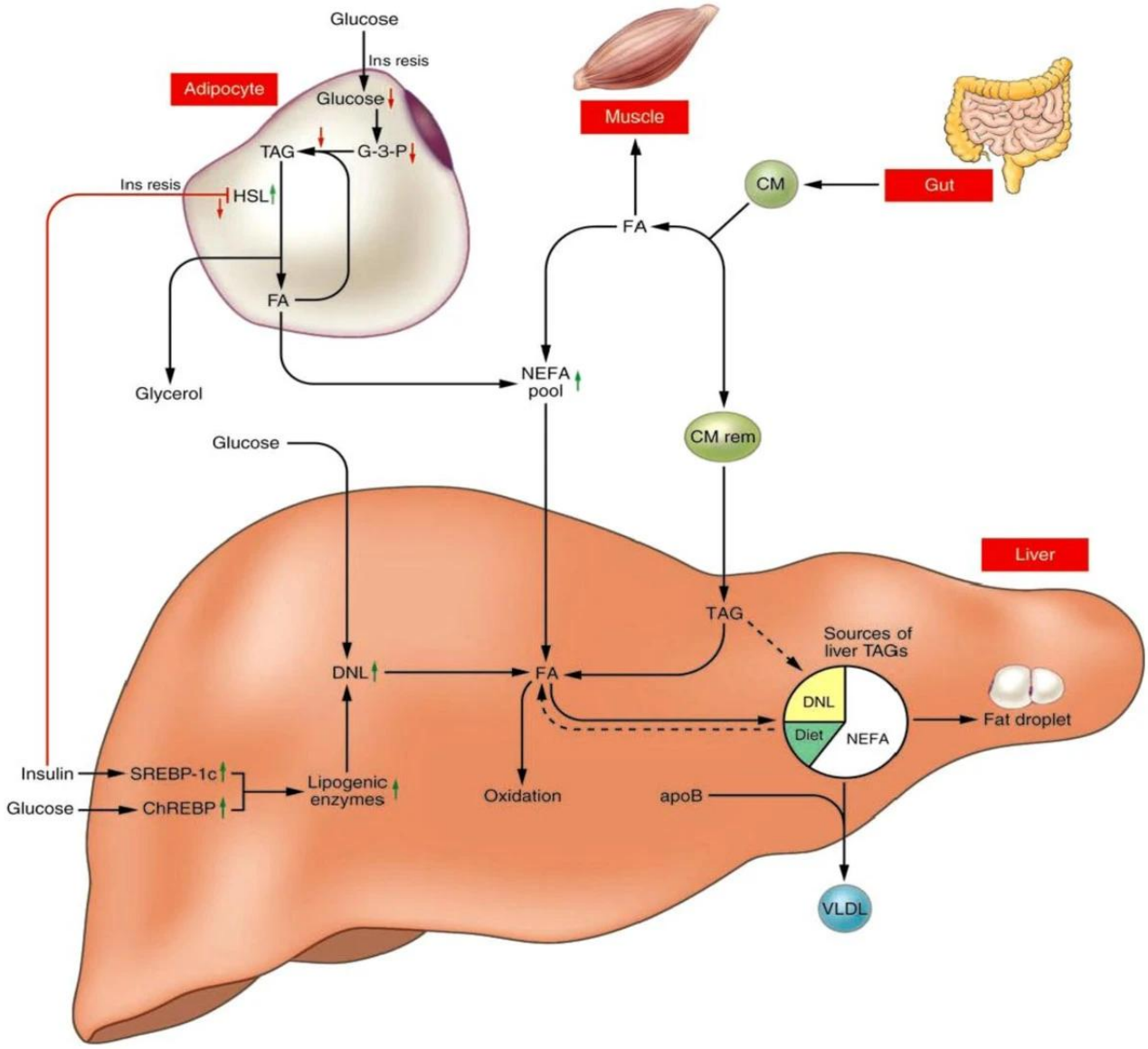

Figure 3: Fat accumulation through lipolysis, de novo lipogenesis and excessive dietary fat and sugar intake [28].

In this condition, lipid homeostasis is disrupted due to higher circulating lipid uptake and *de novo* lipogenesis (DNL), and lower fatty acid oxidation and TAG-rich lipoproteins (VLDL) secretion [29–31]. Briefly, the resulted metabolic shift, associated with insulin resistance and obesity, triggers primarily the inhibition of lipolysis with an increased release of FFAs into the bloodstream, and further transported into the liver [26,32,33]. Moreover, in insulin-resistant states, high insulin levels induce,

through stimulation of transcription factors like SREBP-1c and ChREBP, the activation of enzymes crucial for DNL, such as acetyl-CoA carboxylase (ACC) and fatty acid synthase (FAS) [22,26,34]. Notably, when ACC1 expression is decreased, accumulation of malonyl-CoA occurs, and inhibits carnitine palmitoyl transferase (CPT)-1, which transports fatty acids within mitochondria and reduced mitochondrial β-oxidation [25,26]. The interplay of these mechanisms leads to the progression of steatosis, which in turn can progress to more severe stages.

1.2. Obesity in muscle

Besides accumulating in liver, excess of adipose tissue can trigger steatosis also in other tissues, including skeletal muscle, leading to dysfunctions such as myosteatosis, characterized by ectopic fat accumulation in muscle, and sarcopenia, described as a loss of muscle mass and function [21]. The coexistence of obesity and sarcopenia is a clinical and functional condition, which is increasingly recognized in the scientific and medical communities, called “sarcopenic obesity” (SO), also known as obesogenic sarcopenia [35]. The title “sarcopenia” has its origin from the ancient Greeks, who were referring to a progressive decline of lean mass with the words "sarx" (σάρξ), meaning "flesh", and "penia" (πενία), meaning "loss" or "deficiency". The term was coined for the first time by Rosenberg [36], and recently, the European Working Group on Sarcopenia in Older People (EWGSOP) consider low muscle strength the most prevalent parameter in sarcopenia, thereby confirming the diagnosis by the evidence of low muscle mass [37,21,38].

Given that, sarcopenia has been further investigated and, as Donini et al. described, it is commonly considered a condition related to metabolic changes, chronic inflammation, hormonal imbalances, and lifestyle factors, such as poor nutrition and physical inactivity, whose main hallmark is considered muscle atrophy [35].

1.2.1.1. Skeletal muscle atrophy

Atrophy is characterized by a massive loss of skeletal muscle mass, as a consequence of several physiological conditions or systemic diseases [39]. It leads to a progressive decline in muscle functionality, eliciting falls, , and loss of independence, impacting on the quality of life of patients [40,41].

Skeletal muscle is the largest organ in human, it constitutes approximately 40% of total body weight and accounts 50% of total body proteins [42]. Since several functions are attributed to it, including structural and functional aspect essential for everyday activity [39], its preservation is essential to avoid metabolic dysregulation. It is highly plastic and dynamic considering that it can modify its mass, composition, and strength in response to stimuli, such as exercise, inactivity, nutrition, and disease [39,42]. Hypertrophy or atrophy are fundamentally defined by the two regulatory mechanisms: skeletal muscle protein synthesis (anabolism) and protein degradation (catabolism) [39]. Under normal condition, homeostasis of skeletal muscle mass is orchestrated by a precise equilibrium between these two processes, on the other hand, when the balance between protein degradation and protein synthesis is deregulated towards the former skeletal muscle atrophy occurs.

In this condition catabolic pathways predominate over anabolic ones, among the latter the most studied consists in the activation of serine/threonine kinase Akt, that in turn amplifies the mammalian target of rapamycin (mTOR), with the induction of protein synthesis [43–45]. On the other hand, protein breakdown in skeletal muscle is mainly mediated by two main degradation systems: the ubiquitin-proteasome system (UPS), and autophagy-lysosome system [39,46]. UPS system is activated when muscle-specific E3 ubiquitin ligases, such as atrogin-1/MAFbx and MuRF1, are overexpressed. Given that, several studies have demonstrated that this proteolytic system is upregulated in catabolic condition and activated in cancer patients [39,46], considering it one master

regulator of muscle atrophy alongside autophagy. Meanwhile, autophagy plays a crucial role in regulating myofibers proteostasis since its activation is triggered by cellular stimuli, including lack of nutrients or stress. It contributes to discard and recycle myofibrillar proteins through the formation of autophagosomes [47], whose aim is to encapsulate aggregates or damaged organelles for subsequent lysosomal degradation, through lytic enzymes [48–50]. Among the autophagy-related genes, LC3, Gabarap, and CathepsinL are now accepted markers of autophagy and are dysregulated in various conditions associated with muscle wasting [39,48]. Nevertheless non-selective autophagy is appointed to remove big cytoplasmatic regions, selective autophagy in muscle has gained relevant importance in regulating protein turnover by working in coordination with UPS system [39,46]. Selectivity is facilitated by the involvement of specific adaptor proteins, including Bnip3 and p62 [48], that target specific organelles, such as mitochondria. The accumulation of damaged mitochondria and impaired mitophagy have been identified as additional pro-catabolic stimuli contributing to muscle loss.

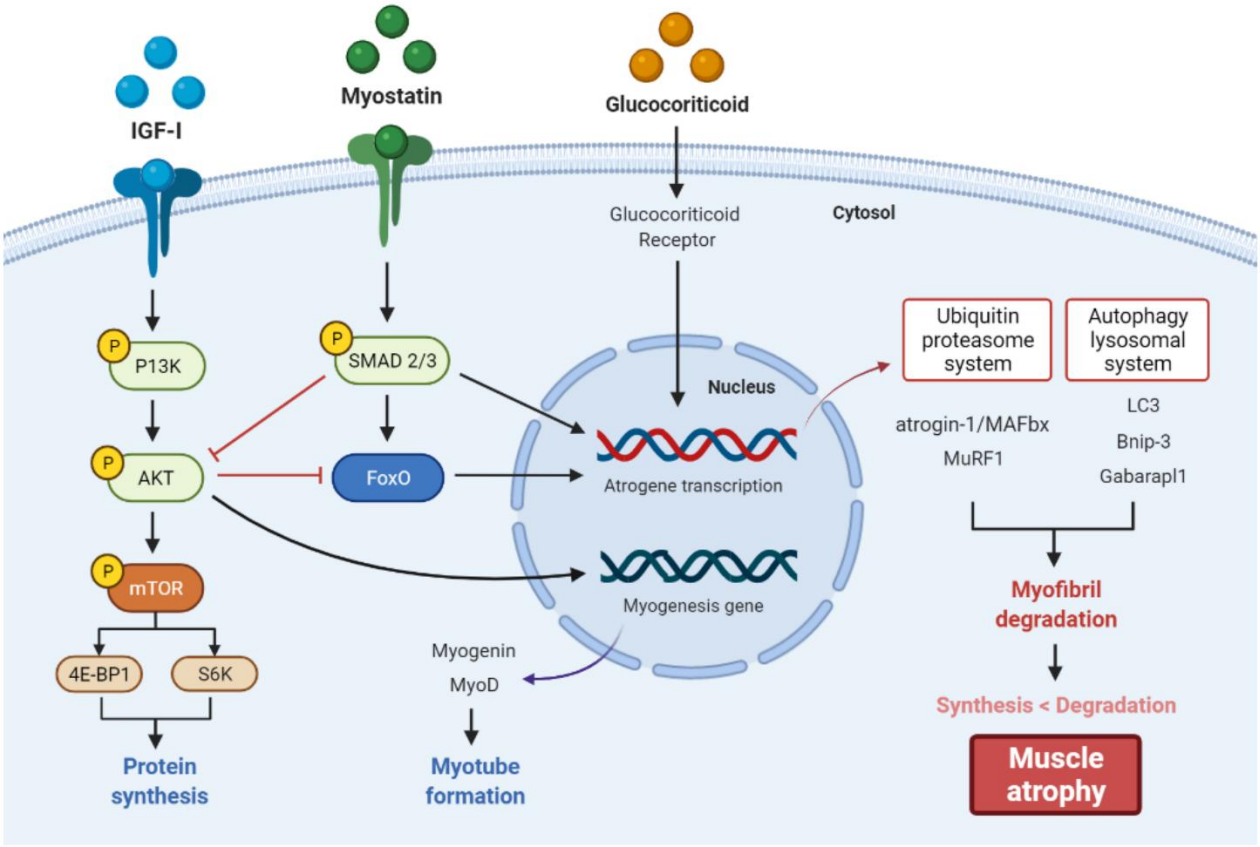

Figure 4: Signalling pathways leading to muscle atrophy. In diverse catabolic states, multiple intracellular signalling pathways stimulate the expression of atrogenes and autophagic genes, resulting in protein degradation via the proteasome and autophagy [51]

Given that, mitochondria cover a central role in the maintenance of skeletal muscle activity, where they exist as an interconnected network often referred to as a reticulum, and morphology relies on the dynamic interplay between fission and fusion events [52]. In brief, fission is required to break the reticulum into smaller fragmented organelles, contributing to the mitochondrial quality control by elimination of impaired or dysfunctional mitochondria, while fusion is conducive to mix and exchange the intramitochondrial contents between mitochondria. The former is regulated by dynamin-related protein 1 (DRP-1), mitochondrial fission factor (Mff), and fission protein 1 (Fis1), the latter by mitofusin 1/2 (Mfn1/2) in the outer mitochondrial membrane and optic atrophy 1 (OPA1) in the inner mitochondrial membrane [15,52,53]. Moreover, mitochondrial dysfunction is

associated with mitochondrial membrane potential impairment, production and accumulation of reactive oxygen species (ROS), and electron transport chain (ETC) dysregulation, all of which exacerbate muscle degradation. The intricate balance between mitochondrial fission, fusion, and mitophagy plays a pivotal role in regulating metabolism and muscle mass. Given that, an equilibrium between anabolic-catabolic pathways is crucial to avoid skeletal muscle loss, while failure of these processes could trigger physio-pathological conditions.

1.3. Bone and obesity

Substantial amount of research has been exploring the relationship between sarcopenic obesity and bone. Despite initially high BMI and bone mineral density (BMD) were considered beneficial for bone strength, obese individual are supposed to be more likely inclined to develop fractures and risk of falls [54].

Bone is a porous, mineralized structure composed of osteoblasts and osteoclasts, blood vessels, and calcium-based mineral crystals (e.g. hydroxyapatite). Bone formation is structured in three passages: 1) production of the osteoid matrix, which is the network composed of osteoclasts within osteoblasts-secreted bone matrix; 2) maturation of the osteoid matrix; 3) matrix mineralization [55]. Two type of bone tissue are observed in the human skeleton: cortical bone and trabecular bone. The former is approximately 80% of the skeleton, dense and compact, with a low turnover rate and high resistance to bending and torsion. The latter accounts for 20% of the skeletal mass, but 80% of the bone surface since it is present in long bones, flat bones, and vertebral bodies. It is less dense and more elastic, with a higher turnover rate, and it is important for metabolism and mechanical support [55].

Several factors obesity-dependent can negatively impact bone formation and homeostasis. High levels of leptin, pro-inflammatory cytokines, such as IL-6 and TNF-α, and FFAs, like palmitate, are

associated with decreased bone formation and lower osteoblastogenesis and increased osteoclastogenesis and bone resorption [54,56]. In addition, adiponectin, Vitamin D, and peptide YY deficiencies in obese individuals further impact negatively bone mass, bone formation, and an overall skeletal health [54,56].

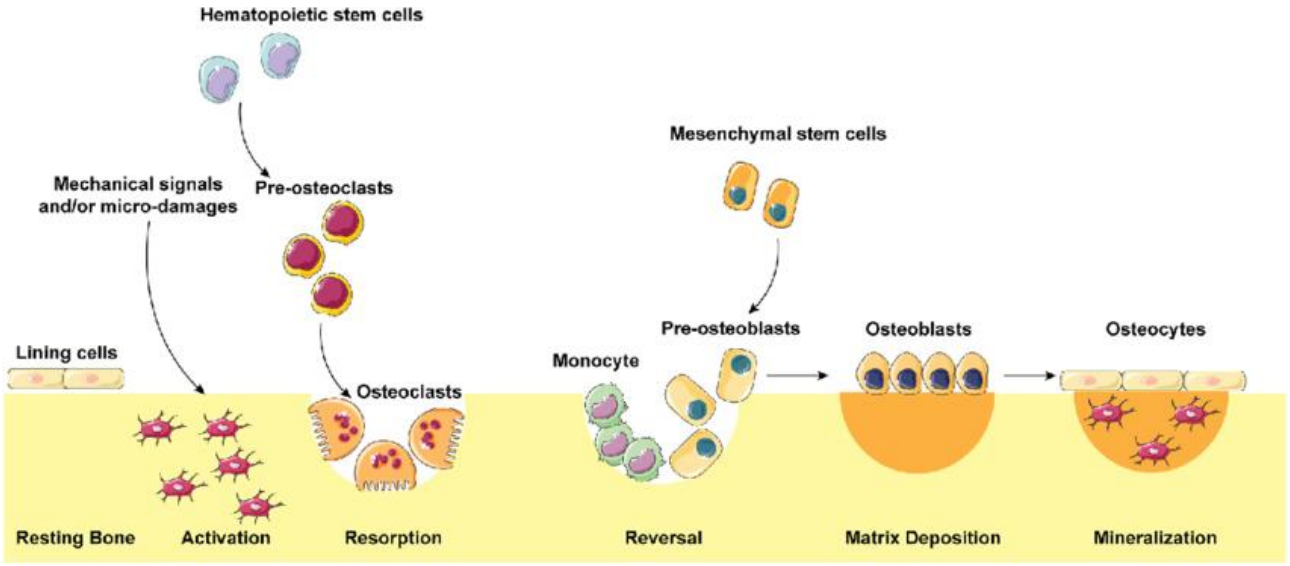

Figure 5: Bone remodelling cycle comprehends different steps, from bone resorption to bone mineralization, and it is catalysed mainly by osteoclasts and osteoblasts [57].

2. Interplay liver-muscle-bone axis

Even though liver, skeletal muscle, and bone appear distinct organs, their intricate networks of communication significantly impact metabolic homeostasis, physical function, and overall health.

The comprehension of this axis paves the way in the understanding of the pathogenesis of some conditions. Liver and skeletal muscle, as mentioned before, are the two main metabolic organs that interact each other to maintain glucolipid homeostasis through secretion of liver-derived hormones, hepatokines, and muscle-derived hormones, myokines. Both hepatokines and myokines exert autocrine/paracrine and endocrine functions that are pivotal in regulating metabolism, for example

glucose uptake, insulin sensitivity, and liver functions. Thus, dysfunction in either liver and skeletal muscle may impact on the other and on the system. Indeed, MASLD and sarcopenia are more often correlated, and their relationship is bidirectional and a vicious cycle, where each condition could exacerbate the other leading to poorer outcomes. In this context, sarcopenia could be both the cause and the consequence of MASLD. Briefly, muscle loss can aggravate steatohepatitis influencing insulin resistance, dyslipidaemia, and systemic inflammation through adipokines and myokines alteration, thereby augmenting liver fat accumulation, on the other hand MASLD can contribute to sarcopenia through pathways that affect muscle protein metabolism and synthesis, leading to muscle wasting [58]. In addition, MASLD and sarcopenia may trigger also osteoporosis affecting bone mineral density (BMD) loss, further impacting risks of falls, and bone fractures [57]. This syndrome is called “osteosarcopenia”, which means the synergistic presence of osteoporosis and sarcopenia, and as a consequence of it, obesity may play a significant role in reverberating bone health [59–61]. Chronic-low grade inflammation triggered by MASLD may induce excessive activation of osteoclasts, whose dysregulated production is associated in the onset of osteoporosis [57]. In this condition, RANKL, a molecule from the TNF superfamily, binds to RANK on osteoclast precursor, promoting their progression and bone resorption [62]

Thus, liver and skeletal muscle are associated also with bone since the former provides metabolic substrates and hormonal signals necessary for bone health, and the latter through its contraction and myokine production is crucial for bone strength and metabolism. In turn, bone provides structural support for muscle function and regulates energy metabolism through production of osteokines.

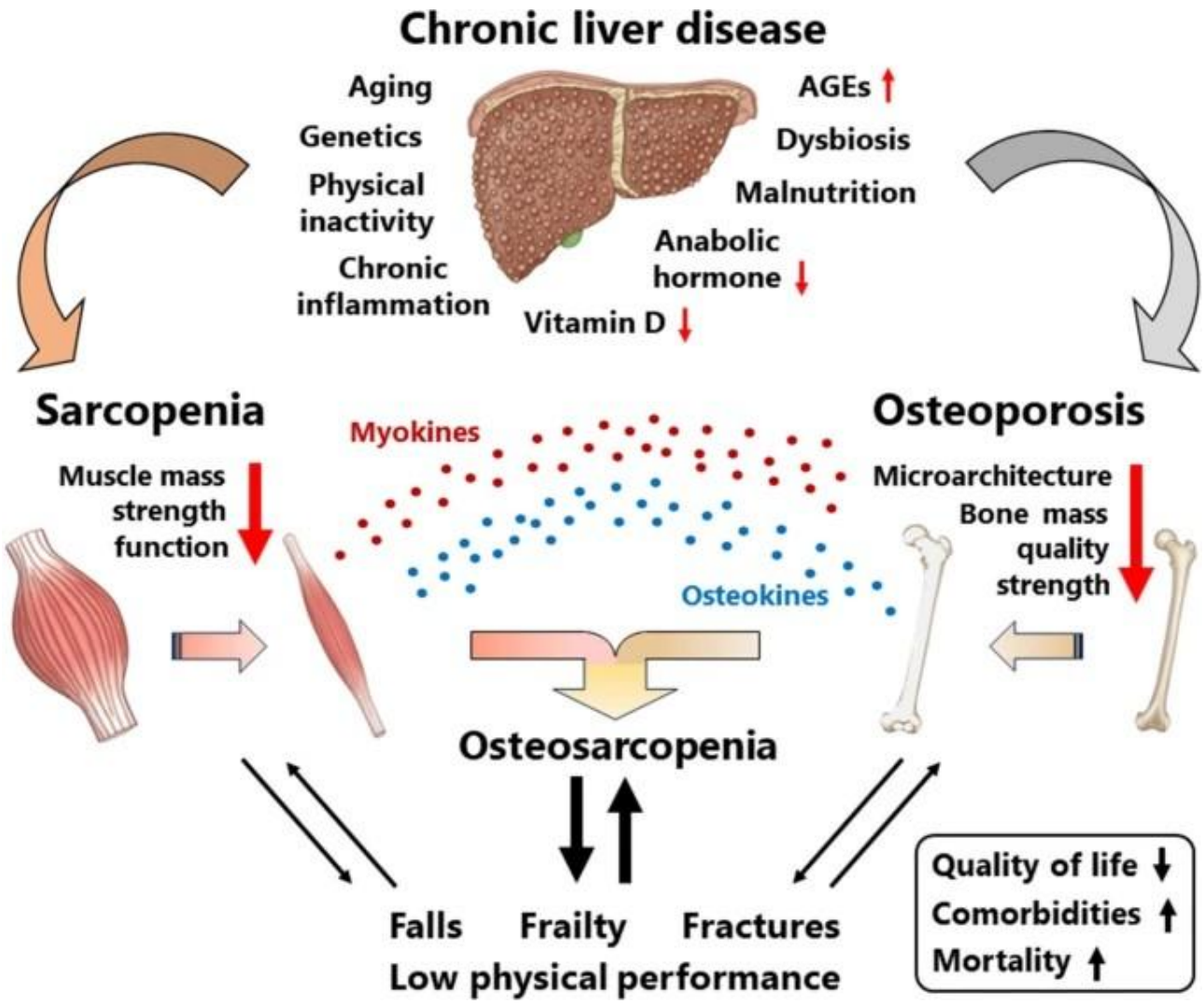

Figure 6: Dysregulation of liver-muscle-bone axis may trigger chronic liver diseases, osteosarcopenia, and the associated comorbidities, with an overall reduction of quality of life and higher mortality [62].

3. Western diet in obesity

The western dietary pattern, called for this reason “western diet” (WD), widespread in industrialized Countries, in particular United States and Europe, where the convenience-driven food culture has become prevalent due to industrialization, urbanization, and the rise of process food industries. Availability of high-calorie and high-fat foods, as well as non-physical entertainment and sedentary

lifestyle are more often studied and documented as key players in the aetiology of several chronic diseases, including T2D, MASLD, CVDs, Alzheimer's disease and several cancers [8,63–65].

WD is characterized by high consumption of processed food, rich in sugars (refined grains) and saturated fats, while being low in fiber (whole grains, fruits, vegetables, legumes) and healthy fats. As a result, this unbalanced diet contains high-energy intake, with an overabundance of simple sugars, and sodium, lacking supply of fibers, vitamins, and minerals, whose levels consumed are below recommendation [66]. Excessive lipid intake from the diet can lead to increased levels of palmitic acid in the blood, which is a saturated 16-carbon fatty acid and it is demonstrated to be the most prevalent saturated fatty acid during WD-feeding [67–69]. Prolonged exposure to saturated fatty acids, like palmitate, is considered to be a risk factor to develop insulin resistance [69].

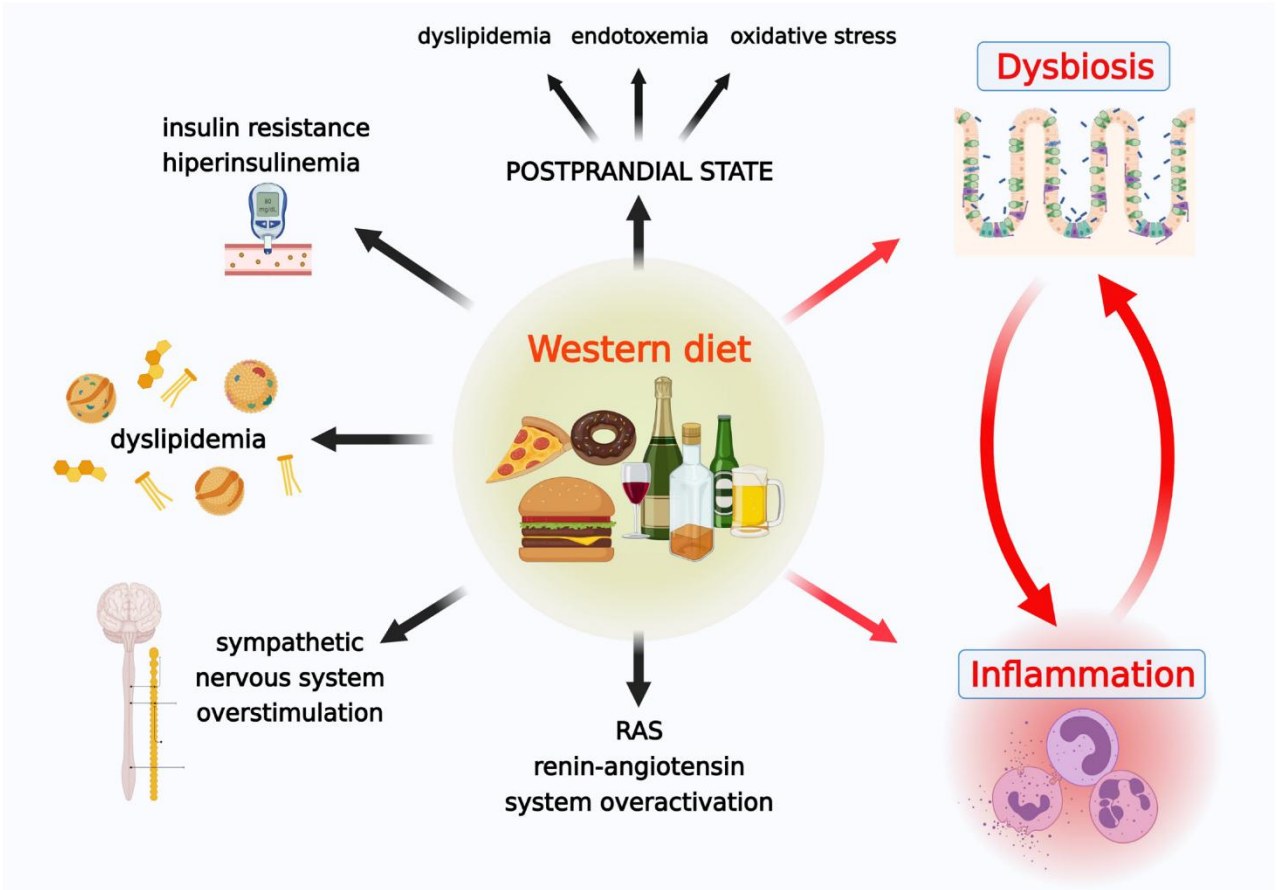

Figure 7: Overview of Western diet: typical foods and drinks with its related potential health complications after long-term consumption [70].

As depicted in FIG 7, chronic surplus of energy intake over energy expenditure, triggers an excess TGs storage in adipose tissue [63,71], which leads to ectopic fat accumulation and metabolic alterations, which can be associated with insulin hypersecretion and hyperinsulinemia, thereby promoting fat storage, lower lipolysis, and dyslipidemia [64]. Moreover, in Malesza et al. is reported how WD is critical in overstimulating and over activating sympathetic nervous system (SNS) and renin-angiotensin system (RAS) inducing high release of molecules, such as norepinephrine (NE) and epinephrine from sympathetic nerves and adrenal medulla, and angiotensin II (ANG II) as the major effector peptide of the RAS [70]. Over-activation of both the SNS and the RAS is implicated in a variety of degenerative diseases, including cardiovascular diseases (CVD) and type 2 diabetes mellitus (T2DM) [64]. Finally, as is widely demonstrated in literature, WD is strongly associated with a chronic low-grade inflammation and oxidative stress, two processes critical in promoting dysbiosis and high intestinal permeability [70,72,73]. Despite WD is frequently used in animal studies to mimic western style lifestyle and nutritional habits, it lacks a precise definition and its composition can vary significantly among studies. Variability in composition and time required for disease progression are important factors that are crucial in influencing the outcome. Although the discrepancy related to the dietary composition and feeding duration, WD is considered, as confirmed in Flessa et al. review, to be a robust model, better than the common high-fat diet alone, that mimic both the histopathology and pathogenesis of human MAFLD, including obesity and insulin resistance [23].

3.1. WD in health complications

As discussed before, WDs have been widely demonstrated to promote weight gain with fat mass accumulation [11,63,64], chronic inflammation [5,36,40,63], insulin resistance [2,5,74], oxidative stress [64,74],

mitochondrial dysfunctions [40,74–76], and metabolic alterations [40,75]. Although western diets share the common characteristic of being high in fat, sugar, and processed foods, and often low in vitamin, fibre, and minerals [77], some studies focus the attention on the percentages of fat and sugar [76], while others on the types of them [33,64,78], or the presence/absence of cholesterol [72]. Various types of WD were designed to mimic human disease in animal models, but no one fully recapitulates human disease, highlighting the need for comprehensive translational approaches [23]. However, depending on the study design, micronutrient ratio and ingredients can vary.

Given this, in our experiment, steatosis in liver was induced by feeding eight-week-old male mice with a high fat/ carbohydrate diet (4.6 Kcal/g) enriched with 1.25% cholesterol Western Diet (WD) for 16 weeks [79].

3.1.1.1. Western Diet as a driver of steatohepatitis in rodents

Given the importance of the topic, WD has been extensively utilized in animal studies in order to induce MAFLD and MASH. Several works in rodent models reported significative results in inducing hepatic inflammation, hepatocellular damage, and fibrosis after both short-term and long-term WD consumption. In Cremonese et al., two or four weeks of WD were enough to induce a more severe hepatic injury and obesity in rats that spontaneously develop MASLD with liver fibrosis and portal hypertension. Moreover, WD leads to a rapid increase in TGs accumulation [72]. On the other hand, western-style diets feeding for longer period in mice exacerbate NAFLD/MASLD progression to NASH/MASH, with more severe inflammation, TGs accumulation, fibrosis, ER stress, and elevated circulating liver enzymes (alanine aminotransferase=ALT; aspartate aminotransferase=AST), indicative for liver damage [23,29,34]. Besides being valid in inducing oxidative stress, insulin resistance, and metabolic changes, WD contributed to hepatic inflammation by impacting gut microbiota dysbiosis, altering intestinal permeability and endotoxemia [23,63].

3.1.1.2. Western diet controversial role in skeletal muscle homeostasis

Although WD is widely discussed to trigger steatohepatitis, knowledge on its role on skeletal muscle is a little bit controversial and not deeply deciphered. WD-feeding is associated with fat deposition in muscle, which in turn affects cell signalling pathways, mitochondrial function, and energy metabolism [76] developing atrophy and muscle weakness. The majority of evidences agrees that WD could be implicated in the onset of atrophy mainly through induction of obesity, insulin resistance, inflammation, and oxidative stress [40,75,80,81]. Indeed, increased consumption of western-style diets and bad habits, besides increasing accumulation of fat mass and promoting progression of MASLD and MASH, they might trigger muscle wasting.

However, there is still a considerable number of works that claim that western-style diets alone are not sufficient in eliciting obesity and muscle atrophy, without altering lean and fat mass [66,82], arguing that it may not represent an appropriate or reliable model to mimic sarcopenic obesity in animals.

3.1.1.3. Bone loss WD-induced

Despite high caloric intake, WD are also characterized by low nutrient density and diminished absorption of essential nutrients, including proteins, calcium, magnesium, and vitamin D, which are fundamental in the maintaining of bone health and muscle mass [78,83,84]. Moreover, consumption of diets rich in fat and sucrose, like the typical western diets, negatively impact turnover rate, with progressive deterioration of bone microarchitecture, including BMD [60,85].

4. Ketogenic diet

Although pharmacological approaches are proposed to counteract obesity, in order to prevent, avoid or simply keep obesity epidemic under control, one of the main approaches that has been studied is the dietary regimen modification [86].

Healthy lifestyle, such as physical activity, and nutritional interventions, including the consumption of a balanced Mediterranean diet, characterized by an adequate content of dairy, fish, and vegetables, have been proposed in order to prevent or mitigate MASLD and osteosarcopenia development [65,78].

Nowadays, among the non-pharmacological therapies, the introduction of the ketogenic diet (KD) or the very-low carbohydrate ketogenic diet (VLCKD) are often proposed [87–89]. In the classical model, KD is a nutritional regimen characterized by very low carbohydrates intake, high-fat and an adequate protein content (55-60% of lipids, 30-35% of proteins, 5-10% of carbohydrates) that causes a shift from the carbohydrates toward fatty acids metabolism. It is a treatment used worldwide from the early 1920s in the therapy of epileptic patients [90,91]. On the other hand, VLCKD differs in a lower percentage of fats and further caloric restriction. However, other strategies simply focus on the caloric intake restriction, with different carbohydrates, fats, and proteins ratios.

KD, due to insufficient level of carbohydrates and elevated fat content, induces a metabolic state called “nutritional ketosis”: a partial beta-oxidation of FFAs finalized to produce ketone bodies (KBs), like beta-hydroxybutyrate (BHB), acetoacetate and acetone. Once produced in liver owing to increase levels of FFAs and acetyl co-A, KBs move from liver and reach extrahepatic tissues, where they are used as the principal source of energy [92–94].

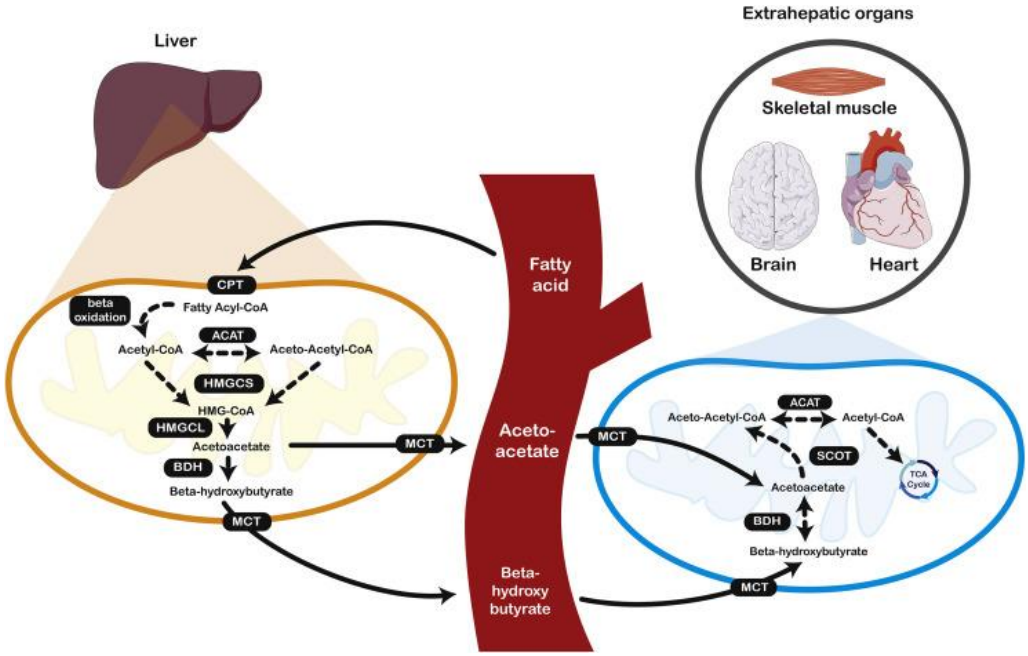

Figure 8: Production of ketone bodies from partial beta-oxidation of fatty acids in liver, with their consequent translocation into extrahepatic tissues through blood circulation [95]

Thus, KD is increasingly proposed as an initial tool able to induce rapid weight loss in obese individuals [93]. According to this, both the Italian Society of Endocrinology (SIE) and the European Association for the study of Obesity (EASO) recognize it as a valid therapeutic option for obesity management, suggesting its use in individuals with severe obesity or obese/overweight with comorbidities, or as supervision of severe obesity before bariatric surgery, emphasizing the importance of a personalized approach and close supervision by healthcare professionals [87,88,96].

Recently, some experimental studies suggested KD effective not only in inducing weight loss, but growing evidences promote KD to be efficient in ameliorating oxidative stress and inflammation, inhibiting NFκB signalling pathway [97], monitoring PI3K/Akt/mTOR signalling pathway [98], and activating the anti-inflammatory cytokine IL-10 that inhibits pro-inflammatory mediators such as TNFα [99]. Consequently, KD is being investigated as a possible new therapeutic strategy in addressing MASLD/MAFLD and T2D [92,100,101]. Nevertheless, low protein/choline and high cholesterol content

typical of the classical KD are hallmarks known to promote steatohepatitis and liver fibrosis in mice fed with KD containing animal-derived lipids [89]. On the other hand, recent data support the induction of ketonemia also with diets sufficient in protein and choline [102]. Indeed, in a small-scale clinical trial, ketosis is considered favourable in counteracting MASLD [103], but the effectiveness in reducing systemic and hepatic inflammation has not been deciphered in detail until now.

Furthermore, KDs may also contribute to the preservation or even improvement of skeletal muscle mass [97]. However, its impact on skeletal muscle homeostasis is a matter of ongoing debate. For instance, Nakao and co-workers reported its negative influence on muscle function and morphology in mice, highlight by lower muscle performances, weights, and myofiber size. These variations were associated with UPS activation, mirrored in the Atrogin-1, MuRF1, and FOXO upregulation [104]. In addition, other studies support its inability in ameliorating body composition or muscle mass, suggesting inconsistent outcomes across experimental models [105].

Furthermore, as previously discussed, liver and muscle represent two of the principal metabolic organs, whose functions are closely correlated with bone homeostasis, particularly if dysregulated. Thus, MAsLD and osteosarcopenia are documented pathophysiologically interconnected [60,62]. Bone is highly dependent on the diet, and KD composition is considered to be poor in essential nutrients and minerals that are necessary for bone health [84]. Due to these nutritional deficiencies, some studies suggest that prolonged adherence to KD may be detrimental for skeletal health, affecting BMD, risk of fractures, and cell homeostasis [57,59,85].

Altogether, these findings underscore the controversial role of KD on skeletal muscle and bone homeostasis. This complexity highlights the need for further systematic studies to clarify whether KD may exert protective or deleterious effects on musculoskeletal tissues, particularly in the context of metabolic dysfunctions, including MASLD and MASH.

5. Introduction to the paper

“Vegetal oil-based ketogenic diet improves inflammation and fibrosis in experimental metabolic dysfunction-associated steatohepatitis”

*Alessia Provera, Naresh Naik Ramavath, Laila Lavanya Gadipudi, Cristina Vecchio, Marina Caputo, **Alessandro Antonioli**, Sabrina Tini, Anteneh Nigussie Sheferaw, Simone Reano, Nicoletta Filigheddu, Marcello Manfredi, Elettra Barberis, Luca Cocolin, Ilario Ferrocino, Monica Locatelli, Massimiliano Caprio, Frank Tacke, Emanuele Albano, Flavia Prodam and Salvatore Sutti*

Frontiers in Immunology (2025)

In this study, we designed and evaluated a novel vegetal oil-based, choline-sufficient ketogenic diet to decipher its safety and therapeutic potential in a murine model of metabolic dysfunction-associated steatohepatitis (MASH), a progressive form of metabolic dysfunction-associated steatotic liver disease (MASLD). Despite MASH is considered as one of the primary complications for obesity and T2D, effective therapies have yet to be validated. Ketogenic diets (KDs) have shown promise in ameliorating metabolic disturbances, although, traditional high-fat, animal-derived KDs have been associated with exacerbated hepatic inflammation and fibrosis in experimental models, limiting their translational value.

In the paper here presented, we demonstrated that nutritional ketosis KD-induced significantly reduced both liver and body weight, improving glucose tolerance. Metabolic improvements in liver are further confirmed by a higher expression of genes and proteins associated with lipid oxidation and glucose metabolism, with a simultaneous reduction in those related with steatosis, insulin resistance, and fibrosis. In accordance, serum analysis confirms lower concentration of markers of hepatic steatosis, lobular inflammation and liver injury, including ALT and DPP-4, with a concomitant reduction in pro-inflammatory and pro-fibrogenic mediators (e.g., TNF-α, IL-12, TGF-β1, Galectin-3, and osteopontin).

Our data indicates that inflammation and fibrosis regression are well appreciated upon KD consumption by the reduced infiltration of TREM2^{+} CD11b^high macrophages and the prevalence of hepatic crown-like structures (hCLSs), hallmarks in MASH progression. Coherently, in cultured macrophages, β-hydroxybutyrate suppressed expression of TREM2 and Galectin-3.

Finally, KD elicited amelioration in the gut microbiota by elevating beneficial bacterial families (e.g., *Oscillospiraceae*, *Ruminococcaceae*) and anti-inflammatory short-chain fatty acids (SCFAs), such as acetate and propionate.

Overall, this work demonstrates that a carefully formulated vegetal oil-based ketogenic diet can safely and effectively mitigate the hallmarks of MASH in mice, including attenuation of liver inflammation and fibrosis, without adverse hepatic effects. These findings highlight the importance of dietary composition in KD and pave the way in considering it as a promising non-pharmacological strategy for MASH and related metabolic disorders. Further investigations are warranted to decipher its long-term safety and clinical transnationality in humans.

frontiers | Frontiers in Immunology

TYPE Original Research
PUBLISHED 01 April 2025
DOI 10.3389/fimmu.2025.1518687

OPEN ACCESS

EDITED BY
Maria Pini,
Haute Autorité de Santé (HAS), France

REVIEWED BY
Toshiyuki Murai,
Osaka University, Japan
Gundappa Saha,
University of Pennsylvania, United States

*CORRESPONDENCE
Salvatore Sutti
salvatore.sutti@med.uniupo.it

†These authors share senior authorship

RECEIVED 28 October 2024
ACCEPTED 03 March 2025
PUBLISHED 01 April 2025

CITATION
Provera A, Ramavath NN, Gadipudi LL, Vecchio C, Caputo M, Antonioli A, Tini S, Sheferaw AN, Reano S, Filigheddu N, Manfredi M, Barberis E, Cocolin L, Ferrocino I, Locatelli M, Caprio M, Tacke F, Albano E, Prodam F and Sutti S (2025) Vegetal oil-based ketogenic diet improves inflammation and fibrosis in experimental metabolic dysfunction-associated steatohepatitis. *Front. Immunol.* 16:1518687. doi: 10.3389/fimmu.2025.1518687

Vegetal oil-based ketogenic diet improves inflammation and fibrosis in experimental metabolic dysfunction-associated steatohepatitis

Alessia Provera[1], Naresh Naik Ramavath[1], Laila Lavanya Gadipudi[1], Cristina Vecchio[1], Marina Caputo[1,2], Alessandro Antonioli[1], Sabrina Tini[1], Anteneh Nigussie Sheferaw[1], Simone Reano[3], Nicoletta Filigheddu[3], Marcello Manfredi[3], Elettra Barberis[4], Luca Cocolin[5], Ilario Ferrocino[5], Monica Locatelli[6], Massimiliano Caprio[7,8], Frank Tacke[9], Emanuele Albano[1], Flavia Prodam[1,2†] and Salvatore Sutti[1*†]

[1]Department of Health Sciences and Interdisciplinary Research Centre for Autoimmune Diseases, University of Piemonte Orientale, Novara, Italy, [2]Unit of Endocrinology, University of Piemonte Orientale, Novara, Italy, [3]Department of Translational Medicine, University of Piemonte Orientale, Novara, Italy, [4]Department of Sciences and Technological Innovation, University of Piemonte Orientale, Alessandria, Italy, [5]Department of Agricultural, Forestry and Food Science, University of Torino, Grugliasco, Italy, [6]Department of Pharmaceutical Sciences, University of Piemonte Orientale, Novara, Italy, [7]Department of Human Sciences and Promotion of the Quality of Life, San Raffaele Roma Open University, Rome, Italy, [8]Laboratory of Cardiovascular Endocrinology, Istituto di Ricovero e Cura a Carattere Scientifico (IRCCS) San Raffaele, Rome, Italy, [9]Department of Hepatology & Gastroenterology, Charité - Universitätsmedizin Berlin, Berlin, Germany

Background and aims: Metabolic dysfunction-associated steatohepatitis (MASH) represents a growing cause of liver cirrhosis and hepatocellular carcinoma (HCC). However, effective therapy for MASH is still lacking. Despite recent studies suggest that ketosis might improve MASH evolution, the mechanisms involved have not been explored since common ketogenic diets cause severe steatohepatitis in mice. In this study, we have investigated the capacity of a new-formulated ketogenic diet (KD) containing vegetal fat in improving liver alterations associated with experimental MASH.

Methods: MASH was induced in C57BL/6 mice by feeding a cholesterol-enriched Western Diet (WD) for up to 16 weeks, followed by switching animals to KD for an additional eight weeks.

Results: We observed that KD administration greatly increased ketone body production and significantly reduced liver and body weights. Moreover, liver proteomic analysis and functional tests evidenced an improved glucose and lipid metabolism along with insulin resistance in KD-fed mice. These metabolic effects were associated with an amelioration in MASH-associated gut dysbiosis and with an improvement of hepatic steatosis, parenchymal injury and liver fibrosis. From the mechanistic point of view mice receiving KD showed a significant reduction

in liver TREM2-positive monocyte-derived macrophages forming crown-like aggregates along with a lowering in the hepatic expression of pro-inflammatory/pro-fibrogenic markers such as CCL2, IL-12, CD11b, α1-procollagen, TGF-β1, osteopontin, and galectin-3. Consistently, *in vitro* experiments showed that β-hydroxybutyrate supplementation reduced TREM2 and galectin-3 expression by cultured Raw 264.7 macrophages.

Conclusions: Altogether, these results indicate that ketogenic diet based on vegetal fat effectively improves MASH metabolic derangements and steatohepatitis, and it might represent a potential therapeutic strategy in this disease.

KEYWORDS

metabolic dysfunction-associated steatotic liver disease, non-alcoholic fatty liver disease, non-alcoholic steatohepatitis, liver fibrosis, liver inflammation, ketone bodies, gut dysbiosis

Introduction

One of the consequences of the worldwide diffusion of overweight and obesity is the increasing prevalence of metabolic dysfunction-associated steatotic liver disease (MASLD) according to the new nomenclature (1). MASLD is the most frequent hepatic alteration in Western and Asian countries with a prevalence in the general population of about 25% reaching up to 70-90% among overweight and obese individuals (2). Although MASLD is more frequent in middle-aged people, its prevalence is also increasing among children in relation to the diffusion of unhealthy dietary habits (3). In about 15-20% of MASLD patients, liver steatosis can progress to metabolic dysfunction-associated steatohepatitis (MASH), a condition characterized by hepatocellular damage, intralobular inflammation, and fibrosis progressing to liver cirrhosis (4). It is estimated that within eight years, 15% of MASH patients will develop clinically evident cirrhosis (4), with a death rate ascribed to MASH-related cirrhosis of about 12-25% (1). Moreover, MASLD is increasingly recognized as an important cause of hepatocellular carcinoma (HCC) (5). Growing evidence indicates that inflammatory mechanisms consequent to the liver recruitment and activation of innate and adaptive immune cells are responsible for the onset of chronic hepatic inflammation in MASH and promote the disease evolution to fibrosis/cirrhosis as well as HCC development (6, 7).

Lifestyle changes, including healthy diet and physical activity are, so far, the most effective interventions in MASLD and significantly reduce liver steatosis and hepatic inflammation, although the effects on fibrosis are controversial (8, 9). In recent years, low carbohydrate ketogenic diets (KDs) derived from the Atkins diet have been increasingly used for weight loss and the treatment of metabolic dysfunctions (10, 11). KDs could be different in calorie amount but are all characterized by a high-fat content that, together with the low-carbohydrate content, shifts the glycolytic metabolism to a lipolytic one inducing the liver production of ketone bodies, including acetoacetate and β-hydroxybutyrate (12). Besides the capacity to sustain cell energy production, ketone bodies exert a variety of favorable effects on lipid metabolism, gene expression, and oxidative stress and have specific anti-inflammatory properties improving neurodegenerative disease, tumors, and heart failure (12). Despite small-scale clinical trials suggest that ketosis might favorably impact MASLD (13), the effectiveness of KDs in reducing systemic and hepatic inflammation has not been investigated in detail since traditional ketogenic diets enriched with animal fat cause extensive steatohepatitis when administered to mice, despite a substantial weight reduction (14). Such an effect is likely due to the combined action of low protein/choline and high cholesterol content, all factors known to promote steatohepatitis in mice (14). Consistently, Long and coworkers have recently reported that cholesterol accumulation along with IL-6 overproduction and c-jun N-terminal kinase (JNK) activation are involved in promoting steatohepatitis and liver fibrosis in mice receiving KD containing animal-derived lipids (15).

To expand the use of KDs in humans, it would be important to devise new formulations and to test in rodents whether these diets are effective in mitigating systemic and hepatic inflammation and might control fibrosis. From recent data showing that ketonemia could be reached also with diets sufficient in protein and choline

Abbreviations: ASVs, amplicon-sequence variants; α-SMA, α-Smooth Muscle Actin; Gal-3, galectin-3; hCLS, hepatic crown-like structures; KD ketogenic diet; MASH, metabolic dysfunction-associated steatohepatitis; MASLD, metabolic dysfunction-associated steatotic liver disease; NAFLD, Nonalcoholic Fatty Liver Disease; NASH, Nonalcoholic Steatohepatitis; MoMFs, monocyte-derived macrophages; OPN, osteopontin; SCFA, short chain fatty acids; TREM-2, Triggering Receptor Expressed on Myeloid cells 2; TGF-1β, Transforming growth factor 1β; TNF-α, Tumor Necrosis Factor-α; WD, Western Diet.

(16), we devised a protein and choline-sufficient KD substituting animal fat with vegetal oil and explored its effects in a mice model of MASH.

Materials and Methods

Mice experimental protocol

4 weeks-old wild-type C57BL/6J male mice were purchased from Envigo (Bresso, Italy) and kept in pathogen-free conditions for four weeks of acclimatization before use. Steatohepatitis was induced by feeding eight-week-old male mice with a high fat/carbohydrate diet (4.6 Kcal/g) enriched with 1.25% cholesterol Western Diet (WD) for 16 weeks. Control animals received a standard chow diet. After MASH induction, mice were randomly divided into two groups, one switching to choline-sufficient KD (6.7 Kcal/g) containing 0.3% as carbohydrates, 9.2% as proteins, and 90.5% as hydrogenated coconut oil and the other continuing with the same WD diet for a further eight weeks. The safety of this new KD formulation was assessed in preliminary experiments by feeding mice for 8 weeks. All the diets were purchased from Laboratorio Dottori Piccioni (Gessate, Italy). At the end of the treatments, mice were anesthetized with sevoflurane, and after checking the anesthesia depth, the blood was collected by cardiac puncture. Afterwards, the mice were euthanized by cervical dislocation. Animal experiments were performed at the animal facility of the Dept. of Health Sciences, University of Piemonte Orientale (Novara, Italy) in compliance with EU ethical guidelines for animal experimentation. The study protocols received ethical approval by the Italian Ministry of Health (authorization N° 411/2020-PR) according to the European law requirements.

Assessment of liver injury and metabolic status

Livers were rapidly removed, rinsed in ice-cold saline, and cut into five pieces. Aliquots were immediately frozen in liquid nitrogen and kept at −80°C until analysis. Two portions of the left lobe from each liver were fixed in 10% formalin for 24h and embedded in paraffin. Serum alanine aminotransferase (ALT) levels and liver triglycerides were determined by spectrometric kits supplied, respectively, by Gesan Production SRL (Campobello di Mazara, Italy) and Sigma Aldrich (Milano, Italy). Circulating Dipeptidyl peptidase 4 (DPP4) and Osteopontin (OPN) were evaluated on serum samples using Luminex® Discovery Assays and Luminex 200™ analyzer (Bio-techne, MI, IT) according to the manufacturer's instructions. Ketone bodies were measured once a week with Keto-Diastix® (Bayer, Basel, Switzerland) according to the manufacturer's indications on mouse urine samples collected during animal handling.

Glucose tolerance test

The glucose tolerance test (GTT) was performed following overnight fasting and the glucose load administration (1.5g/kg) via intraperitoneal injection. Blood sampling has been performed by tail vein incision with sterile needles and the glycemia has been measured at the basal state and 10, 30, 60, 90, and 120 minutes after the glucose load through a glucometer (URight, TD-4279, Munich, Germany).

Histology and immunohistochemistry

Formalin-fixed and paraffin-embedded (FFPE) liver sections (4-µm tick) were stained with hematoxylin/eosin using a Roche Ventana HE 600 automatic staining system (Roche Diagnostics International AG, Rotkreuz, Switzerland), while collagen deposition was detected by Picro-Sirius Red staining. Sections were scored blindly for steatosis and lobular inflammation, as described (17). The extension of Sirius Red was quantified by histo-morphometric analysis using the ImageJ software (https://imagej.nih.gov/ij/). Liver macrophages were evidenced on FFPE liver sections by immunofluorescence staining with anti-F4-80 rat monoclonal (Biolegend, USA) and anti-TREM2 rabbit monoclonal antibodies (Abcam, Cambridge, UK) in combination with secondary antibody cocktail prepared depending on the primary antibodies host species. The image acquisition was performed with Zeiss Observer 7 microscope, and background subtraction was performed with the default settings using the ZEISS software ZEN 3.1 (blue edition). Single-channel grayscale pictures were further processed in FIJI. Immunohistochemistry for galectin-3 was performed using goat polyclonal antibodies provided by R&D Systems (Minneapolis, USA) in combination with a horseradish peroxidase polymer kit (Biocare Medical, Concord, CA, USA). Microphotographs were taken using a Nikon Eclips CI microscope fitted with 20x0.5 and 40x0.75 PlanFluor lens and a DSR12 camera (Nikon Europe BV, Amsterdam, Netherlands) through the NIS-Elements F4.60.00 acquisition software.

Flow cytometry analysis of liver leukocytes

Livers were digested by type IV collagenase (Worthington, USA), and intrahepatic leukocytes were isolated by multiple differential centrifugation steps according to Weide et al. (18). The cell preparations were then subjected to red cell lysis by BD FACS™ Lysing Solution (BD Bioscience, San Jose, CA, USA) and stained using combinations of the following monoclonal antibodies: CD45 (Clone 30-F11, Cat. 12-0451-82), CD3 eBioscience, (Thermo Fisher Scientific, Milano, Italy), CD11b (Clone M1/70, Cat. 101212), F4-80 (Clone BM8, Cat. 123113, Biolegend, San Diego, CA, USA) Thermo Fisher Scientific, Milano, Italy). Sample analysis

was performed using the Attune NxT flow cytometer (Thermo Fischer Scientific, Waltham, MA, USA) and data were elaborated with FlowJo™ Software (BD Biosciences, San Jose, CA, USA).

mRNA extraction and real-time PCR

mRNA was extracted from snap-frozen liver fragments using the TRIzol™ Reagent (Thermo Fischer Scientific, Milano, Italy). cDNA was generated from 1 μg of mRNA using the High-Capacity cDNA Reverse Transcription Kit (Applied Biosystems Italia, Monza, Italy) in a Techne TC-312 thermocycler (Techne Inc, Burlington NJ, USA). Real-Time PCR was performed in a CFX96™ Real-time PCR System (Bio-Rad, Hercules, California, USA) using TaqMan Gene Expression Master Mix and TaqMan Gene Expression probes (Thermo Fischer Scientific, Milano, Italy) reported in Supplementary Materials. All samples were run in duplicate, and the relative gene expression was calculated as $2^{-\Delta Ct}$ over that of the β-actin gene and expressed as a fold increase over the relative control samples.

Microbiota analysis

Mouse stool samples have been collected from cages into sterile plastic tubes once a week for the whole experimental timeframe (T0-24) and promptly frozen and stored at -80°C before microbiota analyses. The cecum samples have been collected at T24 by killing mice and isolating each gut segment along with its content in sterile conditions. The analysis has been conducted on samples collected at the beginning (T0), before (T16), and after (T17) the switching to KD and at the end time-point (T24). DNA extraction from 1000 mg of fecal samples was carried out following the SOP 07 guidelines and procedure developed by the International Human Microbiome Standard Consortium (www.microbiome-standards.org). RNAse treatment was then performed on the extracted DNA, quantified by using the QUBIT dsHS kit, and standardized at 5 ng/μL. The V3-V4 region of the 16S rRNA was amplified using the primers 16SF (5'-TCGTCGGCAGCGTCAGATGTGTATAAGAGACAG-3') and 16SR (5'-GTCTCGTGGGCTCGGAGATGTGTATAAGAGACAG-3') (19), according to the Illumina 16S Metagenomic Sequencing Library Preparation instructions. Amplicons were then purified, tagged, normalized, pooled, and sequenced on the Illumina MiSeq platform (2×250 bp) according to the Illumina protocols. Raw reads were imported in QIIME2 software (https://docs.qiime2.org) for denoising by the qiime dada2 denoise-paired script (20). The amplicon-sequence variants (ASVs) obtained were then used for a taxonomic assignment against the SILVA database. ASVs table was analyzed at the lower taxonomic resolution (genus or family level).

Metabolomic analysis

Plasma short chain fatty acids (SCFAs) were analyzed by using GCxGC-TOFMS as reported in Supplementary Materials.

Proteomics analysis

Changes in the liver protein pattern were performed as described in Supplementary Materials.

In vitro experiments

Raw264.7 cells (ATCC) were cultured ($8x10^5$ cells) in 6-well plates at 37°C in complete DMEM + GlutaMAX™ (Gibco, Thermo Fisher Scientific, Milano, Italy) with 5% CO_2. For the experiments Raw264.7 cells were treated for 48h with either butyrate 50μM (Sigma-Aldrich) or vehicle (ethanol, 0,1%) and then harvested for RNA extraction.

Data analysis and statistical calculations

Statistical analyses were performed by SPSS statistical software 26.0 for Windows (SPSS, IBM, USA) using one-way ANOVA test with Tukey's correction for multiple comparisons or Kruskal-Wallis test for non-parametric values. Significance was taken at the 5% level. Normality distribution was assessed by the Kolmogorov-Smirnov algorithm. Statistical analysis of proteomic data was performed using MarkerView software (Sciex, Concord, Canada) and MetaboAnalyst software (www.metaboanalyst.org). Proteins were considered up- and downregulated using fold change >1.3 or <0.769 and p-value <0.05. The significance of the difference was also analyzed by non-parametric tests using the Prism v.8 software package (GraphPad Software, San Diego, CA, USA), with statistical significance taken at $p < 0.05$. Bioinformatics analysis of proteomic data was performed using Ingenuity Pathways Analysis (IPA) software (Qiagen, Redwood City, CA, USA). ASVs tables were then imported in R-Studio for Principal component analysis and to perform the permutational multivariate analysis of similarities (ANOSIM) by the "vegan" package in R environment. Between-group differences were assessed by the Mann–Whitney test.

Results

Characterization of a new formulation of the ketogenic diet for mice

For assessing the effects of ketosis on rodent MASH evolution, we devised a choline-sufficient KD in which fat consisted of coconut oil hydrogenated to obtain a consistency suitable for shaping pellets. To avoid misleading interpretations due to caloric restriction rather than ketogenesis boosting in preliminary experiments we tested the diet palatability by comparing mice fed *ad libitum* with the standard or ketogenic diets for 8 weeks. In this time frame, we did not observe significant differences regarding food consumption (2.99 ± 0.14 vs. 2.98 ± 0.19 g/die; n.s) and body or liver weights (Figure 1A) while, as expected, urine ketone bodies were significantly increased in KD-fed mice as compared with those receiving standard diet (~40 mg/

ml vs. 0 mg/ml, p<0.0001). Since previous studies have shown that KD diets can cause steatohepatitis (14), histological and biochemical analyses were performed on mice receiving our new KD. Although KD-fed mice showed a slight but not statistically significant increase in serum alanine aminotransferase (ALT) (Figure 1C), histological analysis evidenced negligible steatosis without signs of hepatocellular necrosis and portal/lobular inflammation or fibrosis (Figures 1B, C). Furthermore, differently from what observed by Long and coworkers (15) our vegetal oil containing KD did not cause c-jun N-terminal kinase (JNK) activation (not shown). On the same vein, hepatic transcripts for genes commonly up-regulated in MASH showed an increase only for TNF-α, while those for the leukocyte marker integrin αM (ITGAM; CD11b) and for fibrosis-related marker pro-collagen 1A1 (COL1A1) were unaffected (Figures 1B, C), confirming the safety of our KD formulation in mice.

Effects of the ketogenic diet on metabolic and pathological features of MASH

From these preliminary results, we went on to explore the effects of KD when administered to mice with established MASH. To this aim, mice were fed *ad libitum* with a cholesterol-enriched western diet (WD) for 16 weeks. As expected, WD feeding increased body and liver weights and promoted the development of extensive steatohepatitis associated with appreciable collagen deposition (Supplementary Figure 1). After MASH induction, mice were randomly divided into two groups, one switching to KD and the other continuing with the same WD diet for a further eight weeks (Figure 2A). The results were analyzed by comparing the animals switched to KD with the mice continuing the WD for 24 weeks as well as with starting conditions of mice receiving the WD for 16 weeks. We observed that switching to KD strongly reduced liver weight and lowered by 48% liver triglyceride content, while appreciably reducing body weight (Figure 2B). Such metabolic improvement was accompanied by the up-regulation in the hepatic transcripts of genes implicated in glucose and lipid homeostasis, such as glucose transporter 2 (GLUT2), insulin receptor substrate-1 (IRS-1), and peroxisome proliferator-activated receptor-γ coactivator 1-α (PPARγC1α) (21) (Figure 2C). Additionally, the switch to KD restored the physiological capacity to metabolize glucose in MASH mice, as assessed by the glucose tolerance test (GTT) (Figure 2C). In line with this, bioinformatic analysis comparing liver proteome profiles of mice switched to KD with those remaining on WD revealed that KD influenced different molecular pathways stimulating 77 proteins involved in lipid metabolism (Z score ≥2) while lowering (Z score ≤2), respectively, 32 proteins concerning insulin resistance, 114 proteins related to glucose metabolism, and 44 proteins associated with hepatic steatosis (Figure 2D, Supplementary Table 1).

These changes impacted on MASH features since morphological analyses in hematoxylin/eosin-stained liver sections (Figure 3A) showed that KD administration significantly reduced the histological scores for hepatic steatosis (2.5 ± 0.5 vs. 0.5 ± 0.6 arbitrary units; p<0.005) and lobular inflammation (2.0 ± 0.3 vs. 0.5 ± 0.2 arbitrary units; p<0.01). Furthermore, KD significantly improved hepatic injury as assessed by ALT release as well as by circulating Dipeptidyl Peptidase-4 (DPP4) (Figure 3B), a metabolic marker strictly associated to MASLD/MASH in both rodents and humans (22). Consistently, the improvement of parenchymal injury was accompanied by a lowering in the gene expression of pro-inflammatory markers TNF-α, CCL2, IL-12p40 and CD11b (Figure 3C). The beneficial effects of KD on MASH evolution were also evident when liver damage and inflammation in mice receiving KD were compared to those of mice before diet switching (Supplementary Figure 2).

Ketogenic diet modifies gut microbiota

MASH is often associated with alteration in the intestinal microbiota and the loss of gut barrier integrity, which can contribute to hepatic inflammation by increasing the translocation of bacterial products through the portal flow to the liver (23). From the knowledge that nutritional behaviors can influence gut microbiota composition and, in turn, hepatic inflammatory responses (24), we explored whether changes in gut microbiota could account for the anti-inflammatory properties of KD. To this aim, mouse feces were collected weekly throughout the experimental protocol and microbiota was analyzed by amplicon sequencing. According to previous studies, we observed that MASH associated with severe dysbiosis characterized by a decreased abundance of Lachnospiraceae and Ruminococcaceae and a concomitant raising of Peptostreptococcaceae, Erysipelotrichaceae, Bacteroidaceae and Sutterellaceae (25). Interestingly, the improvement of steatohepatitis in mice receiving KD led to changes in gut microbiota composition that were already appreciable after one week of treatment (Figure 4A). In more detail, KD increased the relative frequency of amplicon-sequence variants (ASVs) with potential anti-inflammatory properties, such as R-Ruminococcus, while decreasing ASVs displaying a potential pro-inflammatory behavior like Sutterella (Figure 4A) (26). The characterization of microbiota composition across the gut segments did not evidence differences in bacterial genera within the cecum, ascending, and descending colon, while they appeared more heterogeneous in the ileum regardless of the diet consumed. Therefore, we did not further consider this portion of the intestine and focused our attention on the colon. Principal component analysis (PCA) was performed on ASVs table in order to highlight shift in the stool microbiota as a function of the dietary regimen along time (Figure 4A). In detail, at the beginning of the experiment (T0) no clear separation between diet was observed, while after 16 weeks of dietary treatment, SD-fed mice showed a clear separation compared with WD- and WD+KD-fed mice, which clustered together (ANOSIM p<0.05). After 17 and 24 weeks of dietary treatment each mice group showed a well-clearly distinguishable bacterial signature and distinct stool microbiota composition, with mice clustering according to the dietary regimen. The separation of the microbiota as a function of the diet was then confirmed also in cecum samples (Figure 4B) (ANOSIM p<0.05). As a microbiota signature, KD promoted the enrichment of beneficial ASVs belonging to Oscillospiraceae, Ruminococcaceae, and

10.3389/fimmu.2025.1518687

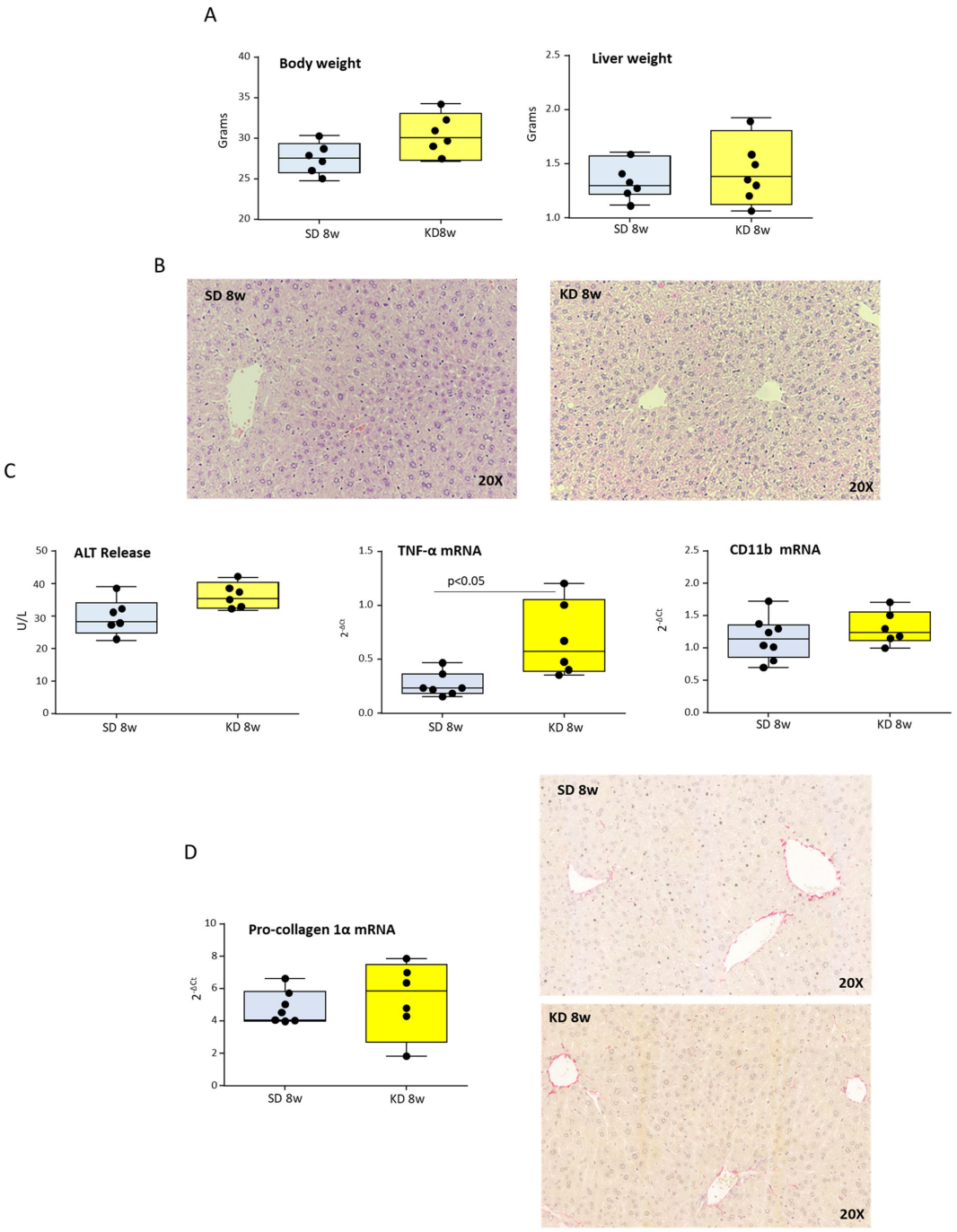

FIGURE 1
Ketogenic diet (KD) administration does not induce hepatic injury, inflammation, or fibrosis in mice. Wildtype C57BL/6 mice were fed with standard (SD) or KD diets for 8 weeks. **(A)** Body and liver weights. **(B)** Hematoxylin/Eosin staining of liver sections (magnification 20×). **(C)** Circulating levels of alanine aminotransferase (ALT) and hepatic transcripts for the inflammatory markers TNF-α and CD11b as evaluated by RT-PCR. **(D)** Intrahepatic collagen deposition as evaluated by the transcripts of procollagen-1α and the staining of liver sections with Sirius Red (magnification 20×). Dots correspond to individual animals and the boxes include the values within the 25th and 75th percentile. The horizontal bars represent the medians, while the extremities of the vertical bars (10th–90th percentile) comprise 80% of the values.

Rikenellaceae. Mounting evidence suggests that microbiota plays an essential role in regulating metabolic and immune functions by producing short-chain fatty acids (SCFAs) (27). To explore the possibility that the health-beneficial properties of KD might be related to the modulation of SCFA production, we analyzed their serological concentrations before and after KD switching. In our hands, KD administration modified SCFA abundance by increasing the circulating levels of propionic and acetic acids by 1.2 and 1.4 folds, respectively ($p<0.05$) (Figure 4C). Conversely, no significant changes were appreciable for butanoic and pentanoic acids (0.06 ± 0.012 vs. 0.04 ± 0.031 ppm, 0.08 ± 0.001 vs. 0.08 ± 0.005 ppm, respectively; n.s.).

10.3389/fimmu.2025.1518687

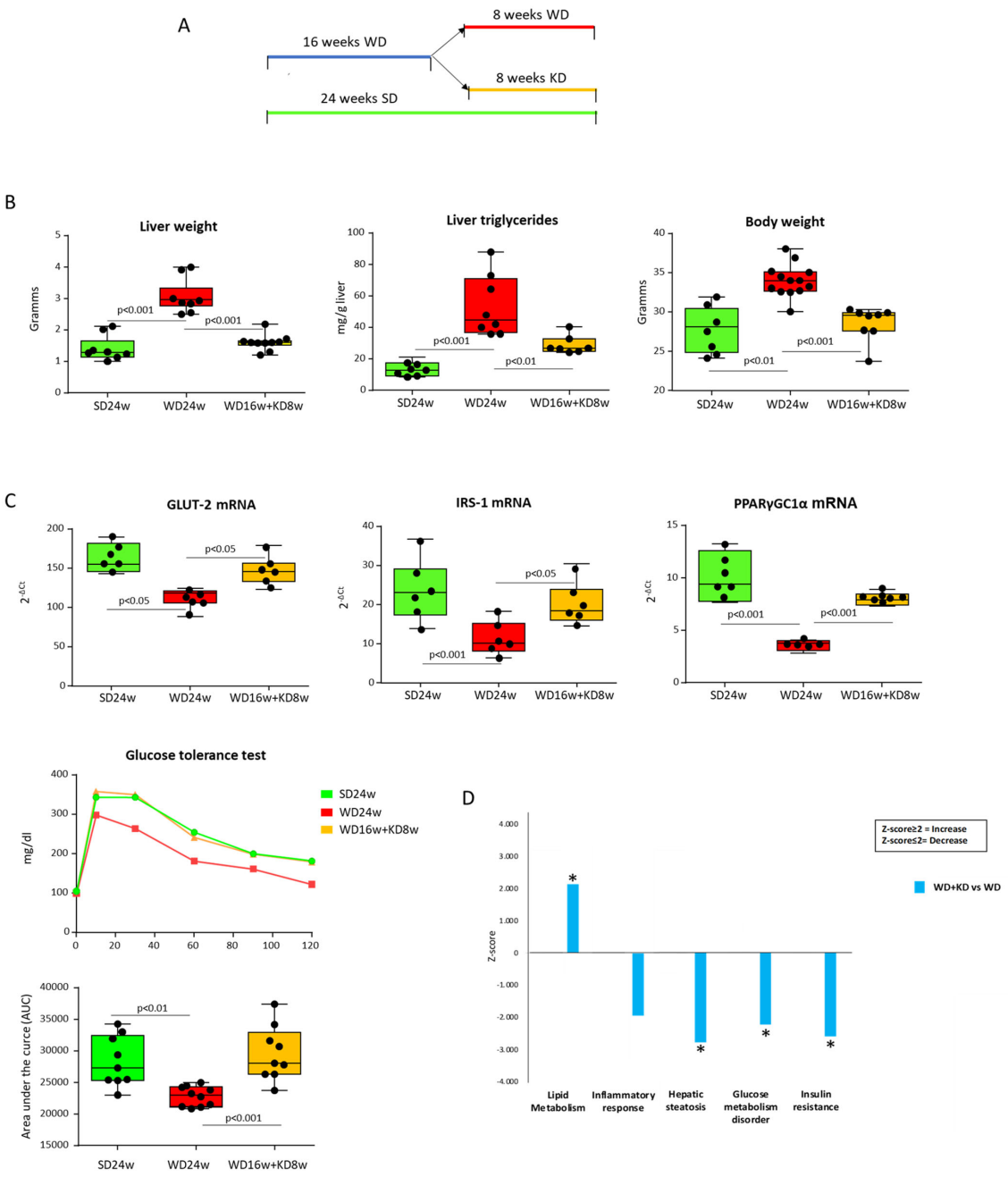

FIGURE 2
Ketogenic diet administration modifies hepatic metabolic functions in mice with MASH. MASH was induced in 8-weeks old wildtype C57BL/6 mice by 16 weeks feeding with Western diet before the switching to ketogenic diet for further 8 weeks (WD16+KD8w). Reference mice received standard diet or WD for 24 weeks (SD24w or WD24w, respectively). **(A)** Experimental Plan. **(B)** Changes in body and liver weights and hepatic triglyceride content. **(C)** Hepatic transcripts for genes of glucose transporter 2 (GLUT2) insulin receptor substrate-1 (IRS-1) and peroxisome proliferator-activated receptor-γ coactivator 1-α (PPARγC1α). RT-PCR values are expressed as fold increase of $2^{-\Delta CT}$ after normalization to the β-actin gene. Glucose tolerance test (GTT) was assessed as area under the curve (AUC). Dots correspond to individual animals and the boxes include the values within the 25th and 75th percentile. The horizontal bars represent the medians, while the extremities of the vertical bars (10th–90th percentile) comprise 80% of the values. **(D)** Ingenuity pathway analysis (IPA) of the changes in liver proteins involved in lipid metabolism, inflammatory response, hepatic steatosis, glucose metabolism and insulin resistance in mice switching to KD as compared to those that received WD only. (*=p<0.05).

10.3389/fimmu.2025.1518687

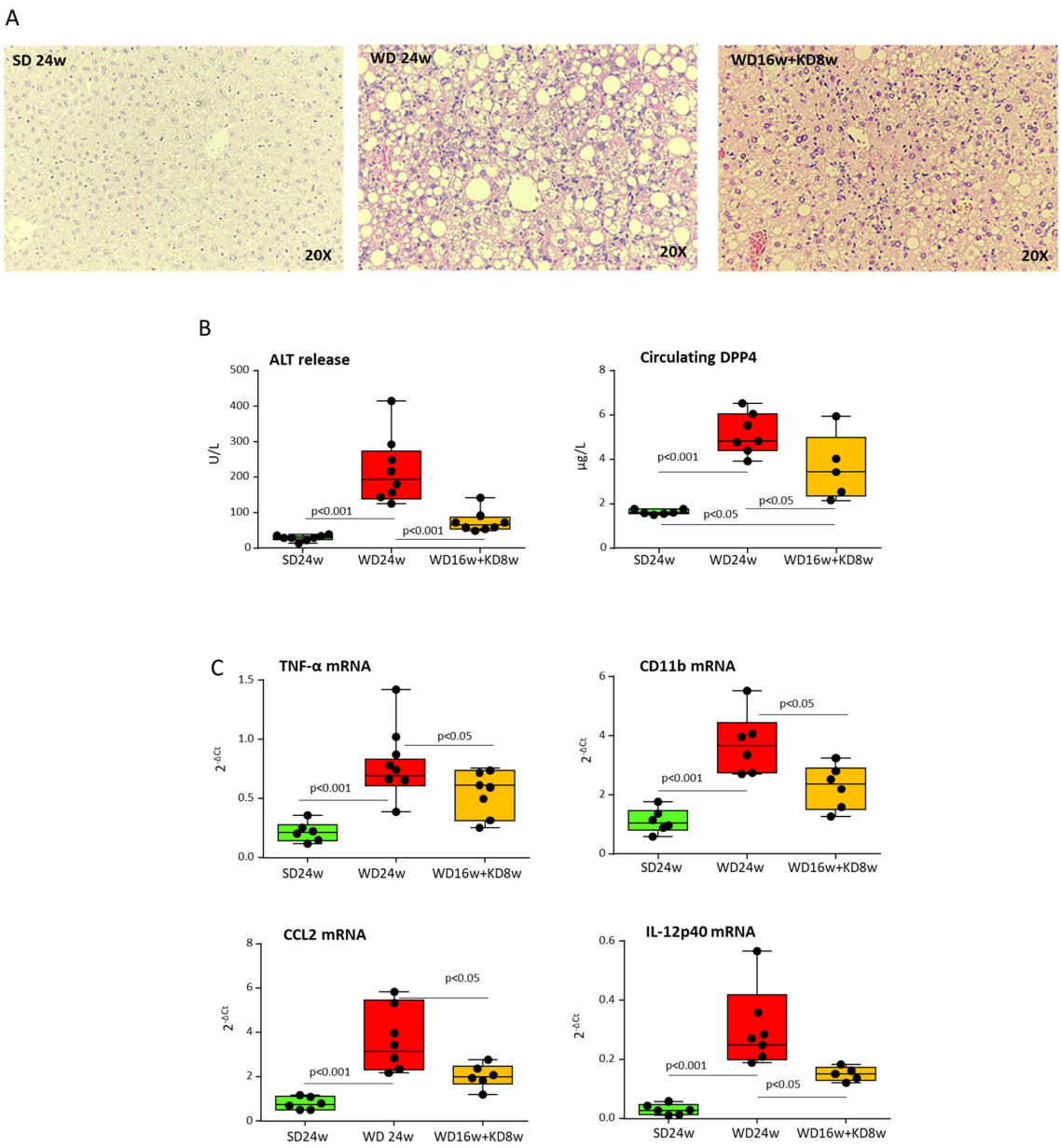

FIGURE 3
Ketogenic diet improves MASH-associated steatosis and hepatic injury in mice. MASH was induced in 8-weeks old wildtype C57BL/6 mice by 16 weeks feeding with Western diet (WD) before the switching to ketogenic diet (KD) for further 8 weeks (WD16+KD8w). Reference mice received standard diet or WD for 24 weeks (SD24w or WD24w, respectively). **(A)** Hematoxylin/eosin-staining of liver sections (magnification 20×); **(B)** Changes in circulating levels of alanine aminotransferase (ALT) and Dipeptidyl Peptidase-4 (DPP4). **(C)** Hepatic gene expression of pro-inflammatory markers TNF-α, CD11b, CCL2, and IL-12p40. RT-PCR values are expressed as fold increase of $2^{-\Delta CT}$ after normalization to the β-actin gene. Dots correspond to individual animals and the boxes include the values within the 25th and 75th percentile. The horizontal bars represent the medians, while the extremities of the vertical bars (10th–90th percentile) comprise 80% of the values.

Ketogenic diet impacts on liver macrophage responses associated with inflammation and fibrosis

From the observation that MASH improvement by our KD formulation associated with changes in gut microbiota impacting on liver inflammation we explored the mechanisms possibly involved. Proteomic analysis showed that among the hundreds of hepatic proteins affected by KD feeding the abundance of galectin-3 (Gal-3) was significantly down-modulated (log-fold change = -0.673; p=0.0028) in 3 out of 5 pathways considered. Gal-3 plays a fundamental role in driving MASH-associated liver fibrosis (28) being produced by a subset of liver infiltrating monocyte-derived macrophages (MoMFs) characterized by the co-expression of the triggering receptor expressed on myeloid cells 2 (TREM2) and CD9 as well as by the production of other pro-fibrogenic mediators such as osteopontin (OPN) (29). These TREM2^{+}-MoMFs also form aggregates surrounding dead/dying hepatocytes, known as hepatic

10.3389/fimmu.2025.1518687

crown-like structures (hCLSs), the prevalence of which strongly correlates with the disease severity and the progression toward fibrosis (29).

In line with these notions, multiparametric flow cytometry evidenced that MASH in WD-fed mice was characterized by an increased hepatic recruitment of pro-inflammatory CD11b^{high}F4/80^{int} MoMFs (Figure 5A), which paralleled with the detection of F4/80^{+}/TREM2^{+} hCLSs within the liver (Figure 5B) and the up-regulation in the transcripts for TREM2, CD9, Gal-3 and OPN (Figure 5C). Interestingly, the switching to KD almost halved the fraction of infiltrating CD11b^{high}F4/80^{int} MoMFs (Figure 5A), strongly reducing the expression of TREM2^{+}-cell markers (Figure 5C) along with the prevalence of hCLSs (23.6 ± 8.1 vs 5.5 ± 2.9 hCLSs/microscopic field; p<0.001) (Figure 5D). From the mechanistic point of view *in vitro* experiments using cultured Raw 264.7 macrophages showed that the supplementation with β-hydroxybutyrate (50 µM) significantly reduced TREM2 and Gal-3 expression (Figure 5E).

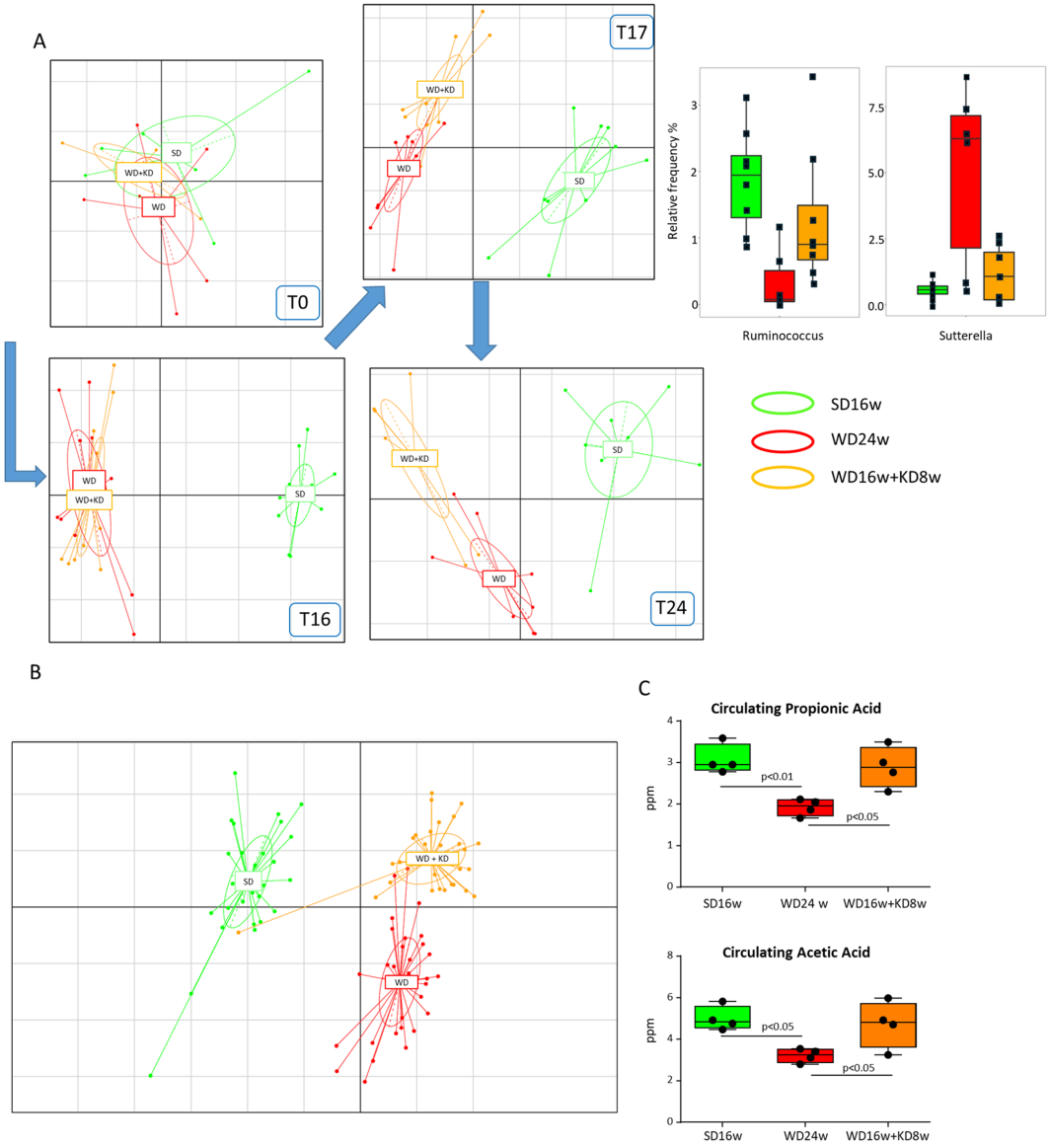

FIGURE 4
Ketogenic diet administration reshapes the gut microbiota in mice with MASH. MASH was induced in 8-weeks old wildtype C57BL/6 mice by 16 weeks feeding with Western diet before the switching to ketogenic diet (KD) for further 8 weeks (WD16+KD8w). Reference mice received standard diet or WD for 24 weeks (SD24w or WD24w, respectively). **(A)** Principal component analysis (PCA) describing the changes in stool microbiota composition at different time points during mice feeding with WD (red) as compared to those remaining in SD (green) or following the switching from WD to KD (orange). **(B)** PCA describing cecum microbiota composition in mice receiving WD, SD or after switching from WD to KD. **(C)** Changes in the serum levels of propionic and acetic acids following mice switching from WD to KD. Dots correspond to individual animals and the boxes include the values within the 25th and 75th percentile. The horizontal bars represent the medians, while the extremities of the vertical bars (10th–90th percentile) comprise 80% of the values.

10.3389/fimmu.2025.1518687

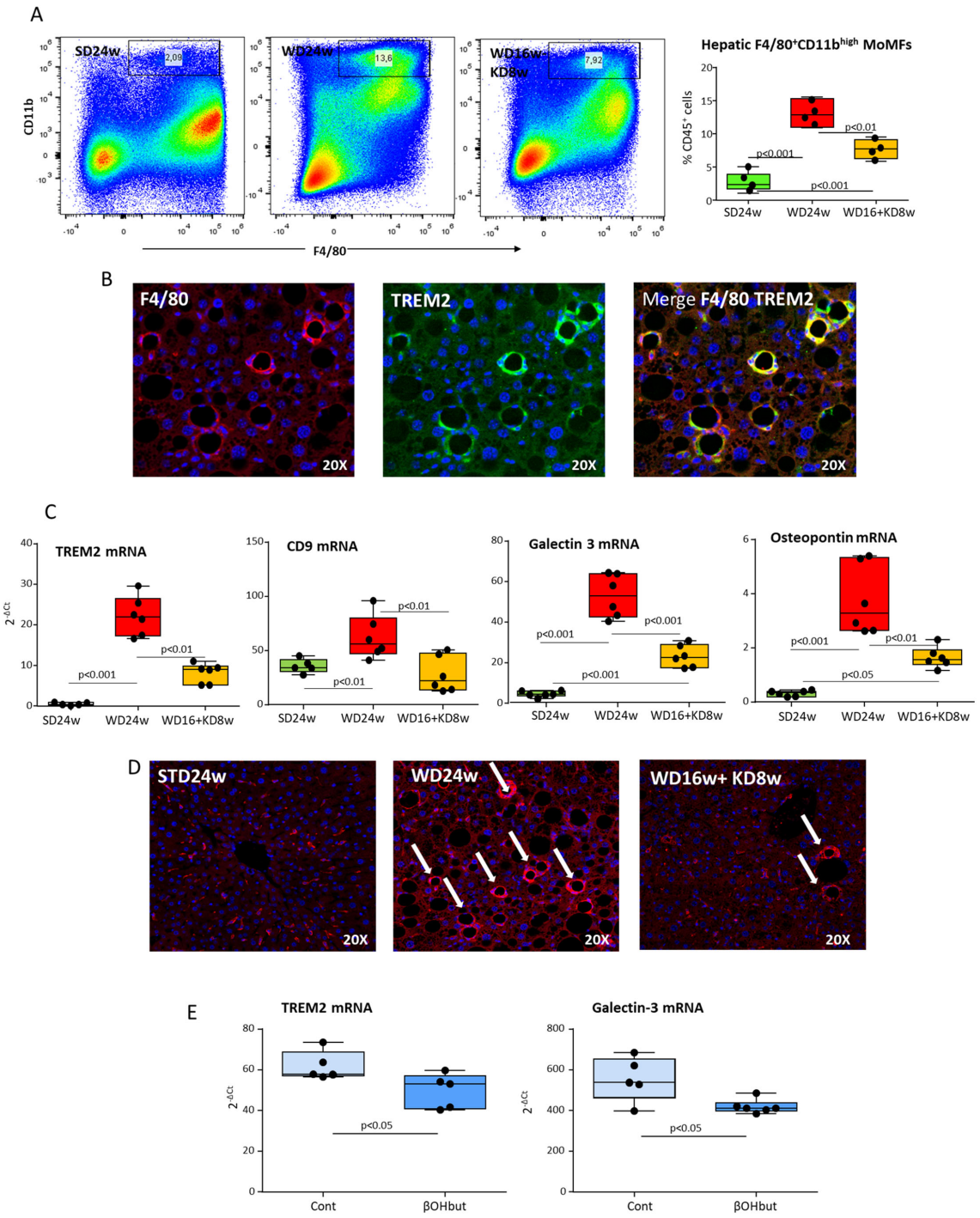

FIGURE 5
Ketogenic diet administration modulates the phenotype of hepatic macrophages and MASH-associated hepatic crown-like structures (hCLSs). MASH was induced in 8-weeks old wildtype C57BL/6 mice by 16 weeks feeding with Western diet (WD) before the switching to ketogenic diet (KD) for further 8 weeks (WD16+KD8w). Reference mice received standard diet or WD for 24 weeks (SD24w or WD24w, respectively). **(A)** Flow cytometry analysis of the distribution of CD11b^{high}/F4-80^{+} monocyte-derived macrophages (MoMFs) within the liver of mice with the different dietary regiments. **(B)** Phenotypic features of liver macrophages forming hCLSs as evidenced by double immunofluorescence of FFPE liver sections stained with fluorochrome-labelled antibodies against F4-80 and TREM2. **(C)** Changes in hepatic transcripts of CD9, TREM2, galectin-3 and osteopontin. Dots correspond to individual animals and the boxes include the values within the 25th and 75th percentile, while the horizontal bars represent the medians. The extremities of the vertical bars (10th–90th percentile) comprise 80% of the values. **(D)** KD effect on the prevalence of hCLSs evidenced by immunofluorescence staining with anti-F4-80 antibodies. **(E)** Effect of β-hydroxybutyrate (β-OHbut; 50 μM) *in vitro* supplementation on TREM2 and galectin-3 expression by cultured Raw 264.7 macrophages. The experimental groups are labelled as Cont (vehicle) and *β*-OHbut and each dot represents an experimental point.

The observation that KD modulated hCLSs, prompted us to investigate whether KD might also have a beneficial impact on liver fibrosis. As expected, steatohepatitis in mice fed with WD for 16 weeks raised the transcripts of the pro-fibrogenic markers procollagen 1α (Col1α) and tumor growth factor 1β (TGF-1β) (Figure 6A) and caused intrahepatic accumulation of collagen fibers, as quantified by Sirius Red staining of liver paraffin sections (Figure 6B). Noteworthy, mice receiving KD showed a significant down-modulation in the Col1α and TGF-1β gene expression along with a remarkable reduction in collagen deposition as compared to WD-fed animals, thus indicating the induction of a substantial regression of the fibrosis (Figures 6A, B). A marked reduction in the prevalence of Gal-3 positive hCLSs was also evident already after 4 weeks from the switching to KD (Figure 6C) in parallel with a lowering in circulating levels of OPN (Figure 6D). These effects were associated with an improvement of fibrosis and of circulating ALT and DPP4 (Supplementary Figure 3C), while they preceded appreciable lowering of steatosis (Supplementary Figure 3B) and the complete offset of hepatic inflammation (Supplementary Figure 3D), indicating that KD has an early and effective impact on the pro-fibrogenic mechanisms involved in MASH evolution to fibrosis/cirrhosis.

Altogether these results indicate that ketogenic diet based on vegetal fat effectively improves MASLD metabolic derangements and reshapes gut microbiota composition while improving steatohepatitis and hepatic fibrosis.

Discussion

Despite the growing clinical relevance of MASLD, there are currently few therapeutic options. According to the European Association for the Study of the Liver (EASL) the guidelines for MASLD management rely on lifestyle changes related to dietary regimen and physical activity (30). Weight loss achieved through caloric restriction in combination with physical activity is at present the only treatment proven to ameliorate liver damage in MASLD patients without severe liver fibrosis (31). Among the dietary regimens proposed to ameliorate liver damage, ketogenic diets (KDs) are increasingly popular for treating obese patients due to their efficacy in inducing weight loss (10, 11). However, the effectiveness of KDs in MASLD/MASH has been questioned because of their high cholesterol content and the lack of essential nutrients such as choline, two factors well known to promote *per se* steatohepatitis in rodents (14). Our results addressed this question demonstrating that, by tuning nutrient composition, it is possible to devise a KD effective in improving MASH.

Hepatocytes are the main responsible for the generation of ketone bodies and, in physiological conditions, ketogenesis disposes of up to two-thirds of the lipids entering the liver. Prolonged exposure to high-fat diets, as in MASLD, progressively impairs ketogenesis likely because of oxidative stress and mitochondrial dysfunction (32). Our newly formulated KD *per se* effectively stimulated ketogenesis due to the high content of coconut oil-derived medium-chain triglycerides which are efficiently metabolized in mitochondria to produce β-hydroxybutyrate, acetoacetate and acetone (33). On the other hand, the use of vegetal oil as the main calorie source avoids cholesterol overload associated with the use of animal fat.

Ketone bodies, besides serving as energy fuel for different tissues, have been shown to exert a variety of biological functions, including the capacity to act as epigenetic modifiers of histones, thus regulating chromatin architecture and gene transcription (12). In line with ketone bodies capacity of regulating gene expression, we have observed that MASH mice switching to KD modulates multiple metabolic pathways involved in hepatic lipid and glucose metabolism as well as insulin responses. In this regard, switching to KD improves glucose tolerance, increasing GLUT2 and IRS-1 expression. This is obtained despite a modest weight decrease, suggesting that ketone synthesis can remove the excess of acetyl-CoA associated with fatty liver and hyperglycemia (34). Indeed, restoring ketone body production improves overall glycemic control even before achieving weight loss (35). Intriguingly, we have also observed that KD promotes the restoration of normal circulating DPP4, a key enzyme in glucose metabolism (36). This strengthens recent findings suggesting DPP4 as a marker of MASLD and the action of DPP4 inhibitors in hepatic fat reduction (37).

Besides improving fatty liver, we also found that, differently from simple dietary restriction, KD effectively counteracts steatohepatitis by lowering hepatic damage and lobular inflammation. These effects can be ascribed to the anti-inflammatory properties of β-hydroxybutyrate that inhibit NF-kB translocation through IκB-α degradation and triggers G-protein-coupled receptor (GPR)109A, abundantly expressed in many immune cells, including monocytes and macrophages (12). At present, hepatic macrophages are considered the main player in MASH progression to fibrosis/cirrhosis by producing pro-inflammatory mediators perpetuating hepatocyte injury and liver inflammation and by directing extracellular matrix production (6). Recent single-cell RNA sequencing analysis of liver infiltrating macrophages has evidenced the phenotype heterogeneity of these cells in both human and rodent MASH (29). The studies also outline the importance of the so-called TREM2 expressing monocyte-derived macrophages (TREM2^{+}-MoMFs) (29), which localize within regions characterized by inflammation, cell death, and extracellular matrix remodeling (38). Furthermore, these cells form hepatic crown-like structure (hCLS) surrounding dying hepatocytes (29). In our hands, KD-fed mice show a significant lowering in the fraction of liver infiltrating CD11b^{high}F4/80^{int} macrophages displaying TREM2^{+}-MoMF features, which parallels with a reduction in hCLSs. Consistently, cultured macrophage supplementation with β-hydroxybutyrate down-modulates the expression of TREM2 and galectin-3, suggesting a specific action of ketone bodies on MASH-associated MoMFs. These findings contrast with previous data showing that KD supplementation fosters hepatic inflammation by promoting macrophage accumulation (39) and increasing the secretion of pro-inflammatory cytokines (15). However, such a discrepancy can be explained by considering that KDs employed in the studies above

10.3389/fimmu.2025.1518687

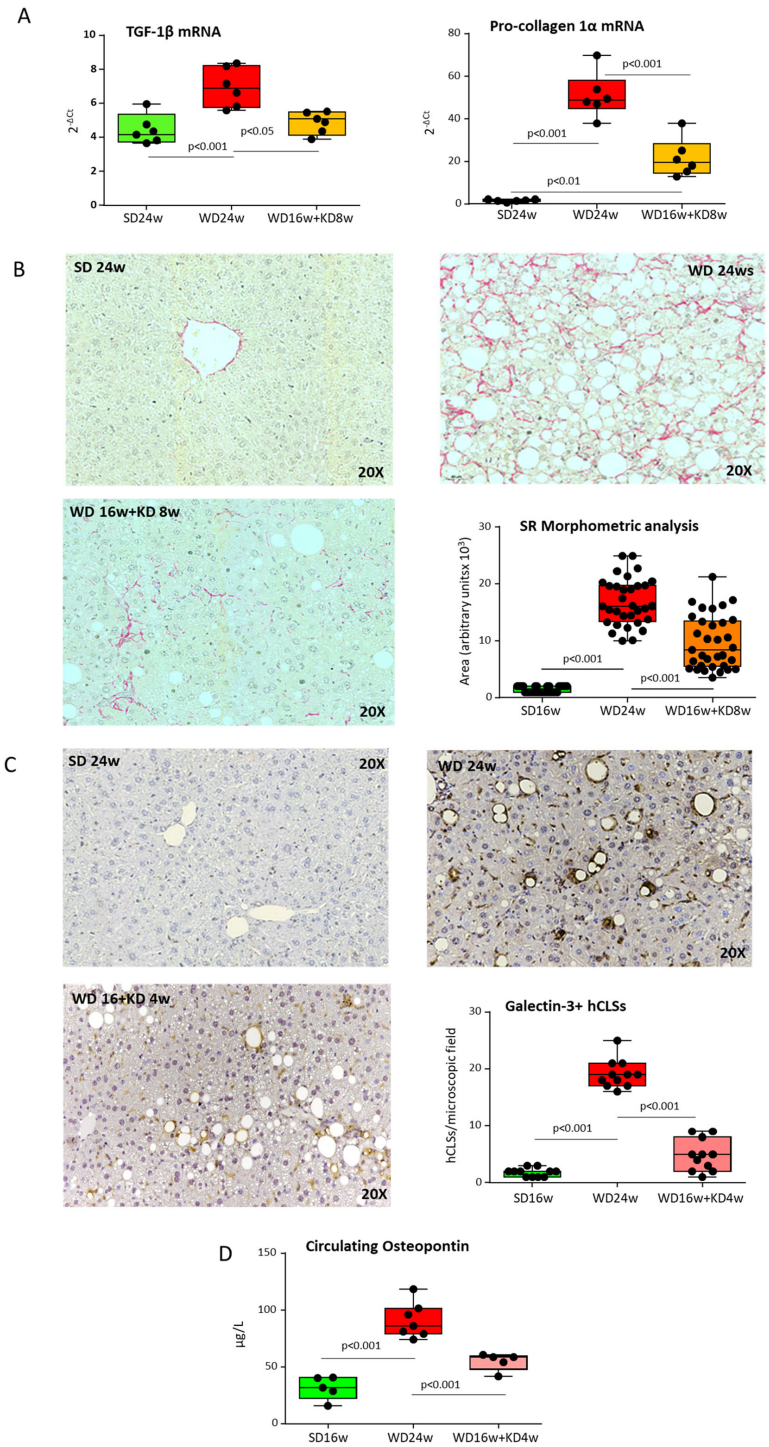

FIGURE 6
Ketogenic diet administration improves MASH-associated fibrosis in mice modulating hepatic crown-like structures (hCLSs) expressing galectin-3 and osteopontin. MASH was induced in 8-weeks old wildtype C57BL/6 mice by 16 weeks feeding with Western diet (WD) before the switching to ketogenic diet (KD) for further 4 (WD16w+KD4w) or 8 weeks (WD16+KD8w). Reference mice received standard diet or WD for 24 weeks (SD24w or WD24w, respectively). **(A)** RT-PCR analysis of the hepatic transcripts for pro-fibrogenic markers TGF-β1 and procollagen-1α. Dots correspond to individual animals and the boxes include the values within the 25th and 75th percentile. The horizontal bars represent the medians, while the extremities of the vertical bars (10th–90th percentile) comprise 80% of the values. **(B)** Effect of 8 weeks feeding with KD on liver fibrosis. The morphological analysis quantification refers to individual readings on liver sections derived from 3-4 animals for each experimental group. **(C)** Effect of 4 weeks feeding with KD on the prevalence hCLSs expressing Galectin-3 (Gal-3) as evidenced by immunohistochemistry with anti-Gal-3 antibodies and **(D)** on circulating levels of osteopontin (OPN). The morphological analysis refers to individual readings on liver sections derived from 3-4 animals for each experimental group.

were rich in cholesterol, which is known to promote hepatic inflammation by stimulating macrophage activation and hCLS formation (40).

Growing evidence suggests that gut dysbiosis represents a common feature in MASLD, supporting disease progression by sustaining hepatic inflammatory responses (41). We have observed that KD reshapes MASH-associated gut microbiota promoting the enrichment of bacterial strains having anti-inflammatory properties such as *Oscillospiraceae*, *Ruminococcaceae*, and *Rikenellaceae* (42). Interestingly, the relative abundance of those bacterial families is decreased in gut microbiota signatures associated with human MASLD, thus supporting their role in maintaining liver health (41). Gut microbiota contributes to the degradation of nutrients, producing bioactive compounds that can modulate host metabolism. Among microbial-derived metabolites SCFAs such as acetate, propionate, and butyrate regulate the immune system and modulate inflammation by influencing activation/differentiation and migration of immune cells, including macrophages (23). Furthermore, nutritional behaviors influence SCFA production along with their metabolic effects. In our hands, KD not only reshapes gut microbiota composition but also significantly modulates SCFA production by raising the serological levels of propionate and acetate. Noteworthy, both these metabolites exhibit anti-inflammatory properties by influencing macrophage functional capacities (43, 44). For instance, acetate inhibits the TLR4 signaling pathway in macrophages through the up-regulation of the tripartite motif-containing protein 40 (TRIM40), reducing their responsiveness to pro-inflammatory stimuli such as damage/pathogen-associated molecular patterns (43). Overall, our results suggest that by modulating gut microbiota, KD can effectively interfere with pro-inflammatory mechanisms involved in promoting steatohepatitis even in the absence of appreciable body weight reduction.

A novel finding concerning the beneficial actions of KD in MASH concerns the improvement of hepatic fibrosis. We have observed that KD supplementation not only ameliorates steatohepatitis, the main factor responsible for stimulating hepatic collagen deposition, but also promotes the regression of already established fibrosis, as evidenced by the early reduction of overall intrahepatic collagen content. Such antifibrotic actions of KD likely involve an effect on TREM-2^{+}-MoMFs, in relation to their capability of producing pro-fibrogenic mediators like OPN and Gal-3 (24). Indeed, both OPN and Gal-3 liver expression are lowered in mice receiving KD in parallel with those of fibrosis markers. The action of KD on the mechanisms supporting hepatic fibrogenesis is consistent with the data by Moore and colleagues (45), showing that dietary supplementation with the ketone ester R, S-1,3-butanediol diacetoacetate (BD-AcAc2) attenuates hepatic stellate cell (HSC) activation and hepatic fibrosis in the context of high-fat diet (HFD)-induced obesity. Conversely, our findings differ from those by Liao et al., who evidence that KD exacerbates carbon tetrachloride (CCl_4)- or thioacetamide (TAA)-induced liver fibrosis (46). Such a discrepancy might represent a specific effect of KD in MASH-related fibrosis and might also depend on the use in Liao's experiments of a cholesterol-rich KD (47), which is known to support hepatic fibrosis along with inflammation (48). Although the beneficial effects of ketosis on hepatic fibrogenesis have been proposed some years ago by Puchalska et al. (12) demonstrating its role in preventing tissue scarring, the present study adds new insights regarding the anti-fibrotic action of ketosis, revealing its capability to also mediate fibrosis regression. KD action on hepatic fibrosis is highly relevant because fibrotic livers are fertile ground for HCC development (5), and the severity of fibrosis is the strongest predictor for disease-specific mortality in MASLD/MASH patients (4). It is now accepted that clinical and experimental liver fibrosis can regress when the causative agent is removed. Such an effect relies on the elimination of myofibroblasts derived from activated HSCs and the progressive degradation of collagen in the fibrous scar (48). The mechanisms leading to fibrosis regression by KD have not been investigated in detail. Puchalska and colleagues (49) have reported that hepatocyte-generated acetoacetate, but not β-hydroxybutyrate, specifically down-modulates fibrogenic responses in liver macrophages *via* mitochondrial metabolism. Nonetheless, we cannot exclude that ketosis might favor macrophage phenotypic conversion to a restorative Ly6C^{low} subset, expressing phagocytosis-associated receptors and secreting matrix metalloproteases which are involved in liver matrix degradation (48). Nonetheless, it is also possible that the changes in the tissue microenvironment due to ketone bodies and microbiota-derived metabolites might modulate innate immune cell memory, which plays an important role in sustaining chronic inflammation and fibrosis (50, 51). In this latter respect, it is plausible that by counteracting the detrimental effects of the maladaptive training of myeloid cells (52), KD-induced modulation of innate immune memory could also positively impact on inflammatory comorbidities often associated with MASH. Further analyses are needed to address these unresolved issues and to gain a more detailed understanding of the mechanisms by which KD administration leads to fibrosis regression.

In conclusion, our findings suggest that the replacement of animal fat with vegetal oil in KD is not harmful in the short term and significantly ameliorates steatohepatitis by restoring essential metabolic functions, counteracting dysbiosis, and reducing the hepatic recruitment of TREM2^{+}-MoMFs. Strikingly, the newly formulated KD also favors the regression of liver fibrosis. Therefore, such a dietary regimen could represent a novel potential therapeutic tool to be exploited for the treatment of MASH-associated fibrosis. Nonetheless, our study suffers from the limitation that the animal model used does not allow to investigate the long-term effects of KD. This is a relevant issue considering that dietary components increased in KDs, particularly cholesterol and saturated fats, are linked to an enhanced risk of chronic kidney diseases, cardiovascular diseases, cancer, diabetes, and Alzheimer's disease (53). Therefore, it would be relevant to verify whether our new KD formulation could help in minimizing these potential risks.

Data availability statement

The datasets presented in this study can be found in online repositories. The names of the repository/repositories and accession number(s) can be found below: PRJNA1175602.

Ethics statement

The animal study was approved by The Italian Ministry of Health. The study was conducted in accordance with the local legislation and institutional requirements.

Author contributions

AP: Data curation, Formal analysis, Investigation, Writing – original draft. NNR: Data curation, Formal analysis, Investigation, Writing – original draft. LLG: Data curation, Formal analysis, Investigation, Writing – original draft. CV: Data curation, Formal analysis, Investigation, Writing – original draft. MarC: Formal analysis, Investigation, Supervision, Writing – original draft. AA: Data curation, Formal analysis, Investigation, Writing – original draft. ST: Data curation, Formal analysis, Investigation, Writing – original draft. AS: Data curation, Formal analysis, Investigation, Writing – original draft. SR: Data curation, Formal analysis, Investigation, Writing – original draft. NF: Conceptualization, Resources, Supervision, Writing – original draft. MM: Methodology, Software, Supervision, Writing – original draft. EB: Formal analysis, Methodology, Software, Writing – original draft. LC: Conceptualization, Data curation, Resources, Writing – original draft. IF: Conceptualization, Data curation, Investigation, Methodology, Supervision, Writing – original draft. ML: Formal analysis, Investigation, Methodology, Writing – original draft. MasC: Conceptualization, Resources, Supervision, Writing – original draft. FT: Conceptualization, Supervision, Writing – review & editing. EA: Conceptualization, Data curation, Formal analysis, Supervision, Writing – original draft, Writing – review & editing. FP: Conceptualization, Funding acquisition, Supervision, Writing – original draft, Writing – review & editing. SS: Conceptualization, Data curation, Formal analysis, Funding acquisition, Investigation, Supervision, Writing – original draft, Writing – review & editing.

Funding

The author(s) declare that financial support was received for the research and/or publication of this article. This work was supported by the University of Piemonte Orientale (grant FAR 2019), FOHN Project – Departments of Excellence 2018-2022– Department of Health Sciences – University of Piemonte Orientale, PRIN grant (2020NCKXBR_004; SIDERALE Project), NODES project M4C2 1.5 of PNRR (grant agreement no. ECS00000036) from the MUR, Cariplo Foundation (prot. 2021–4652) and the Department of Health Sciences (DiSS) of the Università del Piemonte Orientale through the APC initiative.

Acknowledgments

The authors would like to thank Dr Antonio Colasanto for his excellent technical support for the characterization of diet composition; Dr Michela Salvo for histological sample preparation; Dr Valeria Caneparo for High Throughput immunoassays; and Dr Emanuela Agosti for participating in the initial steps of the experimental work.

Conflict of interest

The authors declare that the research was conducted in the absence of any commercial or financial relationships that could be construed as a potential conflict of interest.

The author(s) declared that they were an editorial board member of Frontiers, at the time of submission. This had no impact on the peer review process and the final decision.

Generative AI statement

The author(s) declare that no Generative AI was used in the creation of this manuscript.

Publisher's note

Supplementary material

The Supplementary Material for this article can be found online at: https://www.frontiersin.org/articles/10.3389/fimmu.2025.1518687/full#supplementary-material

References

1. Rinella ME, Lazarus JV, Ratziu V, Francque SM, Sanyal AJ, Kanwal F, et al. A multisociety Delphi consensus statement on new fatty liver disease nomenclature. *J Hepatol*. (2023) 79:1542–56. doi: 10.1016/j.jhep.2023.06.003

2. Younossi ZM, Golabi P, Paik JM, Henry A, Van Dongen C, Henry L. The global epidemiology of nonalcoholic fatty liver disease (NAFLD) and nonalcoholic steatohepatitis (NASH): a systematic review. *Hepatology*. (2023) 77:1335–47. doi: 10.1097/HEP.0000000000000004

3. Nobili V, Svegliati-Baroni G, Alisi A, Miele L, Valenti L, Vajro P. A360-degree overview of pediatric NAFLD: recent insights. *J Hepatol*. (2013) 58:1218–29. doi: 10.1016/j.jhep.2012.12.003

4. Powell EE, Wong VW, Rinella M. Non-alcoholic fatty liver disease. *Lancet*. (2021) 397:2212–24. doi: 10.1016/S0140-6736(20)32511-3

5. Huang DQ, El-Serag HB, Loomba R. Global epidemiology of NAFLD-related HCC: trends, predictions, risk factors and prevention. *Nat Rev Gastroenterol Hepatol*. (2021) 18:223–38. doi: 10.1038/s41575-020-00381-6

6. Subramanian P, Chavakis T. The complex function of macrophages and their subpopulations in metabolic injury associated fatty liver disease. *J Physiol*. (2023) 601:1159–71. doi: 10.1113/JP283820

7. Ramadori P, Kam S, Heikenwalder M. T cells: Friends and foes in NASH pathogenesis and hepatocarcinogenesis. *Hepatology*. (2022) 75:1038–49. doi: 10.1002/hep.32336

8. Promrat K, Kleiner DE, Niemeier HM, Jackvony E, Kearns M, Wands JR, et al. Randomized controlled trial testing the effects of weight loss on nonalcoholic steatohepatitis. *Hepatol (Baltimore Md)*. (2010) 51:121–9. doi: 10.1002/hep.23276

9. Romero-Gómez M, Zelber-Sagi S, Trenell M. Treatment of NAFLD with diet, physical activity and exercise. *J Hepatol*. (2017) 67:829–46. doi: 10.1016/j.jhep.2017.05.016

10. Caprio M, Infante M, Moriconi E, Armani A, Fabbri A, Mantovani G, et al. Very-low-calorie ketogenic diet (VLCKD) in the management of metabolic diseases: systematic review and consensus statement from the Italian Society of Endocrinology (SIE). *J Endocrinol Invest*. (2019) 42:1365–86. doi: 10.1007/s40618-019-01061-2

11. Muscogiuri G, El Ghoch M, Colao A, Hassapidou M, Yumuk V, Busetto L, et al. European guidelines for obesity management in adults with a very low-calorie ketogenic diet: A systematic review and meta-analysis. *Obes Facts*. (2021) 14:222–45. doi: 10.1159/000515381

12. Puchalska P, Crawford PA. Multi-dimensional roles of ketone bodies in fuel metabolism, signaling, and therapeutics. *Cell Metab*. (2017) 25:262–84. doi: 10.1016/j.cmet.2016.12.022

13. Watanabe M, Tozzi R, Risi R, Tuccinardi D, Mariani S, Basciani S, et al. Beneficial effects of the ketogenic diet on nonalcoholic fatty liver disease: A comprehensive review of the literature. *Obes Rev*. (2020) 21:e13024. doi: 10.1111/obr.13024

14. Garbow JR, Doherty JM, Schugar RC, Travers S, Weber ML, Wentz AE, et al. Hepatic steatosis, inflammation, and ER stress in mice maintained long term on a very low-carbohydrate ketogenic diet. *Am J Physiol Gastrointest Liver Physiol*. (2011) 300:G956–67. doi: 10.1152/ajpgi.00539.2010

15. Long F, Bhatti MR, Kellenberger A, Sun W, Modica S, Höring M, et al. Low-carbohydrate diet induces hepatic insulin resistance and metabolic associated fatty liver disease in mice. *Mol Metab*. (2023) 69:101675. doi: 10.1016/j.molmet.2023.101675

16. Ang QY, Alexander M, Newman JC, Tian Y, Cai J, Upadhyay V, et al. Ketogenic diets alter the gut microbiome resulting in decreased intestinal Th17 cells. *Cell*. (2020) 181:1263–75. doi: 10.1016/j.cell.2020.04.027

17. Sutti S, Jindal A, Locatelli I, Vacchiano M, Gigliotti L, Bozzola C, et al. Adaptive immune responses triggered by oxidative stress contribute to hepatic inflammation in NASH. *Hepatol*. (2014) 59:886–97. doi: 10.1002/hep.26749

18. Wiede F, Tiganis T. Isolation and characterization of mouse intrahepatic lymphocytes by flow cytometry. *Methods Mol Biol*. (2018) 1725:301–11. doi: 10.1007/978-1-4939-7568-6_23

19. Klindworth A, Pruesse E, Schweer T, Peplies J, Quast C, Horn M, et al. Evaluation of general 16S ribosomal RNA gene PCR primers for classical and next-generation sequencing-based diversity studies. *Nucleic Acids Res*. (2013) 41:e1. doi: 10.1093/nar/gks808

20. Callahan BJ, McMurdie PJ, Rosen MJ, Han AW, Johnson AJ, Holmes SP. DADA2: High-resolution sample inference from Illumina amplicon data. *Nat Methods*. (2016) 13:581–3. doi: 10.1038/nmeth.3869

21. Shearer AM, Wang Y, Fletcher EK, Rana R, Michael ES, Nguyen N, et al. PAR2 promotes impaired glucose uptake and insulin resistance in NAFLD through GLUT2 and Akt interference. *Hepatology*. (2022) 76:1778–93. doi: 10.1002/hep.32589

22. Trzaskalski NA, Fadzeyeva E, Mulvihill EE. Dipeptidyl Peptidase-4 at the interface between inflammation and metabolism. *Clin Med Insights Endocrinol Diabetes*. (2020) 13:1179551420912972. doi: 10.1177/1179551420912972

23. Vallianou N, Christodoulatos GS, Karampela I, Tsilingiris D, Magkos F, Stratigou T, et al. Understanding the role of the gut microbiome and microbial metabolites in non-alcoholic fatty liver disease: Current Evidence and Perspectives. *Biomolecules*. (2021) 12:56. doi: 10.3390/biom12010056

24. Brandl K, Schnabl B. Intestinal microbiota and nonalcoholic steatohepatitis. *Curr Opin Gastroenterol*. (2017) 33:128–33. doi: 10.1097/MOG.0000000000000349

25. Abenavoli L, Giubilei L, Procopio AC, Spagnuolo R, Luzza F, Boccuto L, et al. Gut microbiota in non-alcoholic fatty liver disease patients with inflammatory bowel diseases: A complex interplay. *Nutrients*. (2022) 14:5323. doi: 10.3390/nu14245323

26. Zhou Y, Zhang F, Mao L, Feng T, Wang K, Xu M, et al. Bifico relieves irritable bowel syndrome by regulating gut microbiota dysbiosis and inflammatory cytokines. *Eur J Nutr*. (2023) 62:139–55. doi: 10.1007/s00394-022-02958-0

27. Silva YP, Bernardi A, Frozza RL. The role of short-chain fatty acids from gut microbiota in gut-brain communication. *Front Endocrinol (Lausanne)*. (2020) 11:25. doi: 10.3389/fendo.2020.00025

28. Mackinnon AC, Tonev D, Jacoby B, Pinzani M, Slack RJ. Galectin-3: therapeutic targeting in liver disease. *Expert Opin Ther Targets*. (2023) 27:779–91. doi: 10.1080/14728222.2023.2258280

29. Peiseler M, Schwabe R, Hampe J, Kubes P, Heikenwälder M, Tacke F. Immune mechanisms linking metabolic injury to inflammation and fibrosis in fatty liver disease - novel insights into cellular communication circuits. *J Hepatol*. (2022) 77:1136–60. doi: 10.1016/j.jhep.2022.06.012

30. Pugliese N, Plaz Torres MC, Petta S, Valenti L, Giannini EG, Aghemo A. Is there an 'ideal' diet for patients with NAFLD? *Eur J Clin Invest*. (2022) 52:e13659. doi: 10.1111/eci.13659

31. Raza S, Rajak S, Upadhyay A, Tewari A, Anthony Sinha R. Current treatment paradigms and emerging therapies for NAFLD/NASH. *Front Biosci*. (2021) 26:206–37. doi: 10.2741/4892

32. Mooli RGR, Ramakrishnan SK. Emerging role of hepatic ketogenesis in fatty liver disease. *Front Physiol*. (2022) 13:946474. doi: 10.3389/fphys.2022.946474

33. Chatterjee P, Fernando M, Fernando B, Dias CB, Shah T, Silva R, et al. Potential of coconut oil and medium chain triglycerides in the prevention and treatment of Alzheimer's disease. *Mech Ageing Dev*. (2020) 186:111209. doi: 10.1016/j.mad.2020.111209

34. Fletcher JA, Deja S, Satapati S, Fu X, Burgess SC, Browning JD. Impaired ketogenesis and increased acetyl-CoA oxidation promote hyperglycemia in human fatty liver. *JCI Insight*. (2019) 5:e127737. doi: 10.1172/jci.insight.127737

35. Paoli A, Bianco A, Moro T, Mota JF, Coelho-Ravagnani CF. The effects of ketogenic diet on insulin sensitivity and weight loss, which came first: the chicken or the egg? *Nutrients*. (2023) 15:3120. doi: 10.3390/nu15143120

36. Ahrén B. Glucose-lowering action through targeting islet dysfunction in type 2 diabetes: Focus on dipeptidyl peptidase-4 inhibition. *J Diabetes Investig*. (2021) 12:1128–35. doi: 10.1111/jdi.13564

37. Carbone LJ, Angus PW, Yeomans ND. Incretin-based therapies for the treatment of non-alcoholic fatty liver disease: A systematic review and meta-analysis. *J Gastroenterol Hepatol*. (2016) 31:23–31. doi: 10.1111/jgh.13026

38. Hendrikx T, Porsch F, Kiss MG, Rajcic D, Papac-Miličević N, Hoebinger C, et al. Soluble TREM2 levels reflect the recruitment and expansion of TREM2+ macrophages that localize to fibrotic areas and limit NASH. *J Hepatol*. (2022) 77:1373–85. doi: 10.1016/j.jhep.2022.06.004

39. Asrih M, Altirriba J, Rohner-Jeanrenaud F, Jornayvaz FR. Ketogenic diet impairs FGF21 signaling and promotes differential inflammatory responses in the liver and white adipose tissue. *PloS One*. (2015) 10:e0126364. doi: 10.1371/journal.pone.0126364

40. Ioannou GN. The role of cholesterol in the pathogenesis of NASH. *Trends Endocrinol Metab*. (2016) 27:84–95. doi: 10.1016/j.tem.2015.11.008

41. Lee G, You HJ, Bajaj JS, Joo SK, Yu J, Park S, et al. Distinct signatures of gut microbiome and metabolites associated with significant fibrosis in non-obese NAFLD. *Nat Commun*. (2020) 11:4982. doi: 10.1038/s41467-020-18754-5

42. Tavella T, Rampelli S, Guidarelli G, Bazzocchi A, Gasperini C, Pujos-Guillot E, et al. Elevated gut microbiome abundance of Christensenellaceae, Porphyromonadaceae and Rikenellaceae is associated with reduced visceral adipose tissue and healthier metabolic profile in Italian elderly. *Gut Microbes*. (2021) 13:1–19. doi: 10.1080/19490976.2021.1880221

43. Al-Lahham S, Roelofsen H, Rezaee F, Weening D, Hoek A, Vonk R, et al. Propionic acid affects immune status and metabolism in adipose tissue from overweight subjects. *Eur J Clin Invest*. (2012) 42:357–64. doi: 10.1111/j.1365-2362.2011.02590.x

44. Yang H, Meng L, Ai D, Hou N, Li H, Shuai X, et al. Acetic acid alleviates the inflammatory response and liver injury in septic mice by increasing the expression of TRIM40. *Exp Ther Med*. (2019) 17:2789–98. doi: 10.3892/etm.2019.7274

45. Moore MP, Cunningham RP, Davis RAH, Deemer SE, Roberts BM, Plaisance EP, et al. A dietary ketone ester mitigates histological outcomes of NAFLD and markers of fibrosis in high-fat diet fed mice. *Am J Physiol Gastrointest Liver Physiol*. (2021) 320:G564–72. doi: 10.1152/ajpgi.00259.2020

46. Liao YJ, Wang YH, Wu CY, Hsu FY, Chien CY, Lee YC. Ketogenic diet enhances the cholesterol accumulation in liver and augments the severity of CCl4

and TAA-induced liver fibrosis in mice. *Int J Mol Sci*. (2021) 22:2934. doi: 10.3390/ijms22062934

47. Teratani T, Tomita K, Suzuki T, Oshikawa T, Yokoyama H, Shimamura K, et al. A high-cholesterol diet exacerbates liver fibrosis in mice via accumulation of free cholesterol in hepatic stellate cells. *Gastroenterol*. (2012) 142:152–164.e10. doi: 10.1053/j.gastro.2011.09.049

48. Kisseleva T, Brenner D. Molecular and cellular mechanisms of liver fibrosis and its regression. *Nat Rev Gastroenterol Hepatol*. (2021) 18:151–66. doi: 10.1038/s41575-020-00372-7

49. Puchalska P, Martin SE, Huang X, Lengfeld JE, Daniel B, Graham MJ, et al. Hepatocyte-macrophage acetoacetate shuttle protects against tissue fibrosis. *Cell Metab*. (2019) 29:383–398.e387. doi: 10.1016/j.cmet.2018.10.015

50. Vuscan P, Kischkel B, Joosten LAB, Netea MG. Trained immunity: General and emerging concepts. *Immunol Rev*. (2024) 323:164–85. doi: 10.1111/imr.13326

51. Mitroulis I, Ruppova K, Wang B, Chen LS, Grzybek M, Grinenko T, et al. Modulation of myelopoiesis progenitors is an integral component of trained immunity. *Cell*. (2018) 172:147–161.e12. doi: 10.1016/j.cell.2017.11.034

52. Li X, Wang H, Yu X, Saha G, Kalafati L, Ioannidis C, et al. Maladaptive innate immune training of myelopoiesis links inflammatory comorbidities. *Cell*. (2022) 185:1709–27. doi: 10.1016/j.cell.2022.03.043

53. Crosby L, Davis B, Joshi S, Jardine M, Paul J, Neola M, et al. Ketogenic diets and chronic disease: weighing the benefits against the risks. *Front Nutr*. (2021) 8:702802. doi: 10.3389/fnut.2021.702802

6. Ketogenic diet besides contributing to a rapid weight loss, it leads to a concomitant muscle wasting.

Ketogenic diet proved to ameliorate MASH metabolic derangements and steatohepatitis after a period of Western diet, suggesting its positive role in ameliorating systemic homeostasis. Moreover, given the increasing evidence supporting the effectiveness of KDs in reducing inflammation, oxidative stress, and improving mitochondrial function, we hypothesized that KDs could hold promise in addressing obesity-related conditions. However, its impact on skeletal muscle homeostasis has not yet been deciphered. Thus, we hypothesized that KD-dependent improvement in liver could be reflected also in skeletal muscle homeostasis, with beneficial effect on muscle mass and force. To this aim, we investigate *in vivo* whether a switch to an *ad libitum* KD after 16 weeks of WD could mitigate or revert detrimental effects WD-induced in muscle. Although liver results are related to the endpoint (16 week of WD + 8 weeks of KD), in the present project, we focus on the firsts timepoints (16 week of WD + 2 or 4 weeks of KD) since we appreciated that KD strikingly decreased not only body weight, but also muscle weight, without altering mice strength. Furthermore, muscle loss was confirmed by a higher expression of genes associated with atrophy and augmented branched chain amino acids (BCAAs) degradation. We then conducted experiments to further investigate the impact of fatty acids and ketone bodies (KBs), respectively upon palmitate (PA) and butyrate (BU) treatments, using the *in vitro* model of C2C12-derived myotubes. Both PA and BU demonstrated to reduce myotube diameters, in association with a diminished mitochondrial membrane potential and an increased ROS production. Finally, we further investigate if different doses of BU could be able to mitigate or revert atrophy. Indeed, our data suggest that the metabolic shift KB-induced is dose-dependent and the finding of the right dose may offer beneficial effects in skeletal muscle homeostasis.

6.1. Introduction

Obesity is a complex, multifactorial condition characterized by excessive fat accumulation in the adipose and other ectopic tissues, such as liver and muscle. It arises primarily from a chronic energy imbalance where caloric intake persistently exceeds energy expenditure 1,2. However, obesity is not merely a consequence of overeating. It is deeply influenced by environmental, genetic, and socio-economic factors.

In recent decades, the global prevalence of obesity has progressively increased, closely mirroring the widespread adoption of the so-called Western diet (WD), a dietary pattern characterized by high intake of saturated fats, refined sugars, and ultra-processed foods, and low consumption of fibers, fruits, and vegetables. This dietary shift, coupled with increasingly sedentary lifestyles and reduced physical activity, has contributed to a dramatic global rise in obesity-related disorders, including type 2 diabetes (T2D), metabolic dysfunction-associated steatotic liver disease (MASLD), cardiovascular diseases (CVDs), Alzheimer's disease, and several types of cancers 3–6.

Among these complications associated to WD consumption, sarcopenic obesity (SO) is increasingly recognized as a clinically significant phenotype within the spectrum of obesity-related disorders. SO is defined by the coexistence of excess adiposity and sarcopenia, the latter referring to the progressive and generalized loss of skeletal muscle mass and functionality 16–18.

The etiology of SO is multifactorial, involving hormonal imbalances (e.g., reduced anabolic hormones such as testosterone and growth hormone), chronic low-grade inflammation, mitochondrial dysfunction, and impaired nutrient signaling 7. Furthermore, ectopic fat accumulation within muscle (i.e., myosteatosis) directly impair muscle contractility and regenerative capacity 19. These pathophysiological changes significantly elevate the risk of mobility impairment, cardiometabolic disease, and mortality 16,17. Given its growing prevalence and clinical

impact, SO is increasingly recognized as a distinct metabolic phenotype requiring targeted therapeutic strategies that address both muscle loss and excess fat accumulation.

Emerging evidence highlights the importance of dietary composition in modulating skeletal muscle homeostasis, and dietary interventions are being explored as non-pharmacological strategies to counteract SO 12,6,20. Among these, the ketogenic diet (KD), a high-fat, adequate protein, low-carbohydrate regimen, has gained attention for its potential to promote weight loss and improve metabolic health 21–23. Indeed, KD alters the energy metabolism by drastically reducing carbohydrate intake, thereby compelling the organism to utilize free fatty acids (FFAs) as the primary energy substrate. This carbohydrate restriction limits glucose consumption, promoting enhanced mitochondrial β-oxidation of FFAs in the liver. As a consequence, acetyl-CoA accumulates and drives hepatic ketogenesis, leading to the production and systemic release of ketone bodies (KBs) such as β-hydroxybutyrate and acetoacetate. These ketone bodies serve as efficient alternative energy source for extrahepatic tissues, including skeletal muscle, brain, and heart, particularly under conditions of low glucose availability. The metabolic reprogramming induced by KD not only supports energy homeostasis, but also influences cellular signaling pathways related to inflammation, oxidative stress, and protein turnover. Indeed, beyond its metabolic effects, KD has been reported to reduce inflammation and oxidative stress through mechanisms involving NFκB inhibition, modulation of the PI3K/Akt/mTOR pathway, and upregulation of anti-inflammatory cytokines like IL-1013–15. Given these metabolic adaptations and their potential to attenuate muscle catabolism and systemic inflammation, the ketogenic diet could represent a promising non-pharmacological strategy to counteract SO. However, the specific impact of KD on skeletal muscle mass and function, particularly in the context of prior WD-induced metabolic dysfunction, remains poorly defined.

To address this, we investigated the effects of a KD intervention following prolonged WD exposure in mice, with a focus on skeletal muscle. Our findings revealed that while KD reduced overall body weight, it also led to reductions in muscle mass and fiber size, without compromising muscle strength. Molecular analyses indicated upregulation of atrophy-related genes and enhanced branched-chain amino acid (BCAA) catabolism. To further dissect the underlying mechanisms, we employed C2C12-derived myotubes cotreated with palmitate (PA), a dominant fatty acid in WD, and butyrate (BU), a representative ketone body in KD. Both compounds at high concentrations induced myotube atrophy, accompanied by mitochondrial dysfunction and increased ROS production. Interestingly, low-dose BU mitigated PA-induced muscle atrophy, suggesting a dose-dependent, protective role of ketone bodies. Targeted modulation of ketone body levels may therefore represent a promising nutritional approach to mitigate sarcopenic obesity.

6.2. Unpublished results

Ketogenic diet is not efficient in influencing muscle performances

To determine if KD has a protective role in counteracting the effects induced by a high fat/carbohydrate diet, steatohepatitis was induced by feeding eight-week-old male mice for 16 weeks with Western Diet (WD) enriched with 1.25% cholesterol. Control animals received a standard chow diet. After MASH induction, mice were randomly divided into two groups, one switching to choline-sufficient KD (6.7 Kcal/g) containing 0.3% as carbohydrates, 9.2% as proteins, and 90.5% as hydrogenated coconut oil and the other continuing with the same WD diet for a further eight weeks. However, despite in Provera et al. analyses were performed at a later endpoint (after 24 weeks), we took in consideration the first four weeks after the switching since mice demonstrated a very fast loss of mass in the previous experiment [79].

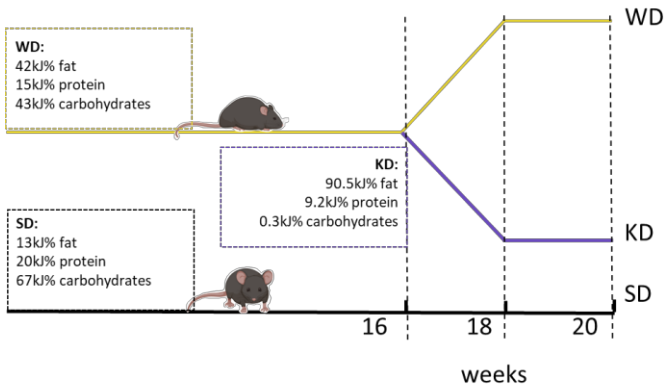

Representative scheme of the experimental plan of the study

Indeed, KD was effective in reducing body weight significantly compared both to SD and WD groups (Fig. 1 A, B). KD beyond lowering liver weight (data not shown), it decreased fat weights, both subcutaneous fat (sFAT), where only a tendency was appreciated (Fig. 1 C), and epidydimal fat (eFAT), in which the KD effect was significative (Fig. 1 D).

Strikingly, in parallel with fat¸ KD compared to SD and WD resulted in decreasing also muscle hindleg weights, including gastrocnemius (GA), tibialis anterior (TA) and quadriceps (QUAD) muscles (Fig. 1 E-F).

Interestingly, each of them showed the same tendency, although at 16 weeks WD mice muscles weighted more, in the successive four weeks weights were similar between WD and SD, while KD after WD promoted muscle wasting, displaying a significant loss of lean mass compared to SD.

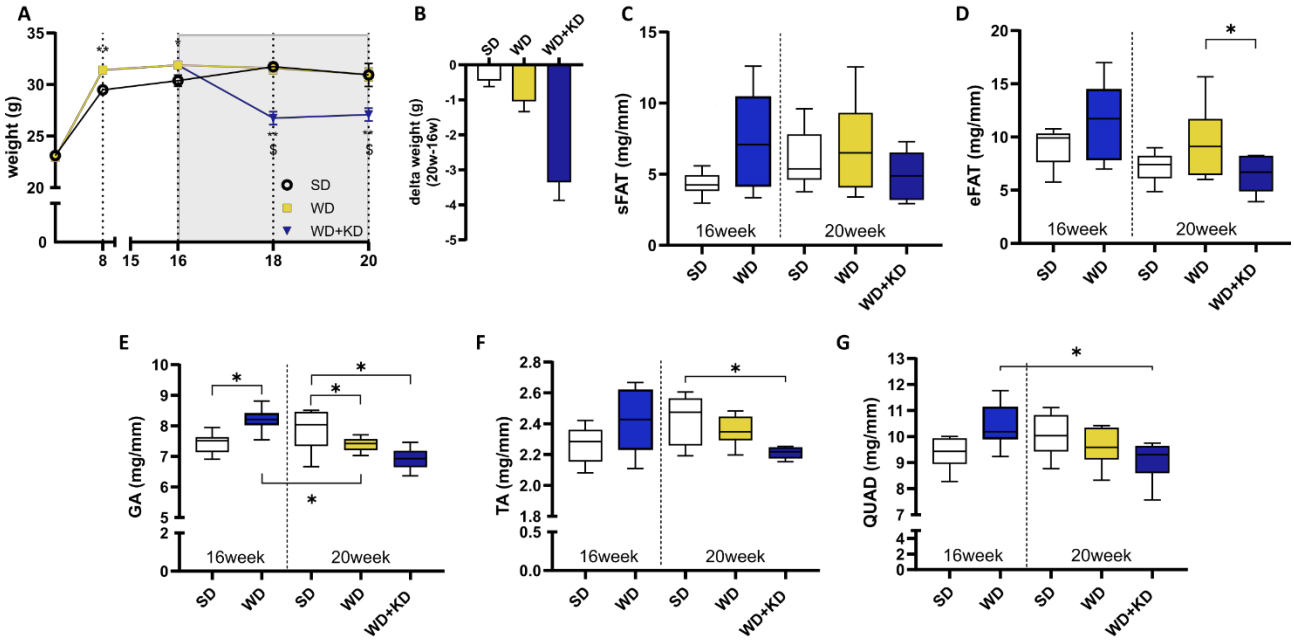

Figure 1: KD-dependent reduction of body, fat, and muscle weights. (**A, B**) Mice were weighted at each timepoint and their weight resulted significant lower upon KD feeding, differences are well appreciated in delta weight graph. (**C, D**) Fat weights display a reduction in epidydimal fat after four weeks of KD. (**E-G**) KD promoted muscle mass loss in gastrocnemius (GA), tibialis anterior (TA), and quadriceps (QUAD) muscles. All the measurements were recorded at 16 and 20 weeks timepoints. Data are presented as means ± SEM. *P < 0.05, **P < 0.01, $ P < 0.05.

However, despite KD was effective in reducing muscle weight, muscle strength was assessed by two different functional tests and differences within the three groups were not appreciated (Fig. 2).

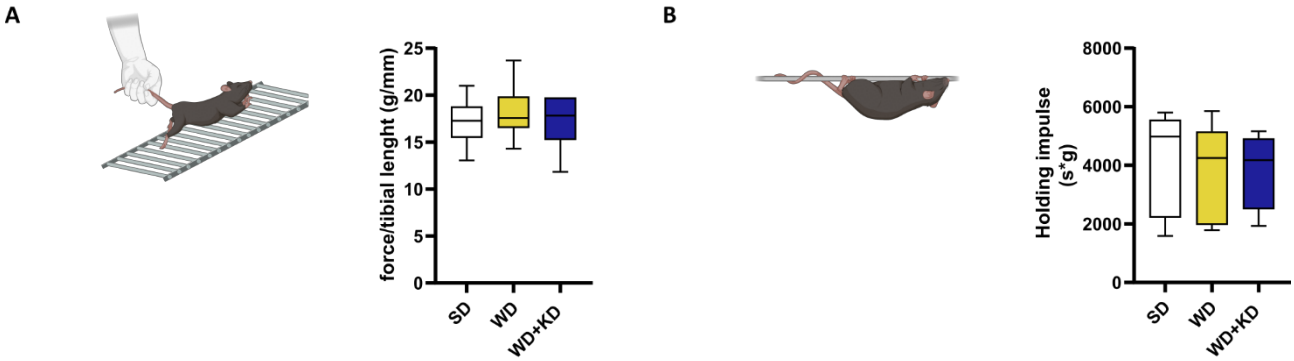

Figure 2: Muscle performances were not influenced by the diets. Representative cartoons and graphs relative of the two different functional tests, grasping test (**A**) and hanging wire test (**B**).

Indeed, we analysed the gastrocnemius myofiber cross-sectional area (CSA) and similarly to the muscle weights even the size distribution followed the same trend: despite before the switch WD CSA distribution shifted toward bigger area compared to SD one, in the successive four weeks their myofiber size displayed comparable values, coherently with the measures of GA weights (Fig. 3 A-F). On the other hand, KD feeding exerted an atrophic effect, thus shifting KD CSA distribution toward smaller area, as represented in Figure 3 E. The highest frequency of KD myofibers size was around 1200 μm^2 and therefore with lower proportion of bigger fibers compared to the other dietary regimens. The mean myofiber size quantification supported the CSA distribution (Fig. 3 F).

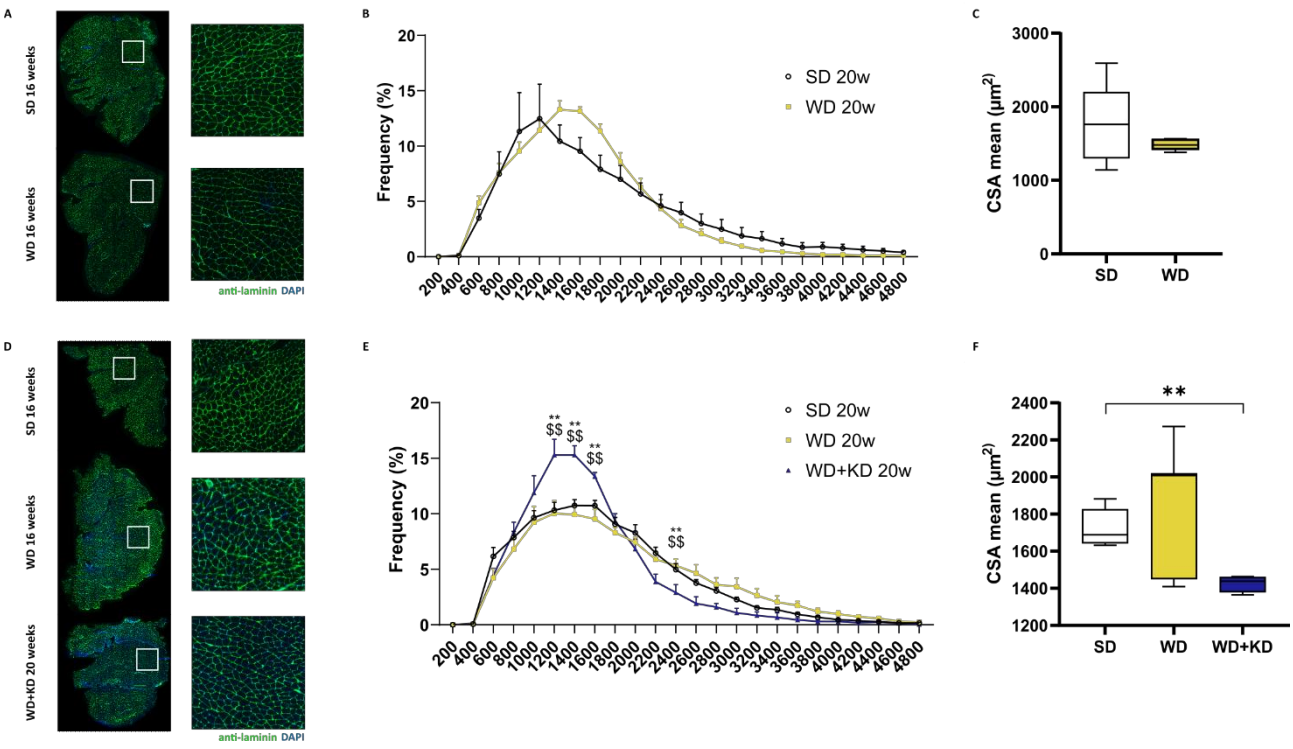

Figure 3: KD reduced cross-sectional area in gastrocnemius muscles. (**A, B**) Frequency distribution of cross-sectional area at 16 and 20 week timepoints. (**C, D**) Representative images of the anti-laminin immunofluorescence, with the relative magnification (**E**) Mean of the myofiber cross-sectional area among the different conditions at 16 and 20 week timepoint. Data are presented as means ± SEM. *P < 0.05, **P < 0.01 vs SD, $ P < 0.05, $$ P < 0.01 vs WD.

To gain insight on the molecular mechanisms that could be related with the CSA shift to smaller fibers, we analysed the expression of the genes responsible of inducing atrophy. Indeed, we evaluated Atrogin-1 (Fbxo32/MAFbx) and MuRF1 (Trim63), which encode muscle-specific ubiquitin ligases and are representative of UPS activation, one of the main mechanisms involved in muscle wasting. In agreement with weights and CSA, atrogenes were not affected before the switching to KD (Fig. 4 A), but then, MuRF1 was upregulated within KD muscles at 20 weeks (Fig. 4 B). These data suggest that atrogenes are mediated by KD, and thus UPS system is activated and responsible in triggering muscle wasting. On the contrary, no distinction between SD and WD alludes that WD in our experiment has not to be considered a good model effective in inducing sarcopenic obesity. Furthermore, also the dysregulation of the autophagy-lysosome system, which is fundamental in protein turnover, could be involved in muscle wasting. We investigated some of the main markers which are responsible in activating autophagy-lysosome system (CathepsinL (Ctsl) and Gabarap), and more in deep Bnip3, mitochondrial fission factor (Mff), and OPA1, fundamental requirements for mitophagy, fission, and fusion to occur [52,53]. The formers resulted downregulated in WD+KD mice, particularly Ctsl (Fig. 4 D). In addition, also Bnip3 appeared reduced coherently with a simultaneous lowering in the Mff gene expression, although they did not reach the significance (Fig. 4 D, E). Indeed, an impairment of the autophagic system, failing turnover of proteins, may take part in inducing muscle atrophy after KD.

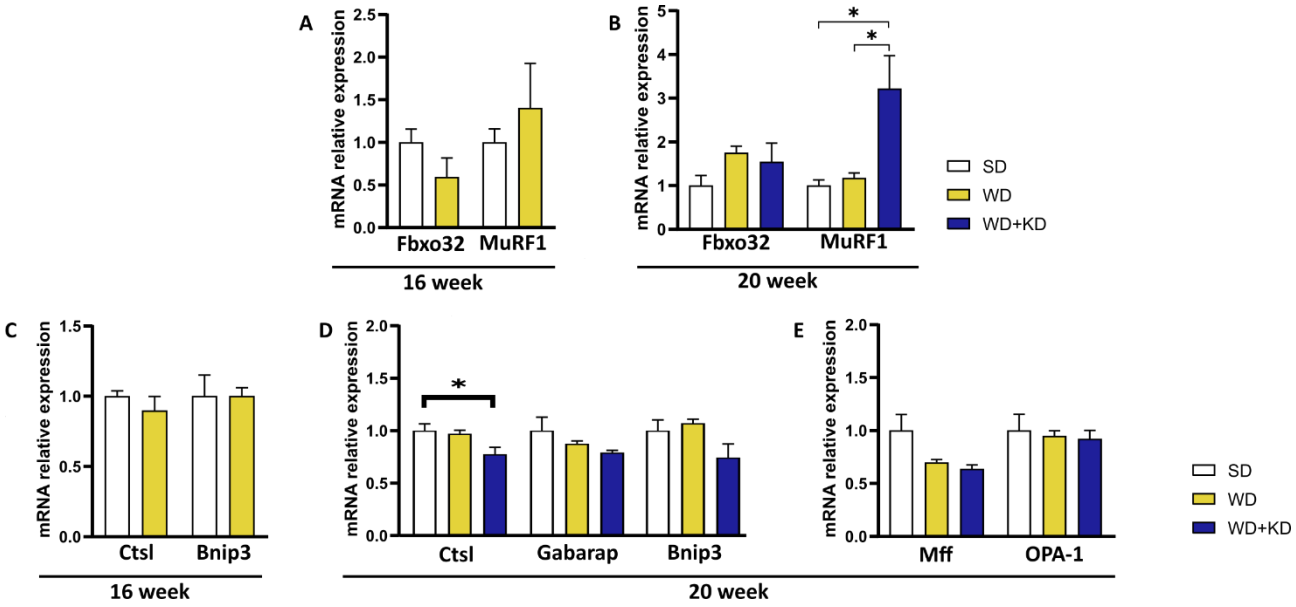

Figure 4: KD induced atrogenes expression, while downregulated genes related with autophagic flux. (**A, B**) The expression of atrogenes Fbxo32 (Atrogin-1) and Trim63 (MuRF1) was assessed by real-time RT-PCR, using Ppif as housekeeping gene. (**C, D**) The expression of the autophagic (Ctsl, Gabarap) and mitophagic genes (Bnip3) and (**E**) of the fission gene (Mff), and of the fusion gene (OPA-1) was assessed by real-time RT-PCR in GA, using Ppif as housekeeping gene. *P <0.05.

Moreover, since atrophy occurs when protein degradation overcomes protein synthesis, we detected the concentration of the branched-chain amino acids (BCAAs), known to be fundamental in protein synthesis, gluconeogenesis, ketone bodies production, and account for average 30-40% of the essential amino acids in muscle proteins [106,107]. Given that, through metabolomic analysis, leucine (Leu), isoleucine (Ile) and valine (Val) levels in TA muscles were analysed, revealing a drastic reduction in the concentration only within the tissues proper of the KD group (Fig. 5 A-C). Studies demonstrated that upon stimuli, including glucocorticoids and fasting, protein breakdown is promoted in skeletal muscle resulting in muscle wasting [51,72]. Several sources highlight the role of KLF15 (Krüppel-like factor 15), a zinc-finger transcription factor, to be determinant in inducing not only protein degradation, but also atrogenes expression and autophagy-lysosome system deregulation [104,107–109].

Moreover, when catabolism is activated, it binds to the promoter region of the mitochondrial enzyme branched-chain aminotransferase 2 (BCAT2), boosting BCAAs catabolism, specifically the reversible transamination of leucine, isoleucine, and valine [107]. Indeed, we investigated Klf15 and BCAT2 expression through qPCR, and curiously we did not appreciate any variation in the KLF15 and Bcat2 mRNA expression at 20 weeks (Fig. 5 D, E). We then deciphered myofiber metabolism through myosin heavy chain isoform immunofluorescence, in which oxidative and glycolytic fibers were quantified to unravel whether diet could influence their proportion. However, coherently with the previous data, any variation in their ratio was assessed at the latest timepoint (Fig. 5 F, G).

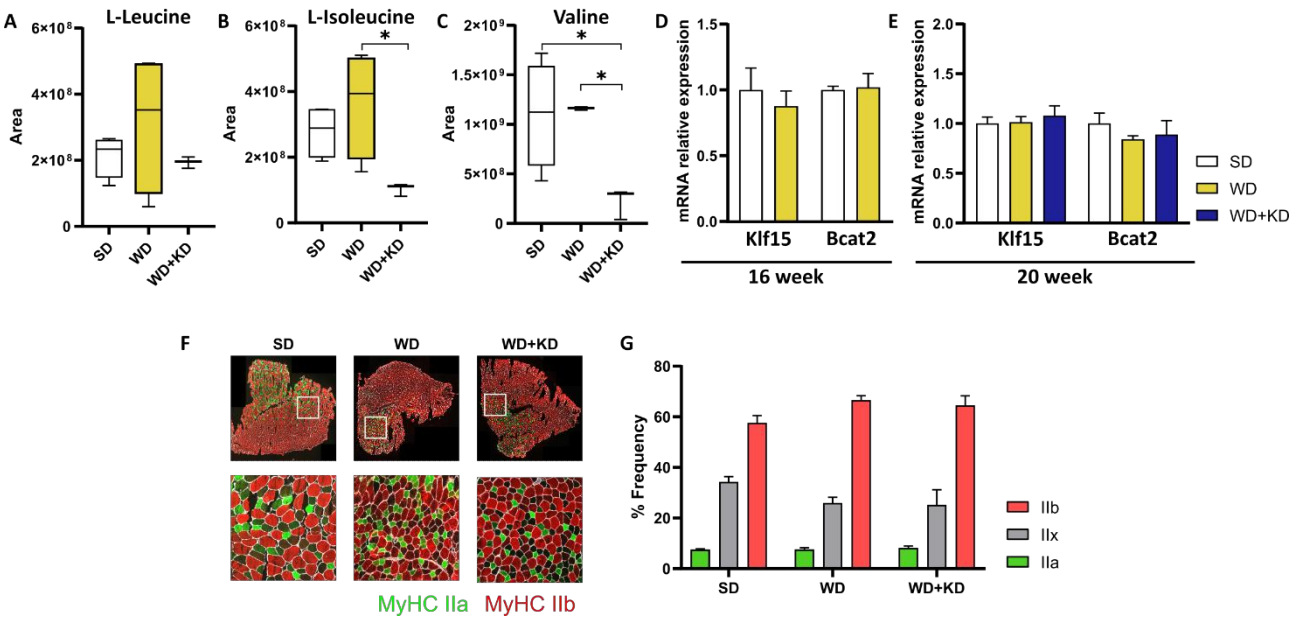

Figure 5: KD induce augmented protein breakdown with the consequent lower BCAAs expression. (**A-C**) metabolomic analysis revealed lower BCAAs concentration within TA muscles at 20 weeks. (**D, E**) The expression of Klf15 and Bcat2 was assessed by real-time RT-PCR, using Ppif as housekeeping gene. (**F, G**) Representative images and fiber proportion graph of MyHC staining in TA muscles and the relative zoom at 20w. Data are presented as mean standard error of the mean (S.E.M), * p<0.05 vs WD. Data were analysed using multiple comparison test ANOVA.

Nevertheless, we supposed that atrophy marked by a reduction in muscle weight, CSA, BCAAs levels and upregulation of atrogenes could be the effect of a putative mechanism activated in the early phases of KD feeding, soon after the switching to another metabolism, thus, we then focus our attention on the intermediate timepoint (18 weeks).

Interestingly, instead of 4 weeks of KD-feeding after 16 weeks of WD, differences among the conditions are more evident upon 2 weeks of KD administration, both in the measurement of weights, suggesting the very rapid KD role in mediating fat and muscle weight, thereby reducing myofiber CSA (Fig. 6).

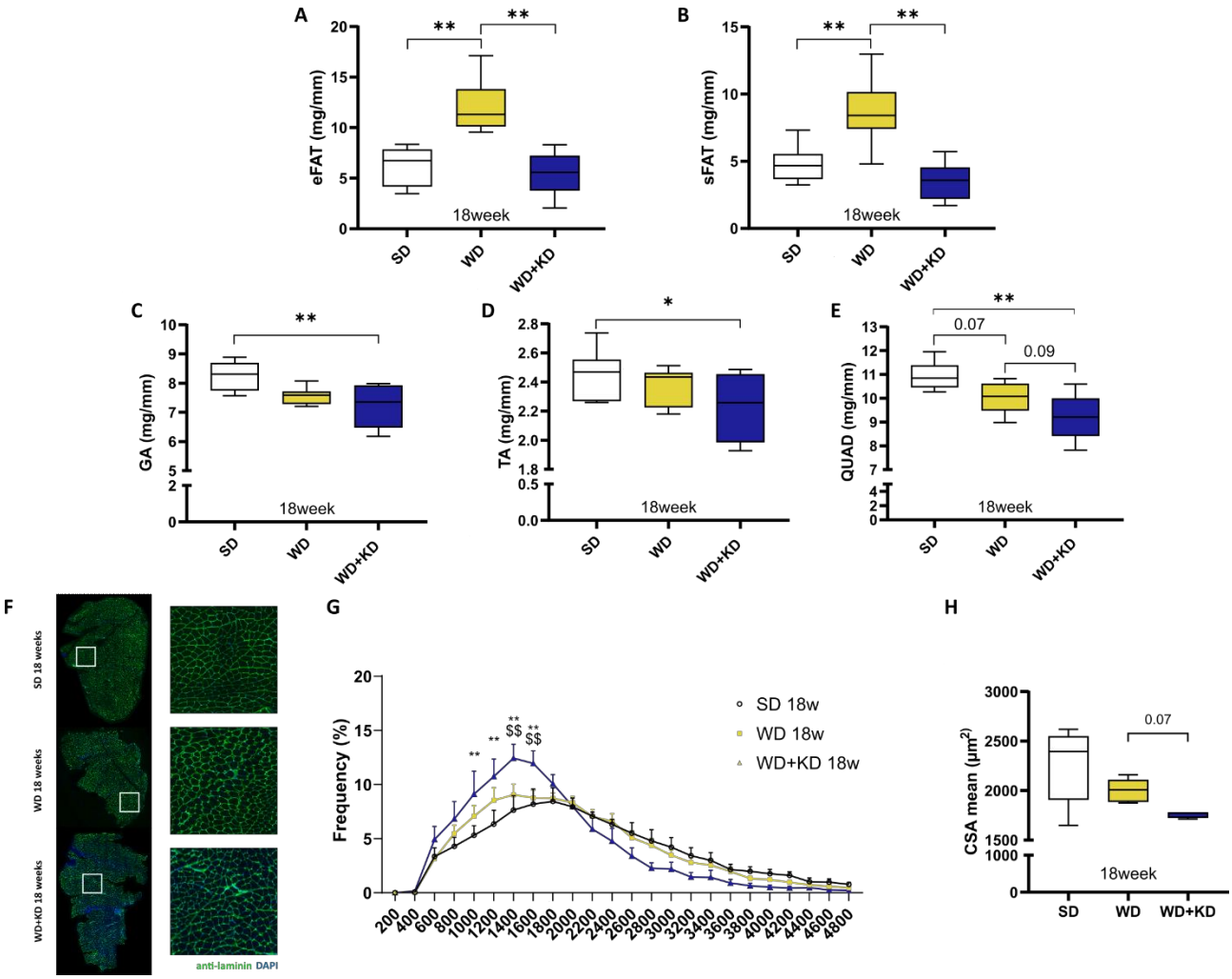

Figure 6: KD elicited fat and muscle loss already from the first two weeks after WD-feeding. (A, B) Fat weights display a significant reduction in subcutaneous and epididymal fat after two weeks of

KD. (C-E) KD promoted muscle mass loss in gastrocnemius (GA), tibialis anterior (TA), and quadriceps (QUAD) muscles. (F, G) Frequency distribution of cross-sectional area at 18 week timepoint and representative images of the anti-laminin immunofluorescence, with the relative magnification (H) Mean of the myofiber cross-sectional area among the different conditions at 18 week timepoint. Data are presented as means ± SEM. *P < 0.05, **P < 0.01 vs SD, $ P < 0.05, $$ P < 0.01 vs WD. All the measurements were recorded at 16 and 20 weeks timepoints. Data are presented as means ± SEM. *P < 0.05, **P < 0.01, $ P < 0.05.

Notably, KLF15 mRNA expression displayed a 3-fold increase within KD group, with consequential BCAT2 elevation (Fig. 7 A). Furthermore, an overall upregulation at the 18th week timepoint of atrogenes (Fbxo32 and MuRF1) and autophagy-related markers (Ctsl, Gabarap, Bnip3, Mff) further support KLF15 role in muscle protein degradation, which is strictly correlated to metabolic shifts induced in the very first phases by this diet (Fig. 7 B, C). In addition, a slight increase of fast-twitch oxidative fibers (IIa) with a simultaneous significant decrease of the fast-twitch glycolytic (IIb) resulted after two weeks of KD switch (Fig. E, F), suggesting that mitochondria-rich oxidative fibers may be used as the primary source for BCAAs degradation Bcat2-mediated that starts in the mitochondrial matrix. Taken these results together, KD-induced muscle atrophy may be the synergistic effect of KLF15-dependent activation of the protein degradation cascade with an exacerbation of UPS and the autophagic/mitophagic pathways.

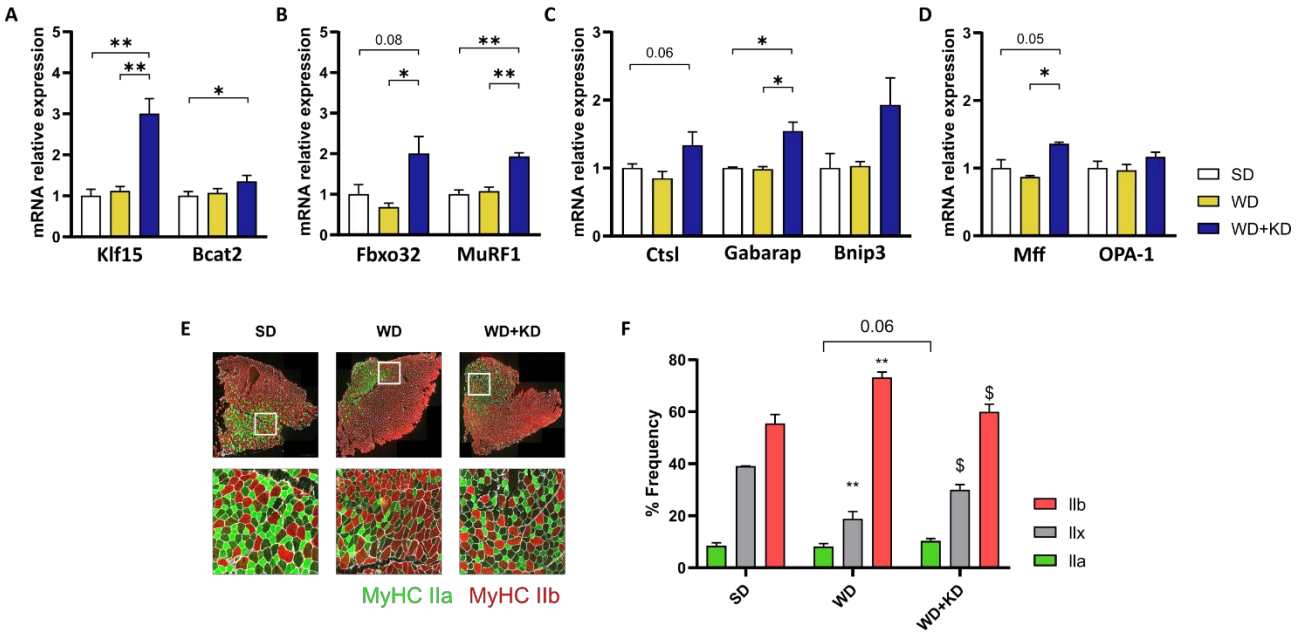

Figure 7: KD modulated gene expression in the early phases after the switching. (**A**)The expression of Klf15 and Bcat2, (**B**) Fbxo32 (Atrogin-1) and Trim63 (MuRF1) (**C**) autophagic and mitophagic genes, respectively Ctsl, Gabarap, and Bnip3, and (**D**) of the fission gene Mff, and of the fusion gene OPA-1 was assessed by real-time RT-PCR in GA, using Ppif as housekeeping gene. (**E, F**) Representative images and fiber proportion graph of MyHC staining in TA muscles and the relative zoom at 20w. Data are presented as mean standard error of the mean (S.E.M), * p<0.05 vs WD. Data were analysed using multiple comparison test ANOVA. Data are presented as means ± SEM. **P < 0.01,*P <0.05 vs SD; $ p<0.05 vs WD.

Dose-Dependent Effects of the Ketone Body Butyrate on Myotube Diameter in the Presence of Palmitate

Meanwhile, to deeper understand WD and KD role in modulating skeletal muscle homeostasis, we used C2C12 myoblasts, an immortalized murine cell line, which is an established cell model widely used to mimic muscle *in vitro*. To this aim, cells were treated with palmitate (PA) and butyrate (BU) since they are reported in literature to be present at high concentration respectively as saturated fatty acid after WD consumption, and as one of the most produced ketone bodies during nutritional ketosis.

We started investigating variation of myotube diameter upon various doses treatment in order to understand whether is present a correlation between dose and myotube diameter. In accordance to literature PA displayed atrophic effect proportionally with dose (Fig. 8 A, B), reducing significantly C2C12 myotube diameter in a dose-response manner [110,111]. Indeed, this result paved the way to use PA500 µM to induce atrophy in our model. Meanwhile, we decided to treat myotubes with 500 µM of BU since in Ang et al. mice that undergone KD for short or long term, specifically for 3 or 10 weeks, reported significantly higher circulating butyrate plasma levels within 0.5-1 mM range [102]. BU behaved atrophic for myotubes leading a 40% reduction of the myotube diameters in comparison with NT ones (Fig. 8 E, F). As reported in Plotkin et al., atrophy is correlated with an exacerbation of protein degradation, and myosin heavy chain (MyHC) protein is the most abundant in skeletal muscle with the pivotal role in muscle contraction [112–114]. Thus, we evaluated MyHC protein expression in our myotubes, both PA 500 µM and BU 500 µM atrophic effect was confirmed also by the reduction in the MyHC protein expression (Fig. 8 C, D, G, H).

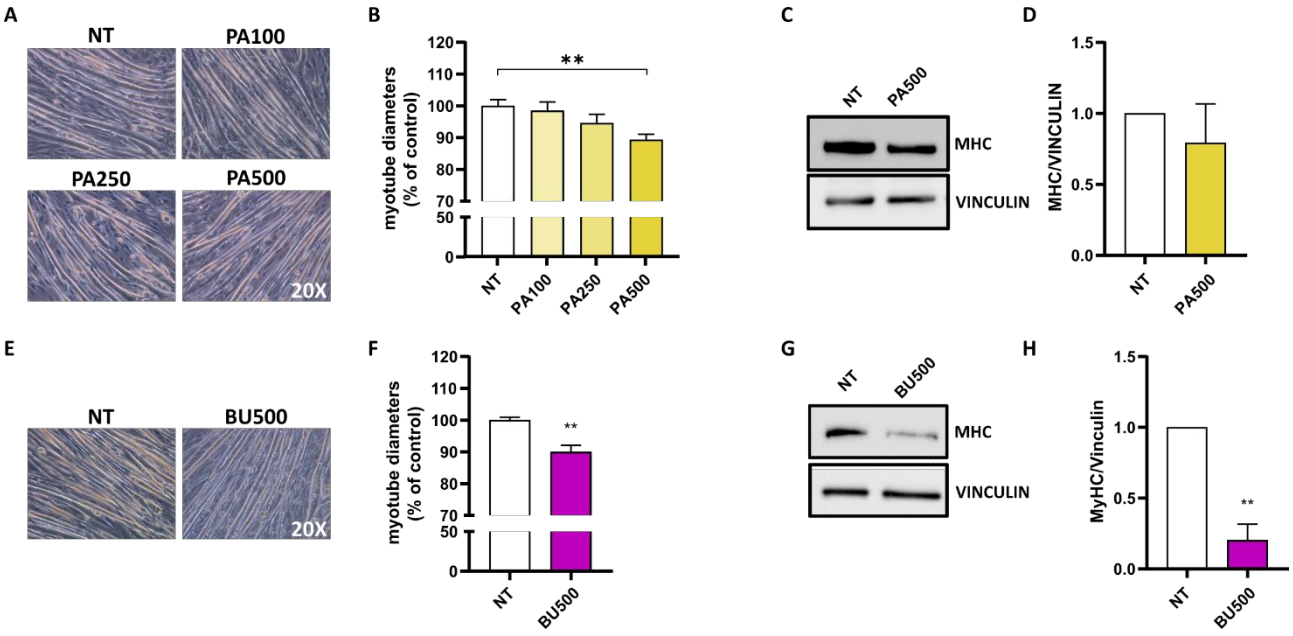

Figure 8: (**A, B**) Myotube diameters were measured after 48 h treatment with 500 µM PA and (**E, F**) 500 µM BU. All treatments were in serum-free medium. For every experiment assessing myotube diameters, at least 10 myotubes for each field, 5 different fields for each replicate, 3 technical

replicates for each treatment were measured. (**C, D, G, H**) Myosin heavy chain expression (MHC) was analysed by western blotting. Relative intensity was normalized on Vinculin. Data are presented as means ± SEM of at least three independent experiments and were analysed using multiple comparison test ANOVA and Student's t-test. * P < 0.05, **P < 0.01.

Indeed, BU 500 µM was used both alone and in co-treatment with PA 500 µM, thereby mimicking KD administered after 16 weeks of WD. In accordance with *in vivo* outcome, as is evident in Fig. 9, BU 500 µM in presence of PA exerted similar behaviour, not only it confirmed the detrimental effect on myotubes, but also it did not carried benefits in counteracting PA-induced atrophy.

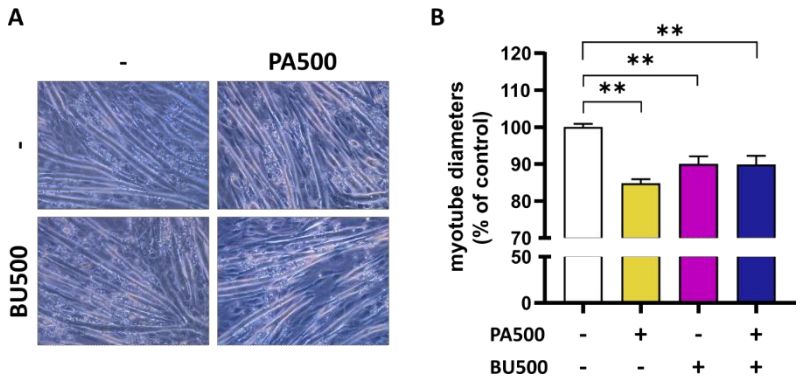

Figure 9: BU500 elicited atrophic effect in C2C12 myotubes both with and without the presence of PA500. (**A, B**) Myotube diameters were measured after 48 h treatment with 500 µM PA, 500 µM BU, and the combination of them. All treatments were in serum-free medium. Data are presented as means ± SEM of at least three independent experiments and were analysed using multiple comparison test ANOVA. * P < 0.05, ** P < 0.01.

In addition, to get insights about the mechanisms that could be implicated in inducing atrophy in our model, we started investigating gene expression of UPS markers. Although no statistical significance differences were appreciated upon PA in both Fbxo32 and Trim63, significant upregulation of them were evident in BU 500 µM treatments (Fig. 10 A, B), with or without PA, confirming the similar results observed in animals (Fig. 4, 7).

Moreover, the synergic participation of palmitate and butyrate triggered an alteration of the autophagic system, with a following magnification of the Gabarap, despite Ctsl gene seemed to be augmented by the treatment of BU alone (Fig. 10 C, D).

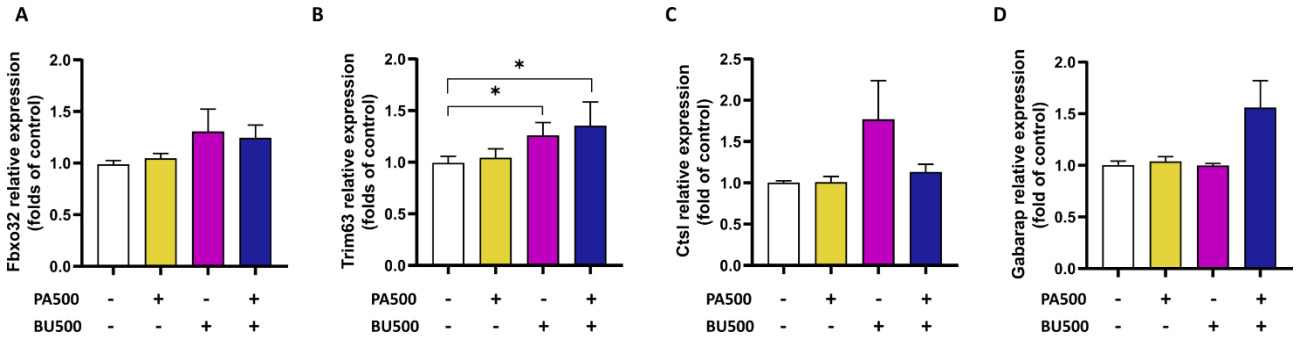

Figure 10: BU500 deregulated both the UPS and the autophagic flux. Relative expression of (**A**) Fbxo32 (Atrogin-1), (**B**) Trim63 (MuRF1), (**C**) Ctsl, and (**D**) Gabarap in C2C12 myotubes was assessed by real time RT-PCR using Gusb as housekeeping gene. Data are presented as means ± SEM. Data are presented as means ± SEM of at least three independent experiments and were analysed using multiple comparison test ANOVA. * $P < 0.05$, ** $P < 0.01$.

Notably, a significant increase of mitophagy was observed in the administration of both the fatty acid and the ketone body (Fig. 11 A). Coherently, the induction of Bnip3 expression was supported by the mitochondrial accumulation, in PA+BU-treated myotubes, of Mff (Fig. 11 B), whose upregulation resulted in mitochondrial membrane potential dissipation that leads to the recruitment of the machinery needed to initiate the putative compensatory mechanism of the autophagic degradation of damaged mitochondria.

Accordingly, PA+BU-induced loss of mitochondrial membrane potential, highlighted by the diffusion of the green cationic dye JC-1 in the cytoplasm, in contrast with the potential-dependent accumulation in healthy mitochondria and fluorescence emission shift from green to red (Fig. 11 C, D).

However, the loss of the membrane potential upon PA+BU treatment did not trigger an increase in the production of reactive oxygen species (ROS) (Fig. 11 E, F).

To further mimic *in vivo* experiment and to deeper comprehend molecular mechanisms that could take part in influencing muscle mass, KLF15-mediated pathway was investigated. Strikingly, mRNA expression of KLF15 transcription factor was modulated differently depending on the time. Despite being similar to the control upon very short-term treatments, specifically after 30 minutes, 6 hours of PA+BU treatment displayed a significant overexpression of the gene (Fig. 11 G).

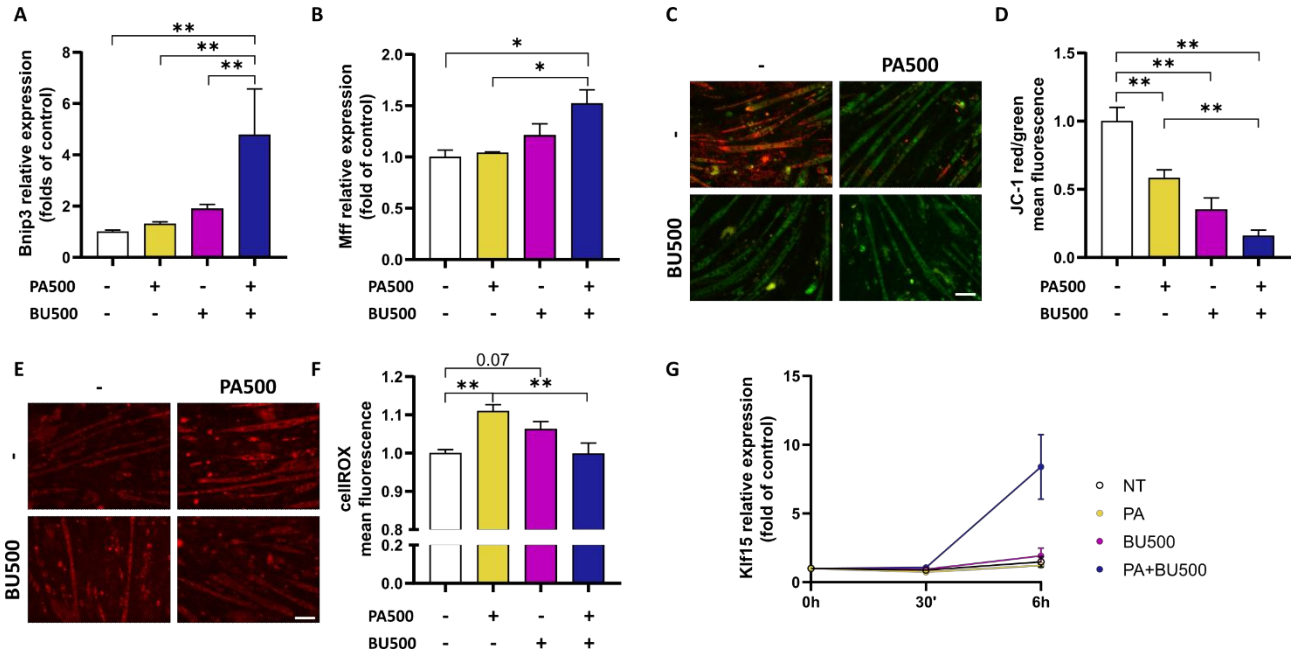

Figure 11: BU500 exacerbated mitochondrial health when combined with PA500. Relative expression of (**A**) Bnip3, (**B**) Mff, in C2C12 myotubes was assessed by qPCR using Gusb as housekeeping gene. (**C, D**) Mitochondrial membrane potential depolarization was evaluated by JC-1 staining after 48 h of treatment. Scale bar set at 100 µm. Bars represent the quantification of the ratio of red/green fluorescence, indicative of membrane polarization. (**E, F**) ROS production was evaluated by CellROX Deep Red reagent and quantified as the fluorescence mean intensity of each myotube. Scale bar set at 100 µm. (**G**) Klf15 relative expression was assessed by qPCR after 30 minutes and 6 hours of treatments using Gusb as housekeeping gene. Data are presented as means

± SEM of at least three independent experiments and were analysed using multiple comparison test ANOVA. ** p<0.01, * p<0.05.

Given the pivotal role of ketone bodies in inducing atrophy in both the models that we decided to investigate, our further aim was to decipher whether changing (decreasing) the dose of the KB could unravel promising results on mitigating, avoiding or reverting PA-induced myotube atrophy.

To this aim we performed a dose-response testing various doses of BU, including 25 µM, 50 µM, 100 µM, 250 µM, and reaching BU 500 µM. Interestingly, although high doses suggested to be toxic for myotubes, leading to a reduction of the diameter, the lower doses did not influence the width of them (Fig. 12 A, B). To confirm these quantifications, a dose-response downregulation of MyHC denoted the toxic effect responsible of inducing protein degradation exerted by high doses of BU (Fig. 12 C, D).

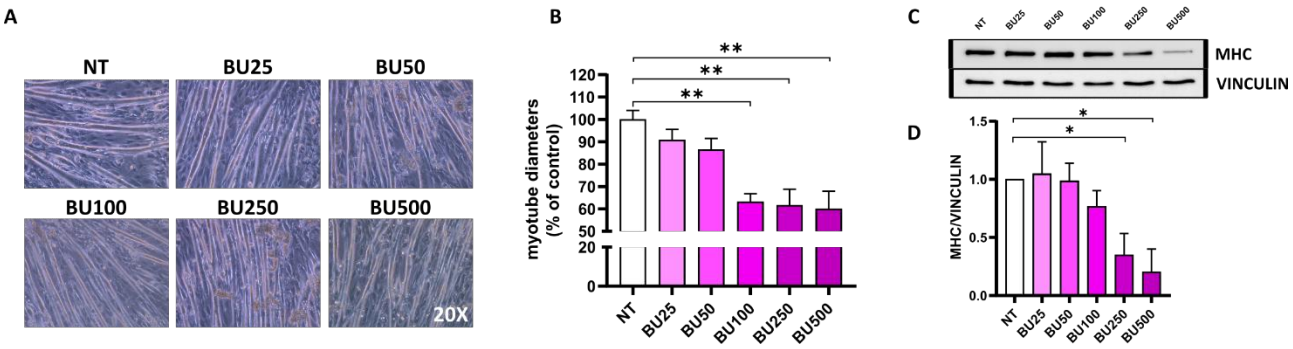

Figure 12: BU dose-dependent atrophic effect. (**A, B**) Myotube diameters were measured after 48 h treatment with BU at various doses, 25 µM, 50 µM, 100 µM, 250 µM, and 500 µM. All treatments were in serum-free medium. (**C, D**) Myosin heavy chain expression (MHC) was analysed by western blotting. Relative intensity was normalized on Vinculin. Data are presented as means ± SEM of at least three independent experiments and were analysed using multiple comparison test ANOVA. * P < 0.05, ** P < 0.01.

Indeed, we decided to focus on BU 50 µM since it displayed the similar amount of the MyHC protein compared to NT. Interestingly, BU 50 µM was able to counteract PA-induced atrophy, with a significative rescue of the diameter thickness, raising up values equal to the NT ones (Fig. 13 A, B). This result paved the way to Fig.ure out whether this dose in the simultaneous treatment with PA could be more promising rather than BU 500 µM.

Coherently with the diameter quantification, no atrogenes or autophagic markers were induced or downregulated upon treatment with BU at low dose, confirming the overall health condition of myotubes (Fig. 13 C-H).

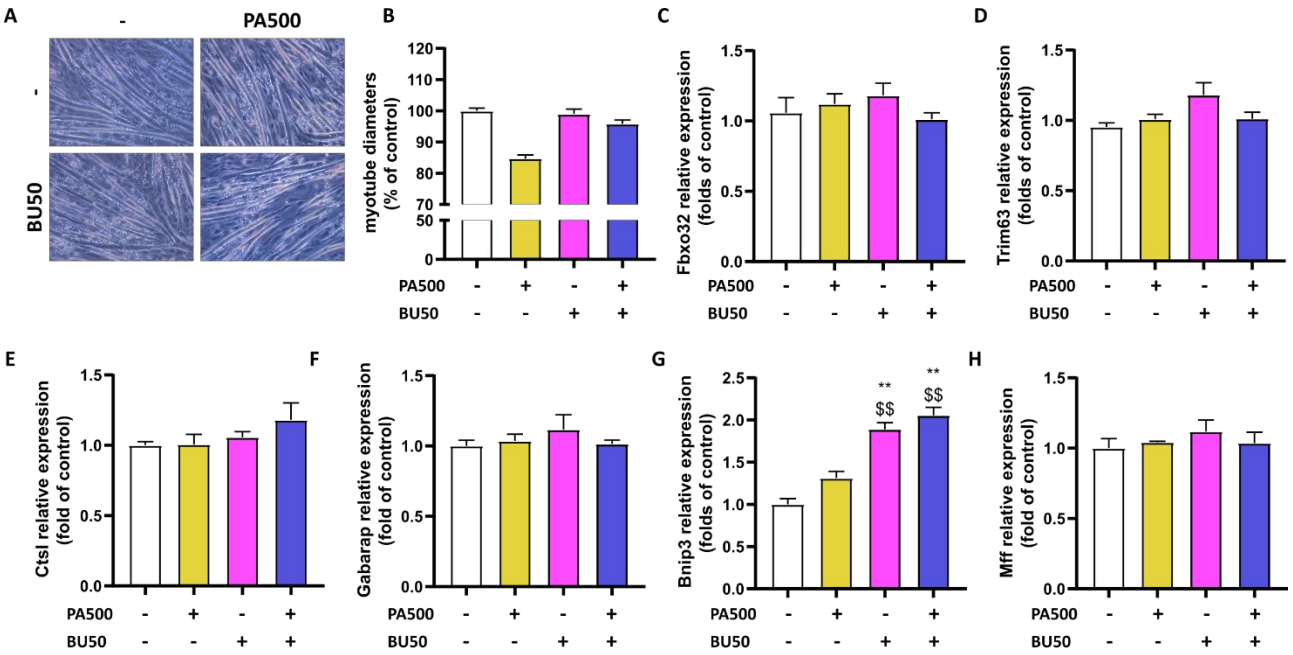

Figure 13: BU 50 µM both in presence and in absence of PA displayed similar results than the NT (**A, B**) Myotube diameters were measured after 48 h treatment with 500 µM PA, 500 µM BU, and the combination of them. All treatments were in serum-free medium. Relative expression of (**C**) Fbxo32 (Atrogin-1), (**D**) Trim63 (MuRF1), (**E**) Ctsl, (**F**) Gabarap, (**G**) Bnip3, and (**H**) Mff in C2C12 myotubes was assessed by real time RT-PCR using Gusb as housekeeping gene. Data are presented as means ± SEM and were analysed using multiple comparison test ANOVA. *P < 0.05, **P < 0.01 vs NT, $ P < 0.05, $$ P < 0.01 vs PA.

However, Bnip3 resulted overexpressed also within BU 50 µM treatments (Fig. 13 G), although its expression appeared lower compared to what BU 500 µM has triggered (Fig. 11 A). To delve deeper in the mitochondrial homeostasis, we moved with further JC-1 assay since mitochondrial membrane depolarization was found deregulated upon PA and BU 500 µM treatments alone and further depolarized in the co-treatment of them. Notably, the 50 µM dose was not only sufficient in abolishing PA-dependent loss of mitochondrial polarization, but also significantly reduced PA-induced production and accumulation of ROS (Fig. 14 A-D), suggesting that the BU-mediated counteraction of atrophy may proceed through this pathway.

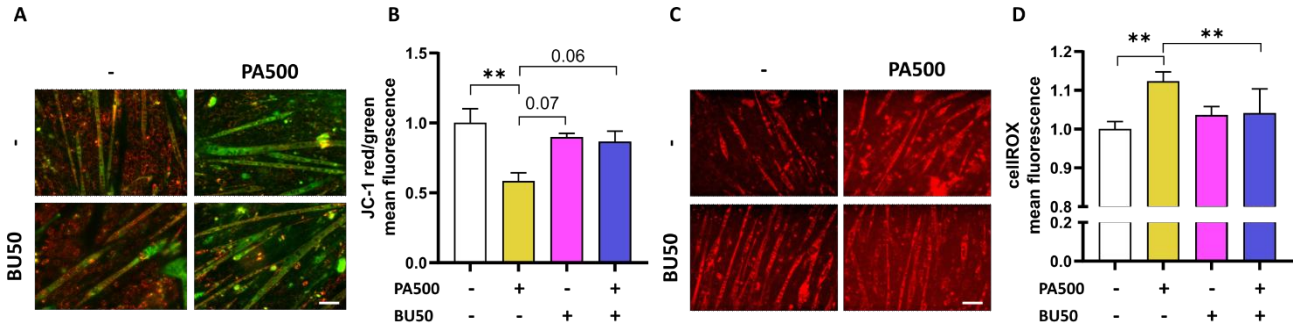

Figure 14: 50 µM BU counteracted PA-induced membrane depolarization and ROS accumulation (**A, B**) Mitochondrial membrane potential depolarization was evaluated by JC-1 staining after 48 h of treatment. Bars represent the quantification of the ratio of red/green fluorescence, indicative of membrane polarization. Scale bar set at 100 µm. (**C, D**) ROS production was evaluated by CellROX Deep Red reagent and quantified as the fluorescence mean intensity of each myotube. Scale bar set at 100 µm. Data are presented as means ± SEM and were analysed using multiple comparison test ANOVA. *P < 0.05, **P < 0.01.

6.3. Discussion

The macronutrient profile proper of KD has been widely investigated both in human and in rodent studies, however, the current body of literature highlights the complex and often contradictory relationship between KD and skeletal muscle health [105]. Several studies have shown that KD can result in muscle fibrosis and atrophy, not reaching a muscle functionality benefit [104,115]. Contradictory results are present in literature deriving both from in animals and in humans studies, due to several reasons, such as composition and amount of Kcalories of the KD regimens, animals models used, baseline clinical condition in patients as well as associations with or without physical activity or exercise programs [85,89,92,97,103]. Our results demonstrated that 2 or 4 weeks of KD feeding after 16 weeks of WD consumption were not effective in counteracting WD-related muscle loss, on the contrary it further triggered muscle atrophy. To deeper elucidate the enigmatic mechanisms that are closely related to WD and KD in skeletal muscle, we employed myoblasts of the C2C12 cell line demonstrating that treatments with high doses of butyrate, in the presence of palmitate, elicited similar results with the ones obtained in the *in vivo* experiment.

First of all, unexpectedly, we observed that KD induced muscle atrophy both compared to SD and WD mice. KD group displayed lower muscle mass and a higher proportion of smaller myofiber cross-sectional area, coherently with the results on mice muscles in Nakao et al. work [104]. These results conflicts with several data in humans. In humans, several studies unraveled the strong effect KD-induced on weight loss, particularly in obese individuals, with significantly large reduction in fat mass, including visceral adipose tissue, [116–118]. However, recently, several Authors raised concerns to strategies for massive weight loss, as bariatric surgery, incretin-based therapies and also KD regimens, which may lead also to a significant decrease in fat free mass (FFM) loss and potentially muscle-bone function impairment, since in humans for every kilogram of weight loss, about 75% is FM loss and 25% FFM loss [119,120]. FFM loss is primarily due to an increased muscle protein

breakdown, more than a decreased protein synthesis, suggesting the critical role of resistant exercise during weight loss [120]. Furthermore, apart from protein or amino acids supplementation during weight loss strategies, KD regimens are considered an effective strategy to counteract FFM loss through a protein sparing effects of KBs [121–123].

The discrepancy between our results in mice and several human studies could be linked to different composition of dietary regimens. KDs composition across different mouse model studies exhibit consistent macronutrient distributions, very high in fat (90-94.8% of kcal), extremely low in carbohydrate (0.1-0.3% of kcal), and notably low in protein (4.8-10% of kcal). Protein intake is considered a central factor contributing in maintenance of strength and lean mass [123,124]. Diversely, human studies in obesity used very low calorie KD, that are characterized by a normal amount of protein on Kg of ideal weight and frequently are supplemented with further amount of essential amino acids [87,125]. Furthermore, protocols in mice skeletal muscle differed also in term of duration and whether dietary treatment is combined with exercise. KD in shorter period, 7 days as Nakao et al. is concerned, displayed worst outcomes [104], on the other hand, in diabetic mice, 6 weeks of KD intervention increased muscle mass, particularly in GA and QUAD muscles, myofiber size, and grip strength, indicating muscle mass and function preservation [126].

In our experiment, despite muscle weight reduction was significant both after 2 and 4 weeks of KD consumption, differences in muscle strength and performances were not appreciated among the mice fed with different diets, suggesting that this period of KD was not able to improve or deteriorate muscle strength and functionality, despite the negative effects on mass. The preservation of muscle strength although a significant decrease in muscle weight could be linked to the fact that our KD regimens included a ~16% of protein on total calories, more similar to human KD models. On the other hand, also in humans conflicting data regarding KD and muscle performances have been published, since this parameter depends on type of performance, duration

of the diet, and individual's training status. Whether KD in athletes may lead in improvement or preservation of muscle strength and performances concomitantly with weight loss [124], in obese individuals the focus is often on preserving functional capacity and preserving lean body mass [116,123,127]. In C57Bl/6J obese mice, after 8 weeks of KD intervention, mice in the KD group exhibited significantly higher running time and distance compared to the obesity control group [128], while in Zhang et al., 4 weeks of KD were not sufficient to influence endurance tests [129]. Interestingly, Nakao and co-workers demonstrated the association between KD and muscle wasting, characterized not only by weight loss, but also by myofiber size reduction, lower muscle performances, and increased expression of the muscle atrophy-related genes (Atrogin-1, MuRF1, FOXO3, and Lc3b) observed in GA, TA and Soleus (SOL) muscles of mice fed for 7 days with KD compared to SD [104]. Furthermore, a large number of researches focused their attention on the FOXO3 signalling pathway triggered by an elevation of reactive oxygen species (ROS), responsible in inducing muscle atrophy through UPS activation and dysregulation of autophagic/mitophagic flux [130], whose exacerbation is widely demonstrated to promote protein breakdown in muscle [131].

Our data suggest that both of the pathways mentioned above were influenced by KD metabolic shift. Despite the upregulation of atrogenes is evident since the first weeks after the switch to KD, the expression of genes related with the autophagy-lysosome system has to be deciphered. Since autophagy may lead a pathological cascade triggering muscular weakness and muscle atrophy both if autophagosome formation is exacerbated or inhibited [132], we speculate that KD initially stimulates the activation of the autophagic flux as a compensatory mechanism necessary to maintain energy homeostasis through the secretion of damaged organelles, and in particular mitochondria, in accordance with Xia et al., in which Is reported that it is stimulated under metabolic shift. However, we suppose that if catabolic stress continues due to ketosis, autophagy might be impaired resulting in failing protein turnover, triggering accumulation of damaged organelles and muscle loss. The

impairment of autophagic flux, highlighted at endpoint by a downregulation of the genes responsible for protein turnover, might be considered key player in the KD-dependent muscle wasting, leading to protein breakdown [48–50].

Consistently, it has been demonstrated that upon pro-catabolic stimuli, including glucocorticoids and fasting, protein breakdown reduces intramuscular BCAA concentration, whose availability is pivotal in maintaining muscle mass through activation of anabolic processes, including mTORC1, the master regulator of protein synthesis levels [51,109].

Moreover, several papers highlighted the role of KLF15, a key transcription factor that integrates glucocorticoid signalling, nutrient status, and catabolic stress [107], to be determinant in influencing BCAA levels by inducing protein degradation through inhibition of mTORC1 activity [133]. In our experiment, while KLF15 levels are constant within SD, WD, and KD at 20 weeks, interestingly, its early upregulation after only 2 weeks of ketosis suggests that the metabolic shift is sufficient to trigger rapidly a cascade of catabolic events that may continue beyond its peak expression. Furthermore, as reported in Shimizu et al. [133], KLF15 inhibits mTOR by activating BCAT2, the muscle-specific mitochondrial enzyme which encodes the first phases of the reversible transamination of leucine, isoleucine, and valine into their corresponding branched-chain α-keto acids (BCKAs). Previous findings established that reduced BCAT2 levels in muscles are associated with high BCAA concentration, which in turn activate mTORC1 and muscle hypertrophy [127]. Additionally, BCAT2 knock out mice increased body weight, augmented protein turnover and whole body insulin sensitivity, but without altering skeletal muscle weight [134]. In accordance with these data, we speculate that the upregulation of BCAT2 and KLF15, marked at 18 weeks in mice that switched diet from WD to KD, may be considered the pivotal pathway that leads to the observed very low BCAA levels, particularly Isoleucine and Valine within TA muscles. Moreover, a higher proportion of oxidative myofibers to the detriment of glycolytic ones suggests that KD-induced metabolic shift

after a period in WD may enhance lipid oxidation, facilitating glycolytic-oxidative myofiber type switch, which in turn leads to increased BCAT2 function in mitochondria, whose expression is reported directly proportional with the number of mitochondria and BCAAs catabolism both in transgenic mice and in C2C12 muscle cells [135]. The higher proportion of oxidative myofibers could also explain the maintenance of muscle performance in the time of our experiment.

Similarly, the elevated mRNA expression of KLF15 in C2C12 myotubes co-treated with palmitate and BU at 30 minutes and 6 hour timepoints, support our hypothesis that this gene may be expressed early, leading to UPS activation, whose triggering is demonstrated to be related with KLF15-dependent proteolysis [108]. Given this, BU at a high (500 μM) concentration, both in absence or in presence of PA, reflecting WD+KD group, significantly reduced myotube diameters and overexpressed mRNA expression of Atrogin-1, MuRF1, and the one of autophagy-related genes, including Bnip3, which is specific for mitochondria. Since mitochondrial dysfunctions are considered central in inducing muscle atrophy [52,53], and BU is associated with increased mitophagy and loss of mitochondrial membrane polarization (MMP) associated with increased of ROS [136], mitochondrial health was assessed through investigation of MMP through JC-1 assay, which confirmed a substantial loss of MMP following PA+BU exposure, a prerequisite for mitophagy to occur. Altogether, PA- and BU- induced muscle atrophy could be mediated by different mechanisms that act both synergistically and distinctly. Despite PA-induced atrophy seems to be an event following mitochondrial dysfunction and ROS accumulation, BU introduction triggered proteolysis through the activation of UPS and deregulation of the autophagic flux.

Furthermore, our findings suggest that the levels of KBs could have different effects on muscle health. Coherently, it has been observed that D-β-hydroxybutyrate infusion could elicit opposite effects in skeletal muscle in healthy males. Although high doses were associated with worst muscle outcomes, lower levels of them were beneficial [137]. Thus, we believed that tailored dose of BU could

potentially mitigate PA-induced myotube atrophy without being detrimental itself. Indeed, a dose-response reduction of myotube diameter we observed confirmed this hypothesis, displaying higher reduction in myotube width concomitantly with higher doses.

Strikingly, BU 50 µM, unlike to what observed upon C2C12-derived myotubes treated with PA+BU 500 µM, not only was neutral if administered alone, but also avoided exacerbation of atrophy with a significative rescue of myotube thickness in the context of PA-induced atrophy when treated in presence of PA. In line with previous findings [110,112], PA exerted atrophic effect on myotubes, both reducing diameter of them and downregulating MyHC protein expression, and BU at low dose could alleviate C2C12 myotube atrophy, by mediating autophagy and inflammation, without affecting the main ubiquitin-mediated protein degradation pathways or proteasome activity, as it is reported in a consistent number of researches [49,138]. Notably, the abolishment of PA-induced MMP with a consequent reduction of ROS accumulation and an overall amelioration of skeletal muscle homeostasis, further underscore the importance of tailoring doses of KBs, suggesting that KD could not be a strategy for all and that KB levels should be modulated in KD regimens to prevent muscle loss and function [123].

Finally, our results highlight a complex interplay between dietary regimen and muscle metabolic regulation, which may be, at least in part, dose-dependent and time-sensitive, with early induction of stress responses that might subside or reverse over time. To delve deeper in the understanding of KD role in skeletal muscle homeostasis, further experiments are necessary to elucidate the mechanism that trigger protein breakdown. To this aim, an amino acid-rich diet should avoid excessive BCAAs degradation [123]. In addition, we suppose that inhibition of KLF15 and BCAT2 may counteract, mitigate, or avoid the catabolic pathway at the basis of KD-induced muscle atrophy. Furthermore, optimization of dietary timing, duration, and nutrient composition, and deciphering more physiologically relevant combination of FFAs and KBs, could help preserving skeletal muscle

functions and mass. In line with this, very recently, it has been demonstrated as a mixture of KBs had different metabolic effects on glucose uptake in L6 myotubes and that BU and acetoacetate together blunted the efficacy of one of them alone [139]. Notably, these outcomes further underscore the need for a more carefully monitored and specialized dietary approach, also in terms of circulating KB levels. Furthermore, more of the positive effects of KD regimens in humans have been observed when coupled with specific programs of physical activity [139], whereas our mice were not subjected to a physical activity program. In clinical studies, particularly in a context of health complications, the consumption of KD should be recommended, tailored, coupled with physical activity and guided by qualified healthcare professionals, such as nutritionists and clinicians, to ensure the effectiveness of the intervention, avoiding undesirable effects, including rapid weight-muscle loss and a possible weight regain once the ketogenic phase in concluded.

6.4. Materials and Methods

Animal experiment

Animal experiment was performed according to procedures approved by the Institutional Animal Care and Use Committee at the University of Piemonte Orientale. The study protocols received ethical approval by the Italian Ministry of Health (authorization N° 411/ 2020-PR, 05 May 2020) according to the European law requirements. All experiments were performed on C57BL/6 male mice, matched for age and weight. Animals were maintained in a 12/12h light/dark cycle with *ad libitum* access to food and drinking water. The animals were bought at 4 weeks of age and were fed a Standard diet prior to the study. Eight-week-old mice were divided into two different groups and were fed *ad libitum* for 20 weeks with Standard Diet (SD: 13 kJ% fat, 20 kJ% proteins, and 67 kJ% carbohydrates) or for 16 weeks with high fat/carbohydrate diet (4.6 Kcal/g) enriched with 1.25% cholesterol Western Diet (WD) (WD: 42 kJ% fat, 15 kJ% proteins, and 43 kJ% carbohydrates). At this timepoint, mice in the latter group were further divided for additional 2 or 4 weeks. Despite a part of them continued in their current diet, the remaining started to assume Ketogenic diet (KD: 90,5 kJ% fat; 9,2 kJ% protein and 0,3 kJ% carbohydrates). All the diets were purchased from Laboratorio Dottori Piccioni (Gessate, Italy).

Mice were euthanized by cervical dislocation, while under general anesthesia (4% isoflurane in the air), at the respective endpoints. Hind-limb muscles such as gastrocnemius (GA), tibialis (TA), and quadriceps (QUAD) were collected, weighed, and stored at -80°C for histology analysis and gene expression.

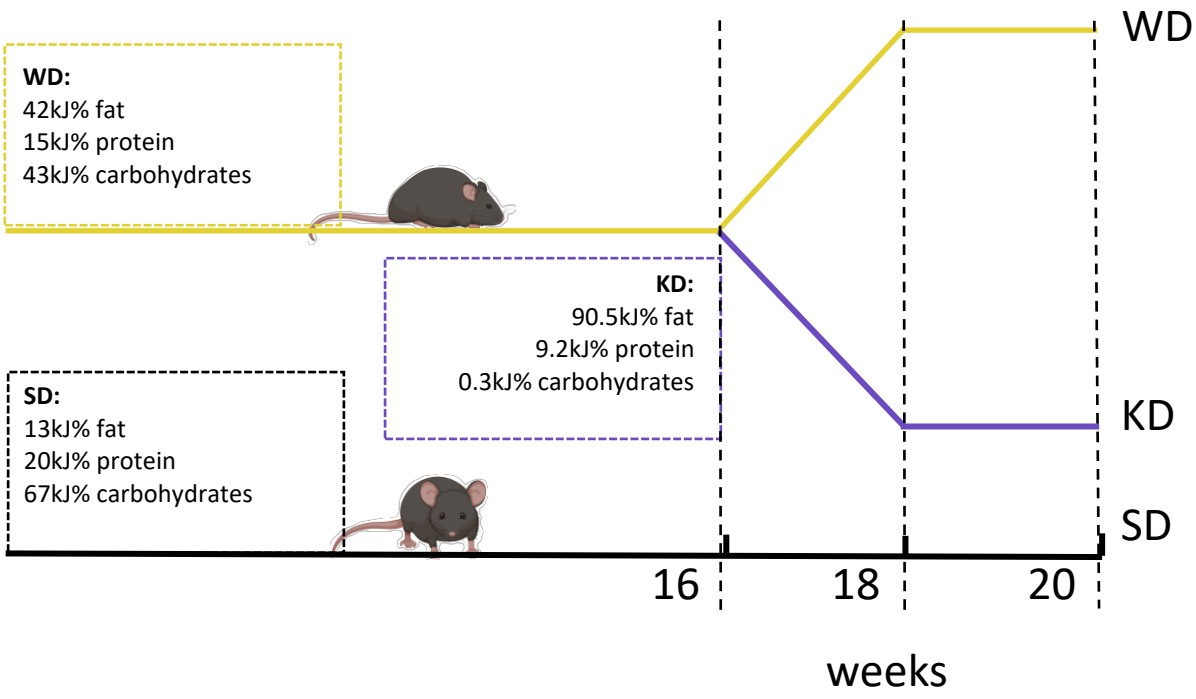

Functional tests

Before being euthanized, mice were subjected to two different functional tests at different time point, in order to decipher whether their muscle strength could be influenced by dietary assumption.

Grasping test

Grasping test is a non-invasive method that can be used to measure mouse strength. This test has been performed using Bioseb grip strength meter and is used to evaluate in vivo muscles performances. It is based on the natural tendency of the mouse to grasp a grid when it is suspended by the tail and carefully pulled backward. A force transducer attached to the grid measures peak resistance force, which is recorded when the mouse is departed from the grid losing grip. An average of 5 repeated pulls for each mouse is recorded in order to reduce the variability between samples [140].

Hanging wire test

Hanging test is performed to determine whole-body muscle strength and endurance of the mouse that uses all four limbs to resist on a suspended wire. The experimental test lasts 180 seconds, in which are recorded both the number of times in which the mouse reaches the extremity and the ones that falls off the wire. Every animal starts with a scores of 10 points, they get 1 point for every <reaching= and lose 1 point for every <falling=. This test can give other important information such as holding impulse (body mass x hang time), which represents the longest time between two successful falls multiplied for body weight.

Histological analysis

CSA immunofluorescence

Muscles were excised, weighted, mounted in Killik embedding medium (Bio Optica Milano SpA), frozen in liquid-nitrogen-cooled isopentane, and stored at -80°C. Transversal muscle sections (7 µm) were cryo-sectioned from the middle part of each muscle.

Myofiber cross sectional areas (CSA) were determined by immunofluorescence with anti-laminin. Slices were fixed in 4% PFA for 20 min, washed, permeabilized with 0.2% Triton X-100 in 1% BSA for 15 min, and blocked with 4% BSA for 30 min. One hour of incubation with primary antibodies at RT was followed by PBS washing and 45 min of Alexa Fluor anti-rabbit 488 secondary antibody at RT. Nuclei were counterstained with DAPI. Eventually, sections were washed in PBS and cover slipped using *SlowFade Gold antifade reagent* (Invitrogen, Thermo Fischer Scientific) mounting medium. Images of whole muscle sections were acquired with Leica TCS SP8 confocal microscope and CSA of fibers quantified with ImageJ software.

MyHC immunofluorescence

MyHC immunofluorescence was performed on mice muscles that have been cut obtaining slices of 4 µm. Firstly these portions have been blocked with 3% BSA for one hour and then properly washed. In order to obtain myofiber type distribution, immunofluorescence for myosin type IIa, IIb and laminin was performed. The slices were probed with different primary antibodies: anti-MyHC Type IIa, anti-MyHC Type IIb, and anti-laminin for one hour at RT and then washed by PBS. Subsequently the portions were incubated with the Alexa Fluor-conjugated secondary antibodies and covered by SlowFade Gold antifade reagent (Invitrogen, Thermo Fischer Scientific) mounting medium.

The cover slips with the muscle slices have been investigated using a Leica TCS SP8 confocal microscope and different images have been collected and analyzed using ImageJ software. In order to obtain a better quantification of the different myosin isoforms, laminin-stained images were optimized enhancing contrast, applying Gaussian blur and despeckle, and subtracting background. Myofiber boundaries were segmented by the plugin "MorphoLibJ". Using the command "analyze particles", it has been possible to count the different fiber areas.

RNA extraction and gene expression

Total RNA from myotubes or 50 mg of tissue was extracted by *RNAzol* (Merck Life Sciences). The RNA was retro-transcribed with the *High-capacity cDNA Reverse Transcription Kit* (Applied Biosystems, Thermo Fisher Scientific), and real-time PCR was performed with the *StepOnePlus* Real-time PCR System (Applied Biosystems, Thermo Fisher Scientific), using the following TaqMan probes (Thermo Fisher Scientific): *Opa1* (Mm00453873_m1), *Mff* (Mm01273401_m1), *Bnip3* (Mm01275600_g1), *Gabarap* (Mm00490678_m1), *Ctsl* (Mm00515597_m1), *Klf15 (Mm00517792_m1), Bcat2 (Mm00802192_m1)*, *Fbxo32* (Mm00499523_m1), *Trim63* (Mm01185221_m1), *Ppif* (Mm00506384_m1), and *Gusb* (Mm01197698_m1).

Metabolomic analysis

For metabolomics analyses, small molecules were extracted form 30 mg of tissue that were transferred in a screw capped tube with 70 mg of glass beads (1mm diameter) 1 mL mixture of acetonitrile (ACN), isopropanol (IPA), and water 3:3:2, with 5 µL of tridecanoic acid (0.5 mg/mL), 5 µL of palmitic acid d31 (0.5 mg/mL), 5 µL of stearic acid d35(0.5 mg/mL), 3.5 µL of glycine d4 (10.07 mg/mL) as the internal standard was added in the screw capped tube. Then the tube undertook four cycles of thirty seconds in the homogenizer, between each cycles the samples were cool down for about a minute in the ice. The samples were vortexed for 15 s and centrifuged for 15 min at 20 °C at 14.5 g. Next, 1 mL of the supernatant was placed in a new tube, dried in a speed vacuum, and stored at -20 °C until derivatization. The samples were at last derivatized with methoximation (20 µL of methoxamine, 80 °C, 20 min) and silylation (30 mL of N,O-Bis(trimethylsilyl)trifluoroacetamide, 80 °C, 20 min) prior to the GCxGC-TOFMS analysis.

For GC-MS, the column was a 30 m Rxi-5Sil MS (Restek Corp., Bellefonte, PA, USA) capillary column with an internal diameter (id) of 0.25 mm and a stationary phase film thickness of 0.25 µm. The inlet was set at 250°C in splitless mode and an aliquot of 1 µL of sample was injected. Electron impact ionization was applied (70 eV). The ion source temperature was set at 250 ◦C, the mass range was 25 to 550 m/z with an extraction frequency of 30 kHz. The acquisition rates were 200 spectra/s.

ChromaTOF version 5.31 was used for the raw data processing. The mass spectral assignment was performed by matching with NIST MS Search 2.3 libraries and a custom library of amino acid standard. Quantification was performed using external calibration curves.

Cell culture and myotube analysis

C2C12 myoblasts (ECACC) were grown at low density in DMEM (Gibco, Thermo Fisher Scientific) supplemented with 10% fetal bovine serum (FBS, Gibco, Thermo Fisher Scientific), 100 U/mL

penicillin, 100 µg/mL streptomycin, and 0.25 µg/mL antimycotic in a humidified 5% CO2 incubator at 37°C. To induce differentiation, cells were allowed to become confluent, and the medium was switched to differentiation medium (DM), consisting of DMEM supplemented with 2% horse serum (GE Healthcare BioSciences), penicillin, streptomycin, and antimycotic as described above. Unless otherwise specified, myotubes were treated in serum-free medium after at least 5 days of differentiation. Differentiated cells were treated in triplicate for 48 hours with 100 µM, 250 µM, 500 µM of Palmitate (PA; Merck Life Sciences, Milan, Italy) and 25 µM, 50 µM, 100 µM, 250 µM, 500 µM of Butyrate (BU; Merck Life Sciences) and co-treatment between PA and BU at the concentration mentioned before. For every experiment were measured at least 10 myotube diameters for each field, five different fields for each replicate, and three technical replicates for each treatment. Myotube diameters were measured with JMicroVision software as previously described.

Western blotting

At the end of the indicated treatments, cells were washed in ice-cold phosphate-buffered saline (PBS) and solubilized with a lysis buffer containing 1% Triton X-100, 0.1% sodium deoxycholate, 0.1% sodium dodecyl sulfate (SDS), 1 mM EDTA, 1 mM EGTA, 50 mM NaF, 160 mM NaCl, 20 mM Tris-HCl, pH 7.4, and supplemented with protease inhibitor cocktail. Lysates were stirred at 4°C for 15 min and centrifuged at 15,000 × *g* for 15 min at 4° C. Protein concentration was determined by BCA protein assay kit. Proteins were resuspended in sample buffer containing 2% SDS, 150 mM dithiothreitol (DTT), and 0.01% bromophenol blue, and 20 µg protein/lane were separated by 10 or 15% SDS-PAGE and transferred to PVDF. Membranes were saturated with 4% BSA, probed with the primary antibodies ON, washed with Tris-buffered saline (TBS) 0.1% Tween, incubated with the appropriate secondary antibody for 1 at RT, visualized with Western Lightning Chemiluminescence Reagent Plus (Perkin Elmer Life and Analytical Sciences), acquired with ChemiDoc Touch (Bio-Rad), and analyzed with ImageLab (Bio-Rad).

Mitochondrial membrane potential

Mitochondrial membrane potential in C2C12 myotubes was assessed using *JC-1 mitochondrial membrane potential assay kit*, according to the manufacturer's instructions (*JC-1 Dye:* Thermo Fisher Scientific; AGCR1- 3568). Briefly, 10 µg/mL JC-1 was added to the culture medium and then mixed gently. Subsequently, cells were incubated in a CO2 incubator at 37°C for 15 min. Images were then acquired through a fluorescence microscope (EVOS™ XL Core Imaging System, Thermo Fisher Scientific). Red emission of the dye represented a potential-dependent aggregation of JC-1 in the mitochondria. Conversely, green fluorescence appearing in the cytosol after mitochondrial membrane depolarization represented the monomeric form of JC-1. The average intensity of red and green fluorescence was measured using ImageJ software, and the ratio of JC-1 aggregate (red) to monomer (green) intensity was then calculated.

Reactive Oxygen Species (ROS) production

To measure cellular ROS production, C2C12 myotubes were stained with *CellROX R Deep Red Reagent* (Thermo Fisher Scientific; C10491) for 30 min at 37°C and washed with PBS. Images were taken using the EVOS™ XL Core Imaging System, and the mean fluorescence signal intensity was measured using ImageJ. For every experiment assessing cellular oxidative stress, at least three myotubes in each field, five different fields for each replicate, three technical replicates for each treatment were measured.

Statistical Analysis

The investigators quantifying the experimental outcomes were blind to the treatments, and the statistic evaluation of the experimental data was performed by another investigator not directly involved in data collection and parameters measurement. Continuous data are presented as the mean ± SEM. Outliers in the measurements were identified by mean of the interquartile range (IQR),

as either below Q1 - 1.5 IQR or above Q3 + 1.5 IQR and excluded from the analysis. The differences among independent groups in continuous data such as myotube diameters, relative mRNA expression or force were evaluated using Student's t-test or one-way ANOVA test followed by Tukey's multiple comparisons test, as indicated in the figure legends, which were conducted upon verification of the normality assumption using the Kolmogorov-Smirnov test (where applicable). Paired t-test was used to compare data measured on the same statistical units. Kolmogorov-Smirnov test was also used to evaluate differences in the CSA distribution between groups. Statistical significance was assumed for $P < 0.05$. Unless otherwise specified, statistical analyses were performed with GraphPad Prism 8 (GraphPad Software).

7. Introduction to the paper

"DIETS DIFFERENTLY AFFECT BONE HEALTH: MURINE MODELS"

Donatella Mentino, Alessia Annicchiarico, Alessia Provera, ***Alessandro Antonioli****,*

Vesa-Matti Leino, Salvatore Sutti, Flavia Prodam, Heikki Y. Suhonen, Grazia Paola

Nicchia, Maria Mastrodonato, Maria Felicia Faienza, Giacomina Brunetti.

Submitted to Journal of Bone and Mineral Research

Bone health is influenced throughout life [141,142] by the co-participation of several factors, which could be genetic, hormonal, and environmental, particularly physical activity and nutrition/diet [143,144]. As previously introduced, liver, muscle, and bone are in close relationship, particularly in metabolic complications, including MASH and associated conditions such a sarcopenia and osteopenia. Therefore, to further complete knowledge on the overall metabolic shift induced by KD, our study also investigated bone health in animals with established steatohepatitis, aiming to evaluate whether a short-term KD intervention could reverse or exacerbate bone damage induced by WD. WD demonstrated harmful for skeletal health in animal models due to its composition, characterized by high levels of carbohydrates and saturated fast, while deficiency of calcium and vitamin D, which are pivotal for bone resorption and overall health [83,84,145]. On the other hand, KD represents an extremely high fat diet with low carbohydrate levels, and until now studies highlight its negative impact on bone microstructure [146].

Our results indicate that the introduction of KD after a period in WD is not effective in mitigating or counteracting WD-induced damage, although further deterioration of bone microarchitecture was appreciated, with a reduction of trabecular bone volume and thickness. Moreover, also cell homeostasis was impaired, speculated by on one side higher osteoclasts number, suggesting enhanced bone resorption, and on the other side lower osteoblasts number, indicating defects in mineralization or a compensatory response to structural bone loss.

Overall, KD did not appear to mitigate WD-induced detrimental effects on bone, on the contrary it further exacerbates them in some cases.

DIETS DIFFERENTLY AFFECT BONE HEALTH: MURINE MODELS

Donatella Mentino PhD (1)*, Alessia Annicchiarico PhDs (2)*, Alessia Provera PhD (3), Alessandro Antonioli PhD (3), Vesa-Matti Leino PhDs (4), Salvatore Sutti PhD (3), Flavia Prodam MD, PhD (3), Heikki Y. Suhonen PhD (4), Grazia Paola Nicchia PhD (2), Maria Mastrodonato PhD (2), Maria Felicia Faienza MD (1)§, Giacomina Brunetti PhD (2)§.

1. Department of Precision Regenerative Medicine and Ionian Area, University of Bari Aldo Moro, Bari, Italy;

2. Department of Biosciences, Biotechnologies and Environment, University of Bari Aldo Moro, Bari, Italy;

3. Department of Health Science, University of Piemonte Orientale, Novara, Italy;

4. X-ray Laboratory, Department of Physics, University of Helsinki, Helsinki, Finland.

*: equal contribution as first authors.

§: equal contribution as last authors.

Conflict of Interest: The authors declare no conflict of interest.

Ethical Approval:

Corresponding author:
Giacomina Brunetti, PhD
Department of Biosciences, Biotechnologies and Environment, University of Bari Aldo Moro,
Via Orabona, 4
70125 Bari, Italy

7.1. Abstract

Bone is a dynamic specialized connective tissue that undergoes continuous remodelling to preserve its health. Bone health is influenced throughout life by a combination of genetic, hormonal, environmental factors, physical activity and diet. The aim of this study is to evaluate the effects of diets on femurs of mice fed for 16 or 20 weeks with normal diet (ND16w and ND20w) or Western diet (WD16w and WD20w) and for 20 weeks with their combinations with ketogenic diet (KD) (WD+ND20w, ND+KD20w, WD+KD20w). Micro-CT analysis on femoral cancellous bone revealed decreased bone volume fraction (BV/TV) and trabecular thickness in mice fed a combined WD+KD20w compared to WD20w ($p<0.05$). Cortical bone thickness was significantly lower in mice fed WD16w and WD20w compared to those fed ND16w and ND20w ($p<0.05$), as well as, in mice fed WD20w and WD+KD20w compared to WD+ND20w ($p<0.01$). Consistently, histological analysis revealed that the number of osteoclasts per bone perimeter on cancellous bone strongly increases in WD+KD20w compared with ND20w and WD20w ($p<0.05$). In addition, a combined KD produced a decrease of the number in osteoblasts in the cancellous bone ($p<0.05$). Whereas, in cortical bone, comparing WD+KD20w with WD20w an increase was observed ($p<0.05$), this suggests that the KD may have differential effects depending on the baseline condition. Osteocyte numbers did not significantly change comparing the different treatments. Mallory staining supports micro-CT results on both cortical and cancellous bone. In conclusion, we demonstrated that different diets with progressively increasing fat content (ND, WD and KD) affect bone health.

Keywords: Diet, Bone health, mouse model, bone cells

7.2. Introduction

Bone is a dynamic tissue that undergoes continuous remodelling to preserve its health, shape, and structural integrity while regulating mineral homeostasis[1,2]. Bone remodelling is a complex biological process that involves the resorption activity of mineralized bone tissue by osteoclasts (OCs) and the production of new bone matrix by osteoblasts (OBs)[3]. It is orchestrated by osteocytes originating from osteoblasts that become embedded in the bone matrix over time. These cells form an extensive network by connecting through long cellular processes within tiny canaliculi. Making up about 90% of bone cells, osteocytes play a crucial role in communicating with surface bone cells and regulating bone remodelling[4]. Together, these processes maintain the dynamic balance of bone renewal and repair, ensuring skeletal health and adaptability over time[5].

Bone health is influenced throughout life[6,7] by a combination of genetic, hormonal, and environmental factors, in particular physical activity and nutrition/diet[8,9]. Calcium and vitamin D intake are the critical nutritional factors most studied until now. Diets with changes in their carbohydrates, protein and fat content, impact differently on bone health, in particular, high-fat content is associated with bone loss[10]. Consistently, using different mouse models and diets, researchers have investigated their impact on bone health showing interesting results for western and ketogenic diets (WD and KD, respectively). Mimicking a Western fast-food diet with a high content of fats and carbohydrates, the WD may have a particularly harmful impact, as it not only contains high levels of saturated fats, processed and simple carbohydrates but is also deficient in calcium and other essential minerals that support calcium absorption and bone health[11,12]. WD showed strong effects on skeletal health as demonstrated in animal models[10]. In detail, in 9-week-old female C57bL/6J mice after 10 weeks of WD the tibial cross-sectional area, cortical thickness, and maximum load were significantly decreased, the serum levels of the OC marker Tartrate-Resistant Alkaline Phosphatase (TRAP) and the pro-osteoclastogenic Receptor activator of nuclear

factor kappa-B ligand (RANKL) were increased[13]. In ovariectomized rats WD significantly decreased bone mineral density (BMD) in the tibia and femora, serum osteocalcin (OCN) levels, urine deoxypyridinoline (DPD) amount, and the OC-specific marker expression cathepsin-K, suggesting that WD affected bone health[14]. Other studies have demonstrated the detrimental effects of a WD on tibial cortical bone[15]. Different studies have reported that the bone loss associated with a WD may be due to the augmented levels of inflammatory cytokines with consequent increased OC activity.

The KD represents an extremely high-fat diet affecting negatively bone microstructure[16]. KDs are also associated with potential negative effects on bone health. Previous research highlighted the impact of KDs on bone mineral content (BMC), osteopenia, osteoporosis, hypercalciuria, urine acidification, hypocitraturia and risk of decreased BMD[16-19]. In detail, Wu et al.[17] using micro-CT in 8-week-old mice for 12 weeks showed that both femoral cancellous and cortical bone were negatively affected. Aikawa et al.[20] fed KD-aged mice under exercise training showing impaired bone mass, cancellous microstructure, and compromised beneficial effects of physical activity on bone health. Liu et al.[21] reported that KD delays the spinal fusion in rats after surgery. Xu et al.[22] reported that rats fed with KD showed high TRAP activity and reduced alkaline phosphatase activity.

Based on this background, we aimd to evaluate the effects of different dietary patterns on bone health in mouse models. We fed mice for 16 and 20 weeks with a normal diet (ND16w, ND20w) or Western diet (WD16w, WD20w), and for 20 weeks with combinations of normal diet + Western diet (ND+WD20w), normal diet+ketogenic diet (ND+KD20w) or Western diet+ketogenic diet (WD+KD20w) to explore whether the swith to a ketogenic diet is protective or detrimental on bone

7.3. Materials and Methods

Mouse models and experiment design

Thirty-five 4-week-old male mice, strain (C57BL/6J) were purchased from Charles River Laboratories Italy (Calco, LC, Italy). After four weeks of acclimatization, 8-week-old mice were fed for 16 and 20 weeks with normal diet (ND16w, ND20w) or Western diet (WD16w, WD20w), and for 20 weeks with combinations of normal diet + Western diet (ND+WD20w: 16 weeks ND + 4 weeks WD), normal diet + ketogenic diet (ND+KD20w: 16 weeks ND + 4 weeks KD) or Western diet + ketogenic diet (WD+KD20w: 16 week WD + 4 week KD20).

Diet composition was the following:

• ND (Control group): mice were fed a standard rodent diet consisting of 13 % Kcal fat, 20 % Kcal proteins, and 67% Kcal carbohydrates (Envigo).

• WD: mice were fed a diet composed of 42% Kcal fat, 15% Kcal proteins, 43% Kcal carbohydrates and enriched with 1.25% cholesterol (Laboratorio Dottori Piccioni, Gessate, Italy).

• KD: mice were fed a choline-sufficient, cholesterol-free diet composed of 90.5% Kcal vegetal fat (hydrogenated coconut oil), 9.2% Kcal proteins, and 0.3% Kcal carbohydrates (Laboratorio Dottori Piccioni, Gessate, Italy).

Animals had free access to diet and tap water ad libitum and were exposed to a 12-hour light/12-hour dark cycle. After 16 and 20 weeks of diet, animals were euthanized by isoflurane and cervical dislocation (Figure 1). Femurs were rapidly removed, fixed with 4% (vol/vol) formaldehyde for 24 hours at 4°C and processed for microcomputed tomography (Micro-CT) and histological analysis.

This animal interventional study is in accordance with the European Law Implementation of Directive 2010/63/EU and all experimental protocols were reviewed and approved by the Veterinary Department of the Italian Ministry of Health (authorization N° 411/2020-PR).

Microcomputed tomography analysis of femurs

For micro-CT, images were acquired using Phoenix Nanotom S (formerly GE, currently Waygate Technologies owned by Baker Hughes Inc) with the following settings: X-ray Tube Voltage (Peak) *U*= 60.00 kVp; X-ray Tube Current *I*=120.00 µA; Integration Time *T*=250.00 ms; Number of Projections *N*=800.00, Magnification *M*= 20.00, Voxel Size (Cubic) cubic, voxel= 5.00 μm^3.

The reconstructed 3D images were then all processed through the exact same image processing and measurement workflow, in which the ImageJ software and its plugins MorphLibJ and BoneJ were used. Segmentation of the 3D images was performed (in 2D) using the image processing method *morphological filtering* on binary images, which were obtained by thresholding the original images with the Auto Threshold algorithm Otsu[23]. The algorithm utilizes the image histogram to calculate a level of brightness that determines whether an individual voxel (3D-pixel) is turned white (if its brightness is above the level) or black (if below). The algorithm Otsu appears to delineate the edge of the bone-density material quite precisely, however, if the delineation is not sufficiently precise, an additional initial filtering of the images or some other thresholding algorithm could feasibly be used.

The cortical parameters measured included cortical thickness (Ct.Th), total cross-sectional area (Tt.Area), cortical bone perimeter (Ct.Pm), and marrow cross-sectional area (Marrow Area). The trabecular parameters measured included bone volume/total volume (BV/TV), number (Tb.N), thickness (Tb.Th), and separation (Tb.Sp).

Histological analysis

To evaluate bone health and perform bone histomorphometry, mouse femurs were decalcified and embedded in paraffin wax. Serial sections, 5 µm thick, were cut using a rotary microtome (Leica RM

2155, Leica, Wetzlar, Germany.)[24,25]. The sections were deparaffinized, rehydrated through graded alcohol series, and stained as follows:

Hematoxylin and Eosin (H&E, Sigma Aldrich, Milan, Italy)[26] staining was applied for osteoblast analysis, assessing osteoblast number per bone cancellous perimeter (N.Ob/Tb.Pm) and per bone cortical perimeter (N.Ob/Ct.Pm). On these same section osteocyte number was determined.

Tartrate-Resistant Alkaline Phosphatase (TRAP, Sigma Aldrich, Milan, Italy) staining solution was used to evaluate osteoclast number per bone cancellous perimeter (N.Oc/Tb.Pm).

Images were captured using a Nikon Eclipse E600 light microscope equipped with a DS-Fi3 microscope camera (Nikon Instruments Ltd., Campi Bisenzio, Florence, Italy).

Masson trichrome Goldner staining was performed using a commercially available kit, according to the manufacturer's instruction (Masson trichrome Goldner Bio-Optica).

All measurements were performed using ImageJ, for Masson evaluation Adobe Photoshop (version 25.12.1) was used.

Statistical analyses

Statistical analyses were conducted using Student's t-test according to the Statistical Package for the Social Sciences software (IBM SPSS, Armonk, NY, USA). Thirty-four mice were used for the analysis ND16w (n= 4), WD16 (n= 5), ND20 (n= 5), WD20 (n= 5), WD+ND20w (n= 6), ND+KD20w (n= 4), WD+KD20w (n= 5). Results were considered statistically significant at $p < 0.05$. GraphPad was used for graphs.

7.4. Results

Diet effects on bone microstructures.

Diet consistently affects bone health, changing the content of carbohydrates, protein and fat in the diet has a different impact on bone health. In the present study, utilizing micro-CT, we analysed the femur microarchitectural features from C57BL/6J mice fed WD, KD and their combination for 16 and 20 weeks (Figure 2, Table 1). Micro-CT analysis of the cancellous bone region of femoral bones showed that mice fed for 16 or 20 weeks with ND or WD respectively did not show significant differences in BV/TV%, while, interestingly, WD+KD20w had a significant BV/TV% decrease compared to mice fed only with WD20w ($p= 0.04$). A similar trend is evident with a significant reduction for Tb.Th comparing WD+KD20w and WD20w, $p= 0.039$. Differently, Tb.N and Tb.Sp did not display significant variation among the different kinds of diet. In cortical bone, a significant decrease in Ct.Th comparing mice fed ND16w or ND20w with those fed WD16w or WD20w was observed ($p= 0.049$ and $p= 0.004$, respectively). Interestingly, mice fed the combined WD+ND20w showed a significant increase in Ct.Th% compared to mice fed WD20w, $p= 0.001$. Furthermore, mice fed the combined WD+KD20w diet showed a significant decrease in Ct.Th% with respect to mice fed the combined WD+ND20w diet ($p= 0.002$). All these data highlight the detrimental effects of KD on cancellous and cortical bone, whereas WD negatively affects cortical bone compared with ND both at 16 and 20 weeks of treatment.

Effect of diets on osteoclast number *ex vivo*.

The interesting findings derived from micro-CT analysis prompted us to count bone cells through histological analysis in cortical and trabecular bone. Histomorphology of trabecular bone using TRAP staining to highlight OCs was performed and the number of OCs per trabecular bone perimeter N.Oc/Tb.Pm assessed (Figure 3). Our results display that mice fed for 16 or 20 weeks with ND or WD

respectively did not show significant differences in OC number on cancellous bone. Interestingly, the number of OCs strongly increases in WD+KD20w mice compared with the ND20w group, (p=0.002). Furthermore, mice fed WD+KD20w with respect to the WD20w group showed a significant enhancement, (p=0.032). Of note, the trabecular bone of mice switching to the KD diet (ND+KD20w and WD+KD20w) displayed a significantly high number of OCs compared to the WD+ND20w group, (p= 0.004 and p= 0.037). These findings support micro-CT results and indicate that the combination of the KD diet with ND or WD over a 20-weeks leads to a marked increase in osteoclast number, suggesting enhanced bone resorption under these conditions.

Effect of diets on osteoblast number *ex vivo*.

The H&E-staining analysis for the number of OB per bone trabecular perimeter (N.Ob/Tb.Pm) of cancellous bone region of femoral bones showed that mice fed for 16 or 20 weeks with WD show a reduction compared to ND (p = 0.036 and p = 0.046, respectively).

The N.Ob/Tb.Pm decreased significantly compared to ND+KD20w versus ND20w (p = 0.041), as well as ND+KD20w versus WD+ND20w (p = 0.020). An increase of osteoblast's number was observed in mice fed WD+ND20w combined diet versus WD20w (p =0.019) similarly to WD+KD20w fed mice compared to WD20w, even if this latter was not statistically significant (Fig.4).

Furthermore, a significant decrease in the OB number per bone cortical perimeter (N.Ob/Ct.Pm) was observed in mice fed combined ND+KD20w diet compared versus ND20w (p = 0.029), instead comparing WD+KD20w with WD20w an increase was observed (p = 0.047). This suggests that the KD may have differential effects depending on the baseline condition.

Comparing the group of mice fed with the WD16w or WD20w diet showed a decrease in the number of OBs *vs* the group fed with the ND16w or ND20w respectively but not statistically significant (Fig.5).

Diets and osteocyte number *ex vivo*.

The results about the strong effects of diet on cortical bone prompted us to evaluate osteocytes. As shown in Fig. 5I-L, H&E staining revealed that osteocyte number per bone surface (Ot.N/BS) did not significantly change comparing the different conditions, although a trend towards the increase is evident comparing the group of mice fed with the WD16w or WD20w *vs* the groups fed with the ND16w or ND20w respectively, and ND+KD20w vs ND20w fed mice; while the group fed with WD+KD20w showed a not significant decrease compared to WD20w.

Effect of diets on osteoid surface.

The obtained results prompted us to evaluate the osteoid surface in both cortical and cancellous bone (Figure 6 - 7). Masson staining evaluations supported Micro-CT results showing an increase of green area (osteoid surface) in cortical bone with the increase of fat in the diet. In detail, a significant increase was evident for WD16w compared to ND16w ($p = 0.03$), WD20w vs ND20w ($p = 0.029$), WD+ND20w vs ND20w ($p = 0.003$) and vs WD20 ($p = 0.050$), ND+KD20 vs ND20 ($p = 0.018$), as well as WD+KD20 vs WD20w ($p = 0.006$) (Figure 6). The highest area of osteoid surface was measured in the WD+KD20 group (2-fold compared with the WD20w group). Cancellous bone evaluation showed a significant increase of osteoid surface comparing WD+KD20w group vs WD20w ($p= 0.004$), thus reflecting micro-CT results (Figure 7). Additionally, a statistically significant increase in osteoid surface was evident comparing WD+ND20w and ND+KD20w vs WD+KD20w ($p= 0.03$ and $p= 0.04$). The obtained data on cancellous bone allowed us to understand the detrimental effect of KD after the WD (WD+KD20w diet) with respect to the ND diet after WD (WD+ND20w diet). Differently, KD after the ND (ND+KD20w group) determined a decrease of osteoid surface with respect to ND20w that, even if not significant, suggested a tendency to the recovery of bone health.

Table 1: MicroCT parameters

	BV/TV%	**Tb.N [1/mm]**	**Tb.Th µm**	**Tb.Sp µm**	**Ct.Th mm**	**Tt.Area mm²**	**Ct.Pm mm**	**Ma.Ar mm²**
ND16	6,36 ± 1,73 vs WD20 p= 0.004	2,75 ± 0,25	51,77 ± 4,51	313,93 ± 27,98	0,1729 ± 0,0087 vs WD16 **p= 0.049**	2,67 ± 0,18	6,66 ± 0,27	1,76 ± 0,13
WD16	6,24 ± 1,29	3,06 ± 0,35	48,14 ± 6,30	282,07 ± 31,80	0,1600 ± 0,0090	2,77 ± 0,35	6,77 ± 0,53	1,91 ± 0,26
ND20	6,31 ± 2,28	2,66 ± 0,19	53,67 ± 6,32	323,53 ± 21,32	0,1688 ± 0,0051 vs WD20 **p=0,0039**	2,65 ± 0,28	6,69 ± 0,39	1,76 ± 0,21
WD20	7,23 ± 2,36	2,88 ± 0,47	52,31 ± 7,59	304,07 ± 62,11	0,1521 ± 0,0078	2,91 ± 0,39	6,96 ± 0,45	2,07 ± 0,32
WD+ND20	5,38 ± 3,19	2,80 ± 0,25	50,37 ± 7,73	309,63 ± 28,98	0,1695 ± 0,0042 vs WD20 **p= 0.001**	2,76 ± 0,47	6,73 ± 0,62	1,86 ± 0,39
ND+KD20	7,68 ± 2,30	2,84 ± 0,08	52,21 ± 1,98	300,45 ± 10,69	0,1750 ± 0,0028 Vs ND20 *p= 0,06*	2,81 ± 0,21	6,82 ± 0,30	1,87 ± 0,18
WD+KD20	4,49 ± 1,09 vs WD20 **p= 0.046**	3,01 ± 0,14	43,19 ± 3,37 vs WD20 **p= 0.039**	289,53 ± 12,59	0,1417 ± 0,0151 vs WD+ND 20 **p= 0.0018**	2,58 ± 0,30	6,52 ± 0,43	1,85 ± 0,29

Bone volume/total volume (BV/TV), trabecular number (Tb.N), thickness (Tb.Th), and separation (Tb.Sp), cortical thickness (Ct.Th), total cross-sectional area (Tt.Area), cortical bone perimeter (Ct.Pm), and marrow cross-sectional area (Marrow Area).

7.5. Discussion

In this work we examine the effects of different dietary patterns ND, WD and KD with progressively increasing fat content, ranging from 13% to 90.5%, on bone health in mouse models. We demonstrated by Micro-CT analysis that in cortical bone a significant decrease was observed in Ct.Th in mice fed with WD16w and WD20w compared to ND16w and ND20w, respectively, as well as mice fed the combined WD+KD20w diet *vs* WD+ND20w diet. Cancellous BV/TV% and Tb.Th decrease in combined WD+KD20w diet compared to mice fed only with WD20w. Consistently, significant differences emerged by OC, OB and osteocyte counting as well as Mallory staining in our samples.

Compared to studies already carried out to investigate the effects of WD and KD on bone health feeding animals for different times, as novelty we evaluated the impact of WD for a long time (20 weeks) and the switching from WD16w to either ND or KD for 4 weeks as well as from ND16w to KD for 4 weeks, specifically WD+ND20w, WD+KD20w, and ND+KD20w. In detail, we displayed a significant reduction in femur Ct.Th caused by WD in both times of 16 and 20 weeks over ND. Previous researche evaluated the impact of WD in Sprangue-Dewley female rats for 10 [15,27] and for 12 weeks[14] and reported that WD negatively affects bone health. In particular, Hou et al.[27] showed that WD decreased the relative size of the femoral neck cortical shell and increased the trabecular core compared to rats fed a control diet. Li et al.[15] found that WD altered bone mechanical properties, in fact, tibias had significantly minor maximum load, failure energy, and tensile stress at the proportional limit than controls. Furthermore, Dong et al.[14] reported detrimental effects of WD on cancellous bone with reduced Tb.BMD in tibia head and femoral end with respect to ND fed rats. Interestingly, Lorincz et al.[13] using female mice fed for 20 weeks with WD demonstrated a significant reduction of CT.Th, cross-sectional area, and load at maximum in tibia.

In line with these findings, we also reported a significant decrease in OB numbers observed in WD compared to ND suggesting that the WD may have a negative effect on OB maintenance or

proliferation. This could be due to the high-fat content and inflammatory nature of the WD, which might impair OB cellular functions. Additionally, the OB number increases in the comparison of WD20w to WD+ND20w suggesting that shifting from WD to ND (dietary intervention) may balance some of the negative effects associated with the WD consumption. These data suggested that this improvement could be linked to the potential for ND components to counterbalance the harmful effects of high fat diet (HFD), and maybe also high sugars content on bone health. Literature data reported a significant decrease of OBs in HFD mice than in ND and consistently serum PINP levels were reduced in the same groups[28]. Interestingly, *in vitro* experiments demonstrated that treating the osteoblastic cell line MC3T3 with NEFA (the fatty acids oleate and palmitate, 1:2 mixture) osteoblastogenesis is impaired as demonstrated by the reduction of RUNX2 levels[29].

Noteworthy, we found that switching to KD from WD induces a decrease of BV/TV% compared to controls along with Ct.Th and Tb.Th, imply a negative effect of either WD or KD on the quality of trabecular and cortical bone in mice. On this vein, Wu et al.[17] and Liu et al.[18] demonstrated that mice fed a KD for 12 weeks exhibited compromised micro-architecture of cancellous bone and the morphological structure of cortical femur, together with altered mechanical properties. These macroscopic features are linked to the increase of OCs number[17,18] and decrease osteocalcin positive cells[18]. An increased TRAP and cathepsin-K mRNA levels were also detected in HFD[28]. Consistently, our histological analysis revealed the number of OCs on cancellous bone strongly increases in WD+KD20w compared with ND20w and WD20w. However, in cortical bone, comparing WD+KD20w diet with WD20w an increase was observed in OBs number, suggesting that KD may have differential effects depending on the baseline condition. Literature data linked the general increased osteoclastogenesis associated to HFD with the enhanced levels of the pro-osteoclastogenic cytokine RANKL as well as RANKL/OPG ratio[29].

It has been reported that RANKL can be produced by osteoblasts as well as adipocytes[30]. In fact, an increased number of marrow adipocytes is linked to HFD. At the cellular level, adipocytes and OBs originate from Bone Marrow Stromal cells, obesity promotes the adipocytes differentiation through the PPARγ pathway and inhibiting OB differentiation, and thus bone formation[31]. Consistently, fat accumulation in the bone marrow stimulates adipogenesis[32], leading to increased production of the pro-inflammatory cytokines by the bone marrow that promote the proliferation and differentiation of OCs, cells responsible for bone resorption. Inflammation leads to increased osteoclastogenesis, which correlates with increased RANKL and decreased OPG. This suggests that HFD may contribute to bone loss by modulating the RANK/RANKL/OPG axis in favour of osteoclastgenesis[33] resulting in heightened OC activity and reduced OB turnover[32].

Interestingly, we did not find significant differences in osteocyte counts associated to the different diets. Our data were supported by literature data that did not reported a significant variation of osteocyte number and markers in HFD[34-36], however an accelerated osteocyte senescence was evident, as demonstrated by the high expression levels of p16 and p21[34]. Dole et al. reported that WD increased perilacunar/canalicular remodeling through osteocyte-intrinsic regulation of enzymes implicated in this signaling, compromise lacuna-canalicular network integrity and mitochondrial activity, and induce cellular senescence[36].

In general, consumption of diets composed of high amounts of saturated fat has been reported to lead to the formation of insoluble soap complexes preventing calcium absorption[13]. Furthermore, it is known that ingestion of sucrose alone determines calcium excretion in the urine or hypercalciuria. Consequently, diets that include both high-saturated fat/sucrose i.e. our WD have a profound effect on skeletal structural integrity also for the effect on calcium absorption and excretion[13].

About human studies, it is clearly known that WD and thus obesity is linked to osteopenia/osteoporosis. However, different authors also focused on KD and bone effect with

contrasting results also depending on Kcalories content, age, gender, the presence of a physical activity protocol. Carter et al. after three months treating with KD no significant changes of bone serum markers detected[37]. Athletes after 3.5 weeks of KD showed an increase of the bone resorption markers[38]. In an additional study, healthy women performing an 8 weeks KD reported an increase of the BMD compared with another female group fed a normal diet[39].

In conclusion, in our animal model the progressive increase of fat in diets led to parallel deterioration of bone health and KD was not able to switch the negative features induced by WD. Thus, a healthy balanced nutrition is a critical step for the skeletal health.

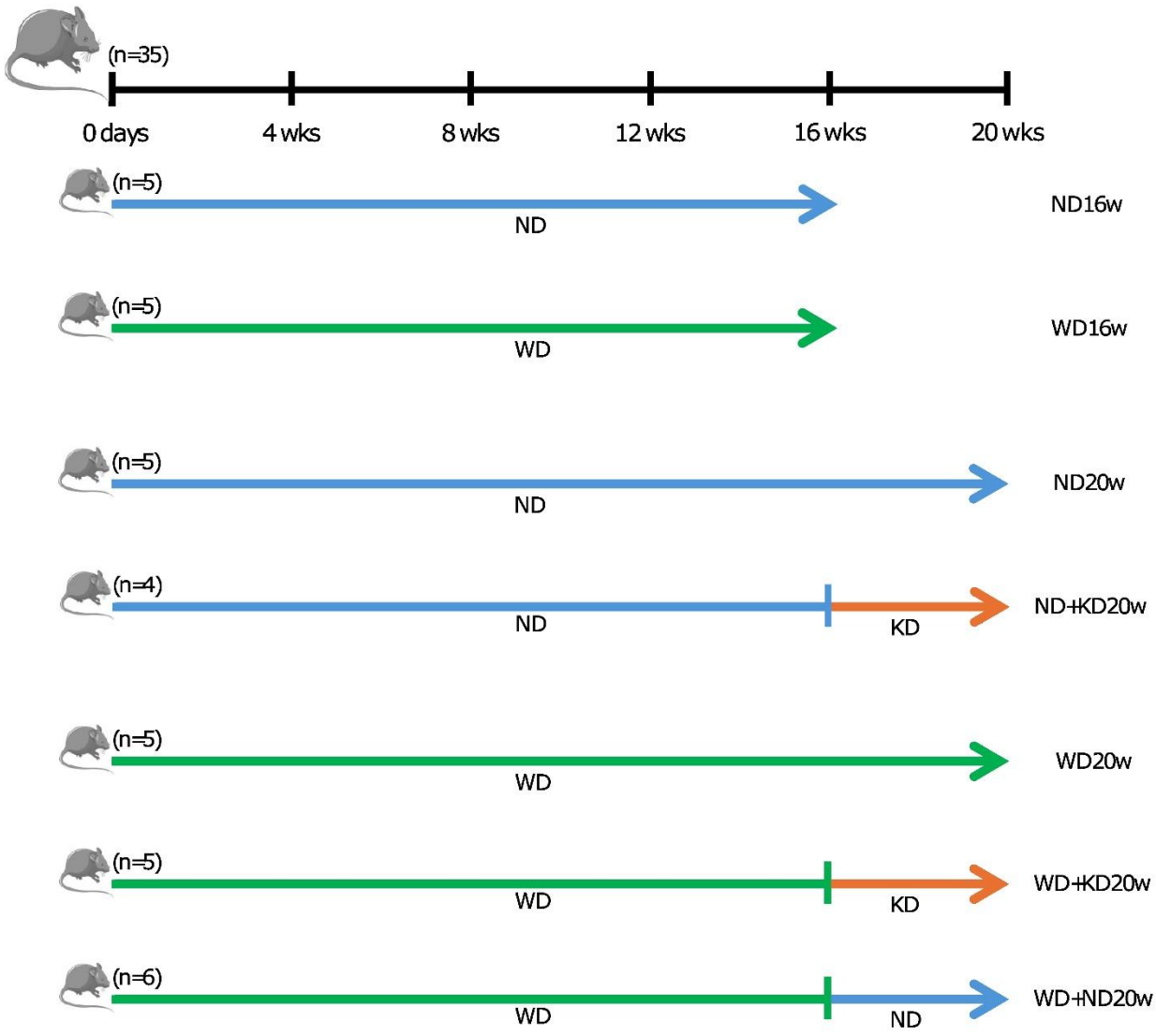
(n=35)
0 days
4 wks
8 wks
12 wks
16 wks
20 wks
(n=5)
ND
ND16w
(n=5)
WD
WD16w
(n=5)
ND
ND20w
(n=4)
ND
KD
ND+KD20w
(n=5)
WD
WD20w
(n=5)
WD
KD
WD+KD20w
(n=6)
WD
ND
WD+ND20w

Figure 1

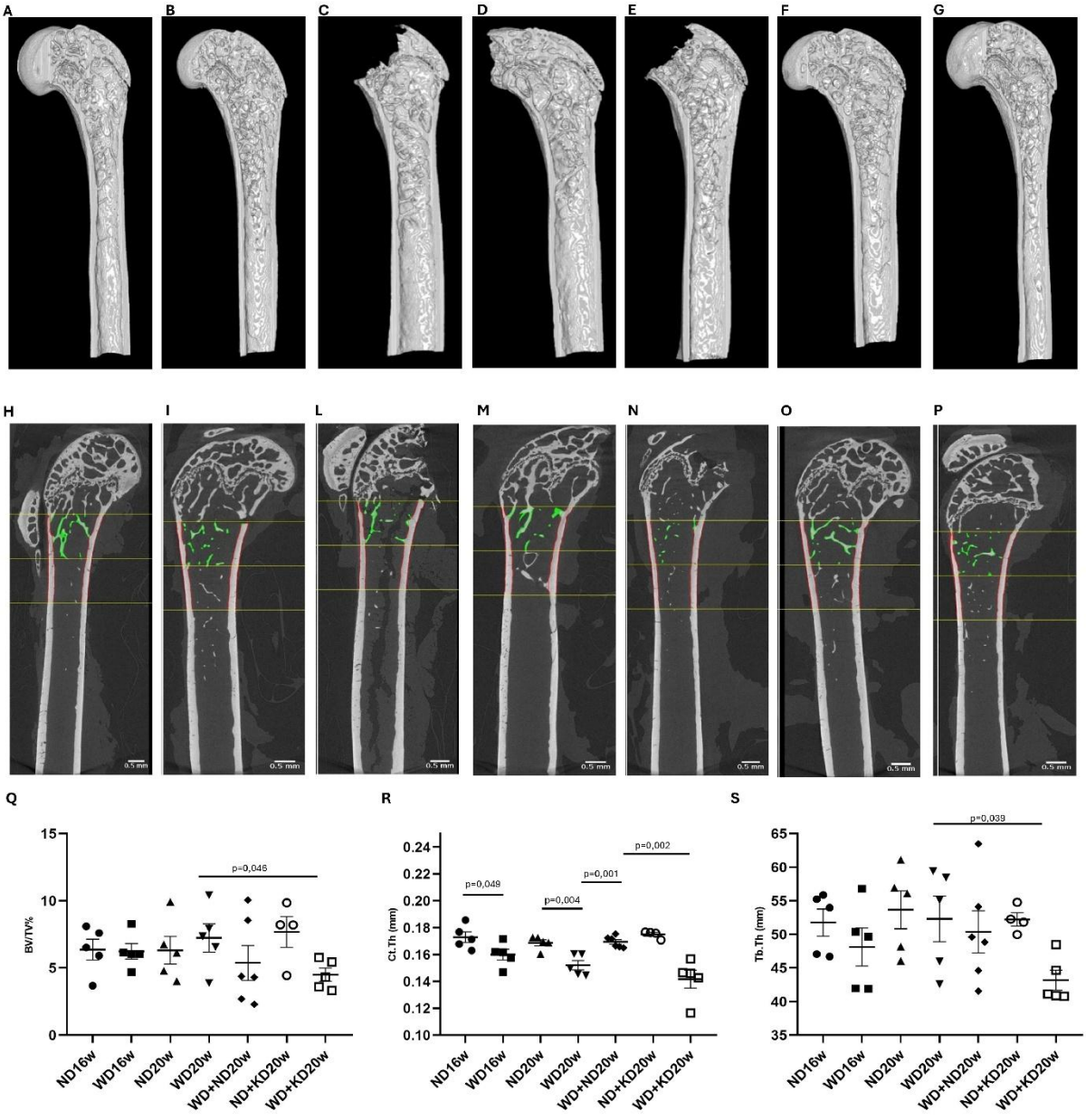
A
B
C
D
E
F
G
H
I
L
M
N
O
P
0.5 mm
Q
BV/TV%
p=0,046
R
Ct.Th (mm)
p=0,049
p=0,004
p=0,001
p=0,002
S
Tb.Th (mm)
p=0,039
ND16w
WD16w
ND20w
WD20w
WD+ND20w
ND+KD20w
WD+KD20w

Figure 2

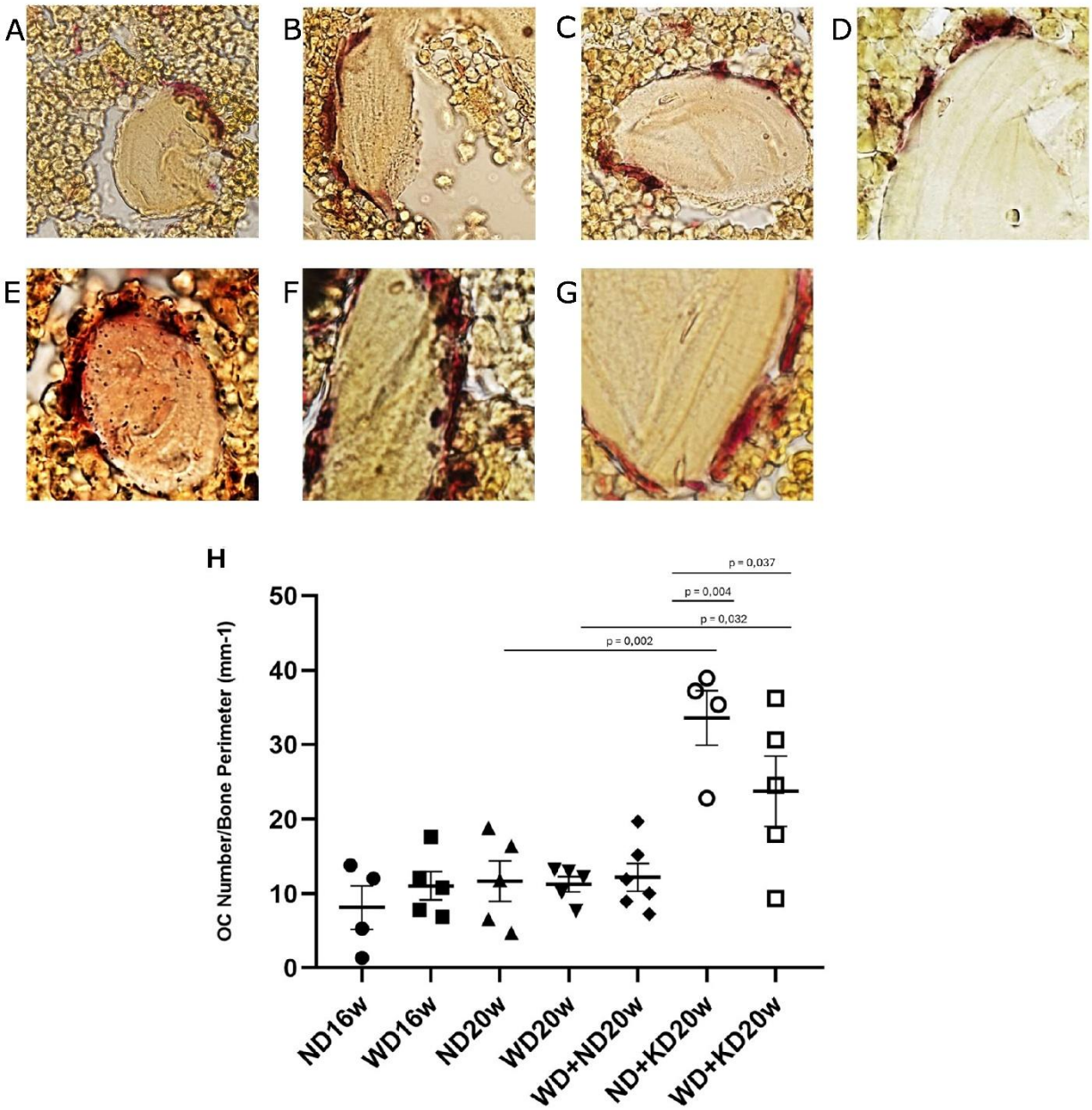
A
B
C
D
E
F
G
H
p = 0,037
p = 0,004
p = 0,032
p = 0,002
OC Number/Bone Perimeter (mm-1)
50
40
30
20
10
0
ND16w
WD16w
ND20w
WD20w
WD+ND20w
ND+KD20w
WD+KD20w

Figure 3

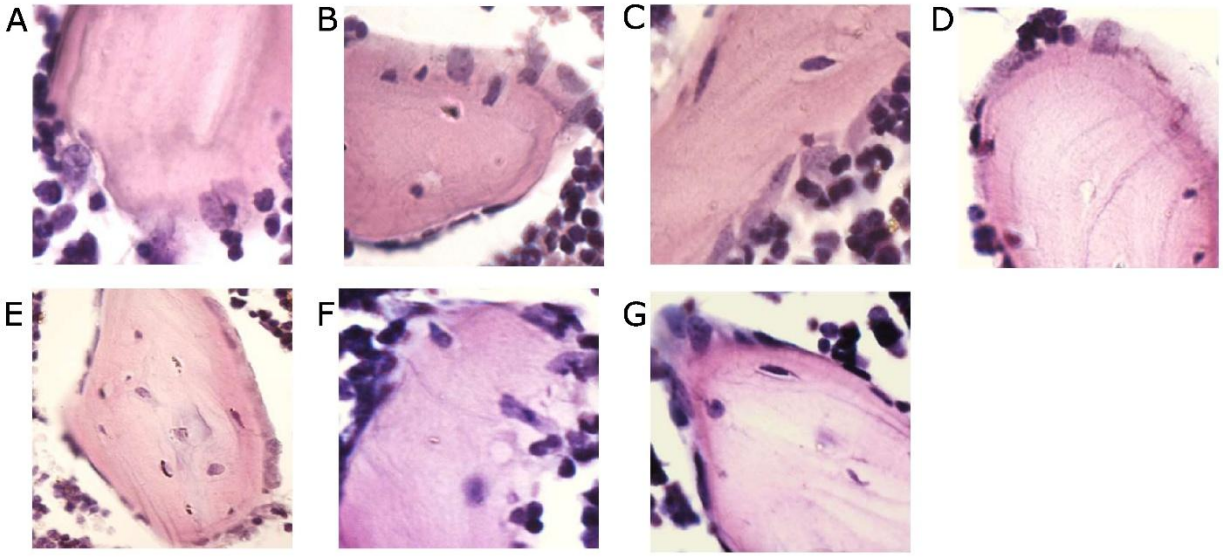
A
B
C
D
E
F
G

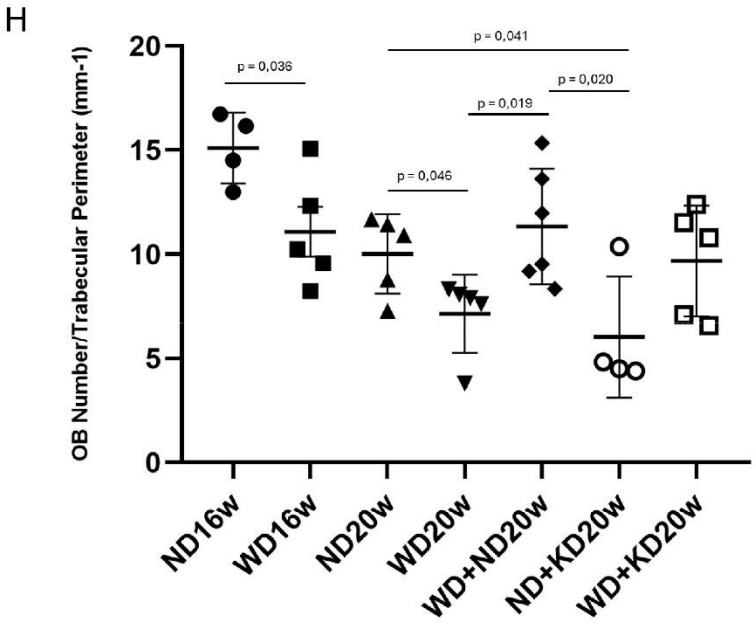
H
OB Number/Trabecular Perimeter (mm-1)
20
15
10
5
0
p = 0,036
p = 0,041
p = 0,020
p = 0,019
p = 0,046
ND16w
WD16w
ND20w
WD20w
WD+ND20w
ND+KD20w
WD+KD20w

Figure 4

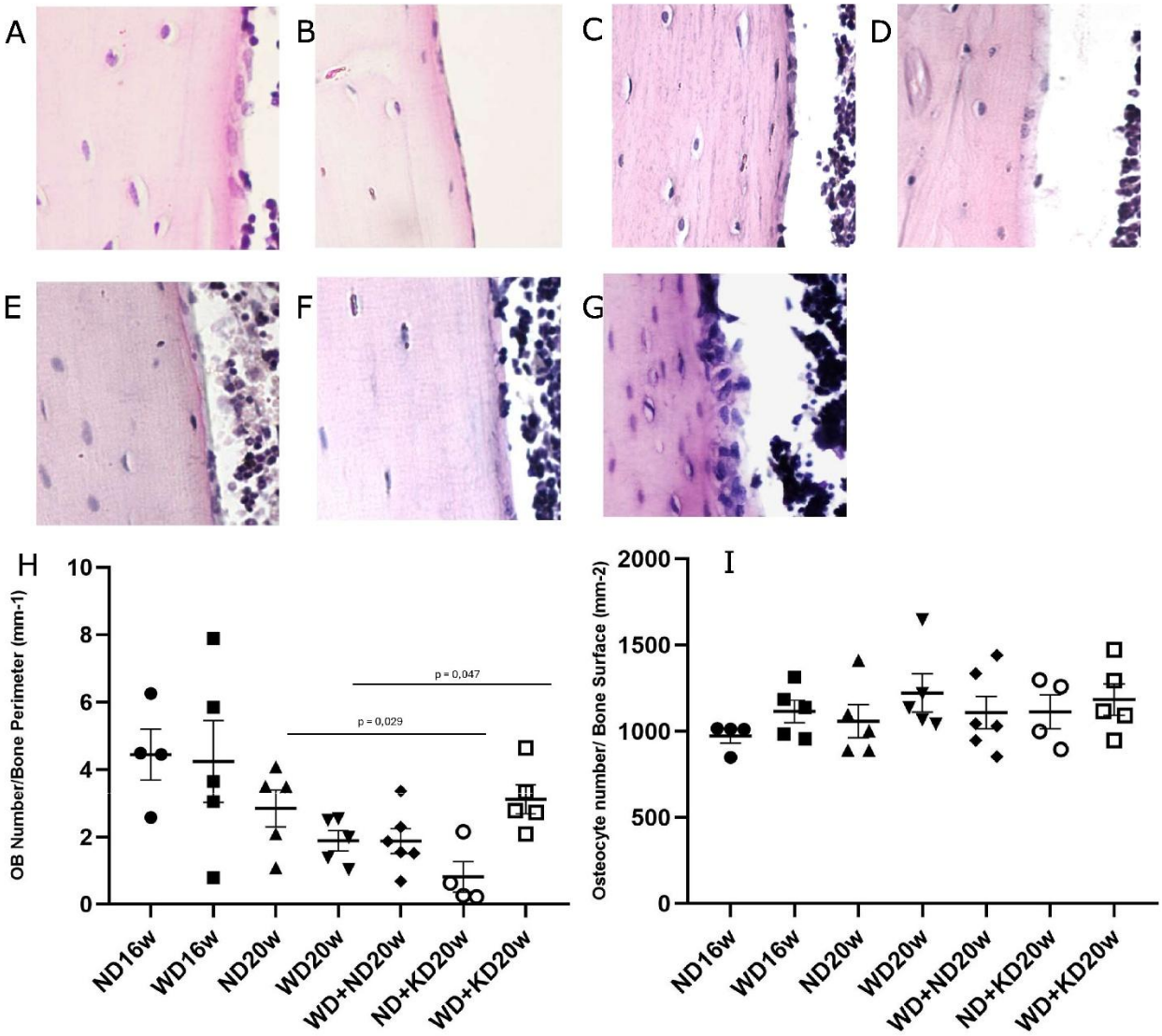
A
B
C
D
E
F
G
H
OB Number/Bone Perimeter (mm-1)
10
8
6
4
2
0
p = 0,047
p = 0,029
ND16w
WD16w
ND20w
WD20w
WD+ND20w
ND+KD20w
WD+KD20w
I
Osteocyte number/ Bone Surface (mm-2)
2000
1500
1000
500
0
ND16w
WD16w
ND20w
WD20w
WD+ND20w
ND+KD20w
WD+KD20w

Figure 5

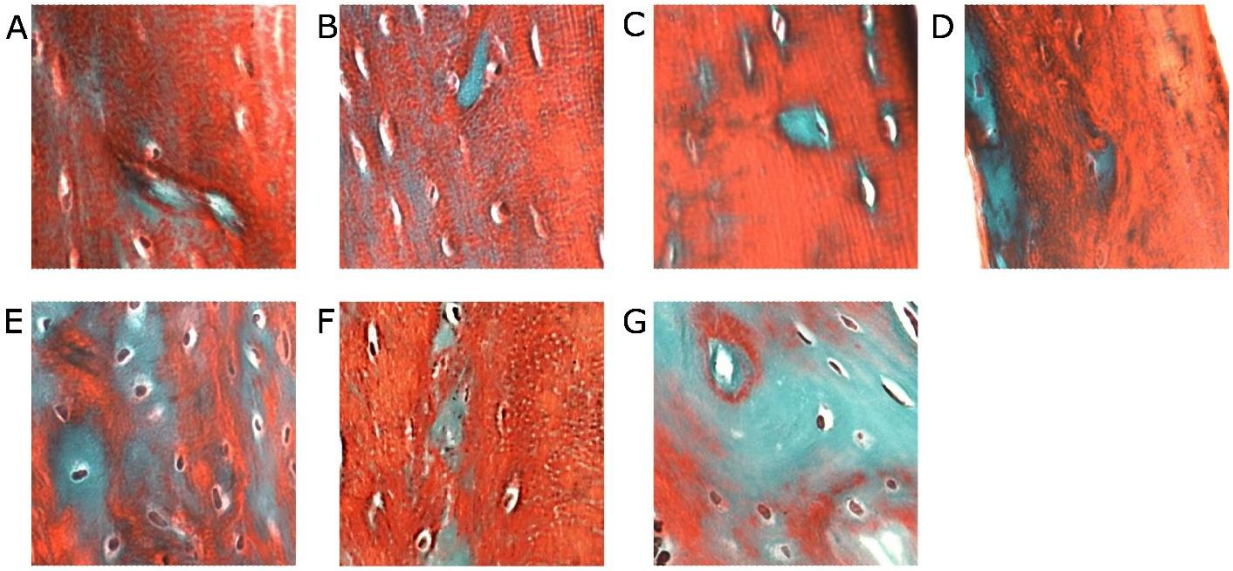
A
B
C
D
E
F
G

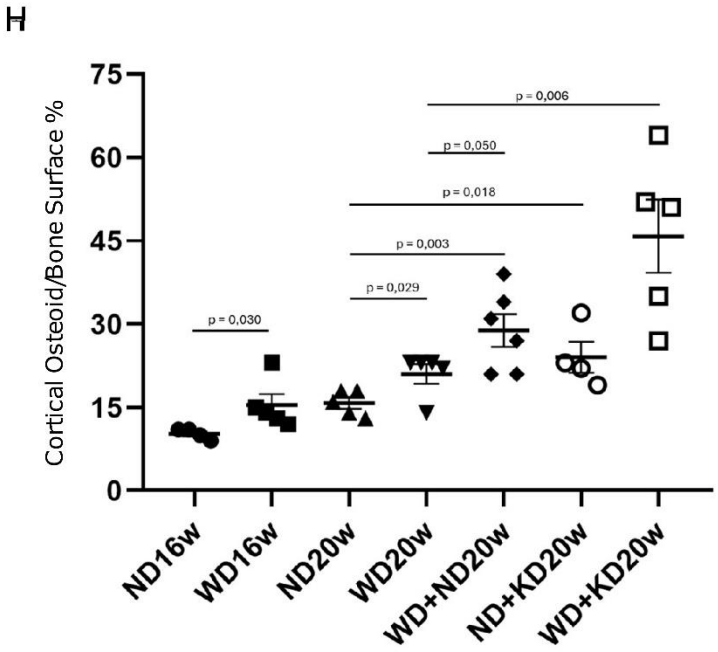
H
Cortical Osteoid/Bone Surface %
75
60
45
30
15
0
p = 0,006
p = 0,050
p = 0,018
p = 0,003
p = 0,029
p = 0,030
ND16w
WD16w
ND20w
WD20w
WD+ND20w
ND+KD20w
WD+KD20w

Figure 6

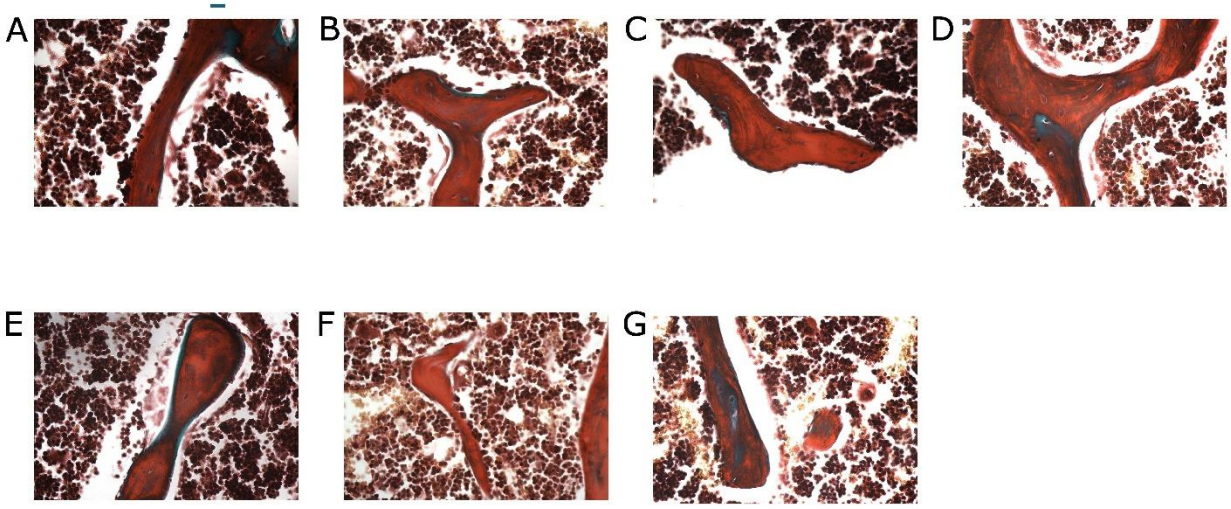
A
B
C
D
E
F
G

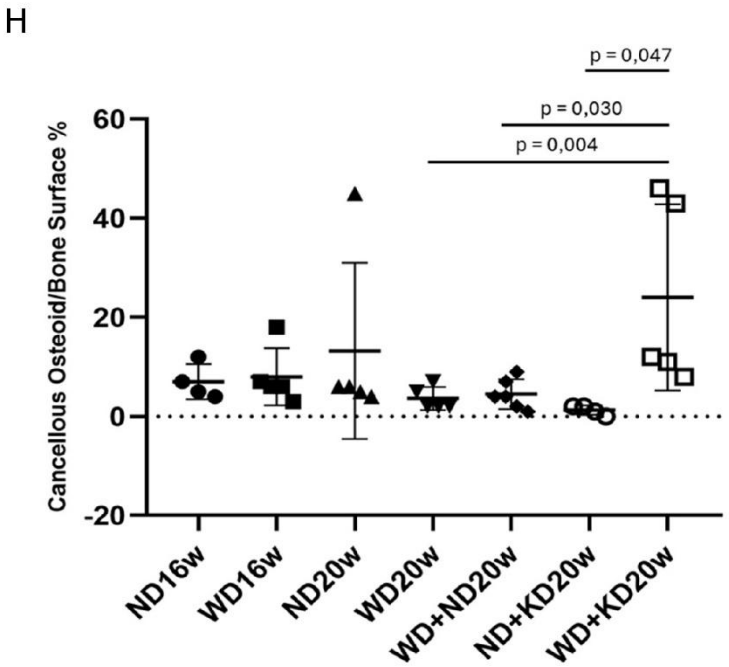
H
p = 0,047
p = 0,030
p = 0,004
Cancellous Osteoid/Bone Surface %
60
40
20
0
-20
ND16w
WD16w
ND20w
WD20w
WD+ND20w
ND+KD20w
WD+KD20w

Figure 7

7.6. Figure legends:

Figure 1. Experimental design. 35 mice were divided randomly into seven groups: 1) n=5 mice fed with normal diet for 16 weeks (ND16w); 2) n=5 fed with Western diet for 16 weeks (WD16w); 3) n=5 mice fed with normal diet for 20 weeks (ND20w); 4) n=4 mice fed with normal diet for 16 weeks and then with Ketogenic diet for 4 weeks (ND+KD20w); 5) n=5 fed with Western diet for 20 weeks (WD20w); 6) n=5 mice fed with Western diet for 16 weeks and then with Ketogenic diet for 4 weeks (WD+KD20w); 7) n=6 mice fed with Western diet for 16 weeks and then with normal diet for 4 weeks (WD+ND20w).

Figure 2: Effect of diets on bone microstructure by Micro-CT. 3D and 2D micro-CT reconstruction images of distal femurs of mice (A - B), Graphs reporting statistically significant data of micro-CT analysis. Data were showed as Mean ± SE.

Figure 3: Effect of diets on OC number in femur bone. Representative images of TRAP-stained osteoclasts in femur section from ND16w (A), WD16w (B), ND20w (C), WD20w (D), WD+ND20w (E), ND+KD20w (F) and WD+KD20w (G) mice, together with osteoclast counts per bone perimeter (H) in femoral trabecular sections from all mice. Data were showed as Mean ± SE. Statistics: Student's t-test. Magnification ×40.

Figure 4: Effect of diets in OB number in femur bone. Representative images of Hematoxylin-Eosin (H&E)-stained osteoblasts in femur section from ND16w (A), WD16w (B), ND20w (C), WD20w (D), WD+ND20w (E), ND+KD20w (F) and WD+KD20w (G) mice, together with osteoblast counts per bone perimeter (H) in femoral trabecular sections from all mice. Data were showed as Mean ± SE. Statistics: Student's t-test. Magnification ×40.

Figure 5: Effect of diets in OB and osteocyte number in cortical femur bone. Representative images of Hematoxylin-Eosin (H&E)-stained osteoblasts and osteocytes in femur section from ND16w (A), WD16w (B), ND20w (C), WD20w (D), WD+ND20w (E), ND+KD20w (F) and WD+KD20w (G) mice,

together with osteoblast counts per bone perimeter (H), and osteocyte counts per bone surface (I) in femoral trabecular sections from all mice. Data were showed as Mean ± SE. Statistics: Student's t-test. Magnification ×40.

Figure 6: Effect of diets on osteoid surface. Representative images of Masson trichrome Goldner stained sections of cortical sections of femurs from ND16w (A), WD16w (B), ND20w (C), WD20w (D), WD+ND20w (E), ND+KD20w (F) and WD+KD20w (G) mice, together with graph reporting the evaluation of osteoid on bone surface (H). Data were showed as Mean ± SE. Statistics: Student's t-test. Magnification ×40.

Figure 7: Effect of diets on osteoid surface. Representative images of Masson trichrome Goldner stained sections of trabecular sections of femurs from ND16w (A), WD16w (B), ND20w (C), WD20w (D), WD+ND20w (E), ND+KD20w (F) and WD+KD20w (G) mice, together with graph reporting the evaluation of osteoid on bone surface (H). Data were showed as Mean ± SE. Statistics: Student's t-test. Magnification ×40.

7.7. References

1. Hadjidakis DJ, Androulakis II. Bone Remodeling. *Annals of the New York Academy of Sciences*. 2007;1092(1):385-396. doi:10.1196/annals.1365.035
2. Wang L, You X, Zhang L, Zhang C, Zou W. Mechanical regulation of bone remodeling. *Bone Research*. 2022;10(1)doi:10.1038/s41413-022-00190-4
3. Jähn K, Bonewald LF. Bone Cell Biology. *Pediatric Bone*. 2012:1-8.
4. Bonewald LF. The amazing osteocyte. *Journal of Bone and Mineral Research*. 2011;26(2):229-238. doi:10.1002/jbmr.320
5. Rowe P, Koller A, Sharma S. Physiology, Bone Remodeling. *StatPearls*. 2025.
6. Weaver CM, Gordon CM, Janz KF, et al. The National Osteoporosis Foundation's position statement on peak bone mass development and lifestyle factors: a systematic review and implementation

recommendations. *Osteoporosis International*. 2016;27(4):1281-1386. doi:10.1007/s00198-015-3440-3

7. Gibson G, Zheng H-F, Tobias JH, et al. WNT16 Influences Bone Mineral Density, Cortical Bone Thickness, Bone Strength, and Osteoporotic Fracture Risk. *PLoS Genetics*. 2012;8(7)doi:10.1371/journal.pgen.1002745

8. Faienza MF, Giardinelli S, Annicchiarico A, et al. Nutraceuticals and Functional Foods: A Comprehensive Review of Their Role in Bone Health. *International Journal of Molecular Sciences*. 2024;25(11)doi:10.3390/ijms25115873

9. Cashman KD. Diet, Nutrition, and Bone Health. *The Journal of Nutrition*. 2007;137(11):2507S-2512S. doi:10.1093/jn/137.11.2507S

10. Natelson DM, Lai A, Krishnamoorthy D, Hoy RC, Iatridis JC, Illien-Jünger S. 2019;doi:10.1101/2019.12.23.887018

11. Peterlik M, Cross HS. Vitamin D and calcium deficits predispose for multiple chronic diseases. *European Journal of Clinical Investigation*. 2005;35(5):290-304. doi:10.1111/j.1365-2362.2005.01487.x

12. DeSalvo KB, Olson R, Casavale KO. Dietary Guidelines for Americans. *Jama*. 2016;315(5)doi:10.1001/jama.2015.18396

13. Lorincz C, Reimer RA, Boyd SK, Zernicke RF. High-fat, sucrose diet impairs geometrical and mechanical properties of cortical bone in mice. *British Journal of Nutrition*. 2010;103(9):1302-1308.

14. Dong X-L, Li C-M, Cao S-S, Zhou L-P, Wong M-S. A high-saturated-fat, high-sucrose diet aggravates bone loss in ovariectomized female rats. *The Journal of nutrition*. 2016;146(6):1172-1179.

15. Li K-C, Zernicke RF, James Barnard R, Li AFY. Effects of a high fat-sucrose diet on cortical bone morphology and biomechanics. *Calcified Tissue International*. 1990;47(5):308-313. doi:10.1007/bf02555914

16. Peng Y, Zhong Z, Huang C, Wang W. The effects of popular diets on bone health in the past decade: a narrative review. *Frontiers in Endocrinology*. 2024;14doi:10.3389/fendo.2023.1287140

17. Wu X, Huang Z, Wang X, et al. Ketogenic Diet Compromises Both Cancellous and Cortical Bone Mass in Mice. *Calcified Tissue International*. 2017;101(4):412-421. doi:10.1007/s00223-017-0292-1

18. Liu Q, Xu X, Yang Z, et al. Metformin Alleviates the Bone Loss Induced by Ketogenic Diet: An In Vivo Study in Mice. *Calcified Tissue International*. 2018;104(1):59-69. doi:10.1007/s00223-018-0468-3

19. Bergqvist AGC, Schall JI, Stallings VA, Zemel BS. Progressive bone mineral content loss in children with intractable epilepsy treated with the ketogenic diet. *The American Journal of Clinical Nutrition*. 2008;88(6):1678-1684. doi:10.3945/ajcn.2008.26099

20. Aikawa Y, Yamashita T, Nakai N, Higashida K. Low-carbohydrate, high-fat diet, and running exercise influence bone parameters in old mice. *Journal of Applied Physiology*. 2022;132(5):1204-1212. doi:10.1152/japplphysiol.00789.2021

21. Liu Q, Wang X, Huang Z, et al. Ketogenic diet delays spinal fusion and decreases bone mass in posterolateral lumbar spinal fusion: an in vivo rat model. *Acta Neurochirurgica*. 2018;160(10):1909-1916. doi:10.1007/s00701-018-3616-7

22. Xu X, Ding J, Wu X, et al. Bone microstructure and metabolism changes under the combined intervention of ketogenic diet with intermittent fasting: an in vivo study of rats. *Experimental Animals*. 2019;68(3):371-380. doi:10.1538/expanim.18-0084

23. Herbst EC, Felder AA, Evans LAE, Ajami S, Javaheri B, Pitsillides AA. A new straightforward method for semi-automated segmentation of trabecular bone from cortical bone in diverse and challenging morphologies. *Royal Society Open Science*. 2021;8(8)doi:10.1098/rsos.210408

24. Mentino D, Scillitani G, Marra M, Mastrodonato M. Seasonal changes in the liver of a non-hibernating population of water frogs, Pelophylax kl. esculentus (Anura: Ranidae). *The European Zoological Journal*. 2017;84(1):525-535. doi:10.1080/24750263.2017.1395482

25. Carlucci R, Mentino D, Semeraro D, Ricci P, Sion L, Scillitani G. Comparative histochemical analysis of intestinal glycoconjugates in the blunthead pufferfish Sphoeroides pachygaster and grey triggerfish Balistes capriscus (Teleostei: Tetraodontiformes). *Journal of Fish Biology*. 2019;94(1):122-131. doi:10.1111/jfb.13871

26. Mentino D, Nicchia GP, Frigeri A, et al. Altered glycosylation in secreting cells of the gastric glands of aquaporin-4-deficient mice. *Microscopy Research and Technique*. 2024;87(8):1836-1848. doi:10.1002/jemt.24563

27. Hou JCH, Zernicke RF, Barnard RJ. High fat-sucrose diet effects on femoral neck geometry and biomechanics. *Clinical Biomechanics*. 1990;5(3):162-168. doi:10.1016/0268-0033(90)90019-3

28. Zheng Y, Yan J, Zhang X, et al. Dietary intervention reprograms bone marrow cellular signaling in obese mice. *Frontiers in Endocrinology*. 2023;14doi:10.3389/fendo.2023.1171781

29. Beier EE, Inzana JA, Sheu T-J, Shu L, Puzas JE, Mooney RA. Effects of Combined Exposure to Lead and High-Fat Diet on Bone Quality in Juvenile Male Mice. *Environmental Health Perspectives*. 2015;123(10):935-943. doi:10.1289/ehp.1408581

30. Yu W, Zhong L, Yao L, et al. Bone marrow adipogenic lineage precursors promote osteoclastogenesis in bone remodeling and pathologic bone loss. *Journal of Clinical Investigation*. 2021;131(2)doi:10.1172/jci140214

31. Cao JJ, Gregoire BR, Michelsen KG, Shi X. Deficiency of PPARγ in Bone Marrow Stromal Cells Does not Prevent High-Fat Diet-Induced Bone Deterioration in Mice. *The Journal of Nutrition*. 2021;151(9):2697-2704. doi:10.1093/jn/nxab173

32. Halade GV, Rahman MM, Williams PJ, Fernandes G. High fat diet-induced animal model of age-associated obesity and osteoporosis. *The Journal of Nutritional Biochemistry*. 2010;21(12):1162-1169. doi:10.1016/j.jnutbio.2009.10.002

33. Bai Y-D, Yang F-S, Xuan K, Bai Y-X, Wu B-L. Inhibition of RANK/RANKL signal transduction pathway: A promising approach for osteoporosis treatment. *Medical Hypotheses*. 2008;71(2):256-258. doi:10.1016/j.mehy.2008.03.021

34. Eckhardt BA, Rowsey JL, Thicke BS, et al. Accelerated osteocyte senescence and skeletal fragility in mice with type 2 diabetes. *JCI Insight*. 2020;5(9)doi:10.1172/jci.insight.135236

35. Suresh S, Alvarez JC, Dey S, Noguchi CT. Erythropoietin-Induced Changes in Bone and Bone Marrow in Mouse Models of Diet-Induced Obesity. *International Journal of Molecular Sciences*. 2020;21(5)doi:10.3390/ijms21051657

36. Dole NS, Betancourt-Torres A, Kaya S, et al. High-fat and high-carbohydrate diets increase bone fragility through TGF-β–dependent control of osteocyte function. *JCI Insight*. 2024;9(16)doi:10.1172/jci.insight.175103

37. Carter JD, Vasey FB, Valeriano J. The effect of a low-carbohydrate diet on bone turnover. *Osteoporosis International*. 2006;17(9):1398-1403. doi:10.1007/s00198-006-0134-x

38. Heikura IA, Burke LM, Hawley JA, et al. A Short-Term Ketogenic Diet Impairs Markers of Bone Health in Response to Exercise. *Frontiers in Endocrinology*. 2020;10doi:10.3389/fendo.2019.00880

39. Vargas-Molina S, Carbone L, Romance R, et al. Effects of a low-carbohydrate ketogenic diet on health parameters in resistance-trained women. *European Journal of Applied Physiology*. 2021;121(8):2349-2359. doi:10.1007/s00421-021-04707-3

Published papers:

- Provera A, Ramavath NN, Gadipudi LL, Vecchio C, Caputo M, **Antonioli A**, Tini S, Sheferaw AN, Reano S, Filigheddu N, Manfredi M, Barberis E, Cocolin L, Ferrocino I, Locatelli M, Caprio M, Tacke F, Albano E, Prodam F, Sutti S. Vegetal oil-based ketogenic diet improves inflammation and fibrosis in experimental metabolic dysfunction-associated steatohepatitis. Front Immunol. 2025 Apr 1;16:1518687. doi: 10.3389/fimmu.2025.1518687. PMID: 40236713; PMCID: PMC11996634.
- Dietary fructose: from uric acid to a metabolic switch in pediatric metabolic dysfunctionassociated steatotic liver disease Faienza MF, Cognetti E, Farella I, **Antonioli A**, Tini S, Antoniotti V, Prodam F. Dietary fructose: from uric acid to a metabolic switch in pediatric metabolic dysfunction-associated steatotic liver disease. Crit Rev Food Sci Nutr. 2024 Aug 19:1-16. doi: 10.1080/10408398.2024.2392150. Epub ahead of print. PMID: 39157959.
- Antoniotti, V., Amore, M., Caputo, M., Fania, C., Mancioppi, V., Casoli, G., Tini, S., **Antonioli, A.**, Aimaretti, G., Rabbone, I., Bellone, S., & Prodam, F. (2023). Glucose Alterations, Insulin Resistance, Arterial Hypertension, and Renin are Strictly Associated in Pediatric Obesity. Journal of the Endocrine Society, 7(8), bvad088.
- Antoniotti, V., Caputo M., **Antonioli A.**, Spadaccini D., Tini S., Aimaretti G., & Prodam F., (2023). Microbiota e patologie endocrino-metaboliche. L'endocrinologo 24, 111-119.
- Spadaccini, D., Guazzotti, S., Goncalves Correia, F. P., Daffara, T., Tini, S., **Antonioli, A.**, Aimaretti, G., Marzullo, P., Caputo, M., Antoniotti, V., & Prodam, F. (2022). Beyond bariatric surgery and weight loss medicaments. A systematic review of the current practice in obesity rehabilitative inpatient programs in adults and pediatrics. Frontiers in nutrition, 9, 963709.

8. References

1. Geiger, A. E. *et al.* Dual effects of obesity on satellite cells and muscle regeneration. *Physiol. Rep.* 8, (2020).
2. Serra, D., Mera, P., Malandrino, M. I., Mir, J. F. & Herrero, L. Mitochondrial Fatty Acid Oxidation in Obesity. *Antioxid. Redox Signal.* 19, 269–284 (2013).
3. Phelps, N. H. *et al.* Worldwide trends in underweight and obesity from 1990 to 2022: a pooled analysis of 3663 population-representative studies with 222 million children, adolescents, and adults. *The Lancet* 403, 1027–1050 (2024).
4. Busetto, L. *et al.* A new framework for the diagnosis, staging and management of obesity in adults. *Nat. Med.* 30, 2395–2399 (2024).
5. Moriggi, M. *et al.* Skeletal Muscle Proteomic Profile Revealed Gender-Related Metabolic Responses in a Diet-Induced Obesity Animal Model. *Int. J. Mol. Sci.* 22, 4680 (2021).
6. Akhmedov, D. & Berdeaux, R. The effects of obesity on skeletal muscle regeneration. *Front. Physiol.* 4, (2013).
7. Bischoff, S. C. & Schweinlin, A. Obesity therapy. *Clin. Nutr. ESPEN* 38, 9–18 (2020).
8. Meldrum, D. R., Morris, M. A. & Gambone, J. C. Obesity pandemic: causes, consequences, and solutions—but do we have the will? *Fertil. Steril.* 107, 833–839 (2017).
9. Khanna, D., Khanna, S., Khanna, P., Kahar, P. & Patel, B. M. Obesity: A Chronic Low-Grade Inflammation and Its Markers. *Cureus* (2022) doi:10.7759/cureus.22711.
10. Huttunen, R. & Syrjänen, J. Obesity and the risk and outcome of infection. *Int. J. Obes.* 37, 333–340 (2013).
11. González Jiménez, E. Obesidad: análisis etiopatogénico y fisiopatológico. *Endocrinol. Nutr.* 60, 17–24 (2013).
12. Tsigos, C. *et al.* Management of Obesity in Adults: European Clinical Practice Guidelines. *Obes. Facts* 1, 106–116 (2008).

13. Pellegrinelli, V., Carobbio, S. & Vidal-Puig, A. Adipose tissue plasticity: how fat depots respond differently to pathophysiological cues. *Diabetologia* 59, 1075–1088 (2016).

14. Pirola, L. & Ferraz, J. C. Role of pro- and anti-inflammatory phenomena in the physiopathology of type 2 diabetes and obesity. *World J. Biol. Chem.* 8, 120 (2017).

15. Das, S., Mukhuty, A., Mullen, G. P. & Rudolph, M. C. Adipocyte Mitochondria: Deciphering Energetic Functions across Fat Depots in Obesity and Type 2 Diabetes. *Int. J. Mol. Sci.* 25, 6681 (2024).

16. McMurray, F., Patten, D. A. & Harper, M. Reactive Oxygen Species and Oxidative Stress in Obesity—Recent Findings and Empirical Approaches. *Obesity* 24, 2301–2310 (2016).

17. Manna, P. & Jain, S. K. Obesity, Oxidative Stress, Adipose Tissue Dysfunction, and the Associated Health Risks: Causes and Therapeutic Strategies. *Metab. Syndr. Relat. Disord.* 13, 423–444 (2015).

18. Kubes, P. & Jenne, C. Immune Responses in the Liver. *Annu. Rev. Immunol.* 36, 247–277 (2018).

19. Crewe, C., An, Y. A. & Scherer, P. E. The ominous triad of adipose tissue dysfunction: inflammation, fibrosis, and impaired angiogenesis. *J. Clin. Invest.* 127, 74–82 (2017).

20. Virtue, S. & Vidal-Puig, A. Adipose tissue expandability, lipotoxicity and the Metabolic Syndrome — An allostatic perspective. *Biochim. Biophys. Acta BBA - Mol. Cell Biol. Lipids* 1801, 338–349 (2010).

21. Altajar, S. & Baffy, G. Skeletal Muscle Dysfunction in the Development and Progression of Nonalcoholic Fatty Liver Disease. *J. Clin. Transl. Hepatol.* 8, 1–10 (2020).

22. Boccatonda, A. *et al.* From NAFLD to MAFLD: Definition, Pathophysiological Basis and Cardiovascular Implications. *Biomedicines* 11, 883 (2023).

23. Flessa, C.-M. *et al.* Genetic and Diet-Induced Animal Models for Non-Alcoholic Fatty Liver Disease (NAFLD) Research. *Int. J. Mol. Sci.* 23, 15791 (2022).

24. Idilman, I. S., Ozdeniz, I. & Karcaaltincaba, M. Hepatic Steatosis: Etiology, Patterns, and Quantification. *Semin. Ultrasound CT MRI* 37, 501–510 (2016).

25. Badmus, O. O., Hillhouse, S. A., Anderson, C. D., Hinds, T. D. & Stec, D. E. Molecular mechanisms of metabolic associated fatty liver disease (MAFLD): functional analysis of lipid metabolism pathways. *Clin. Sci.* 136, 1347–1366 (2022).

26. Wang, D. Q. -H., Portincasa, P. & Neuschwander-Tetri, B. A. Steatosis in the Liver. in *Comprehensive Physiology* (ed. Terjung, R.) 1493–1532 (Wiley, 2013). doi:10.1002/cphy.c130001.

27. Rinella, M. E. & Sookoian, S. From NAFLD to MASLD: updated naming and diagnosis criteria for fatty liver disease. *J. Lipid Res.* 65, 100485 (2023).

28. Liu, Q., Bengmark, S. & Qu, S. The role of hepatic fat accumulation in pathogenesis of non-alcoholic fatty liver disease (NAFLD). *Lipids Health Dis.* 9, 42 (2010).

29. Yang, P. *et al.* Western diet induces severe nonalcoholic steatohepatitis, ductular reaction, and hepatic fibrosis in liver CGI-58 knockout mice. *Sci. Rep.* 10, 4701 (2020).

30. Yang, M. *et al.* Western diet contributes to the pathogenesis of non-alcoholic steatohepatitis in male mice via remodeling gut microbiota and increasing production of 2-oleoylglycerol. *Nat. Commun.* 14, 228 (2023).

31. St-Amand, R., Ngo Sock, É. T., Quinn, S., Lavoie, J.-M. & St-Pierre, D. H. Two weeks of western diet disrupts liver molecular markers of cholesterol metabolism in rats. *Lipids Health Dis.* 19, 192 (2020).

32. Gonzalez, A. *et al.* Role of Oxidative Stress in Hepatic and Extrahepatic Dysfunctions during Nonalcoholic Fatty Liver Disease (NAFLD). *Oxid. Med. Cell. Longev.* 2020, 1617805 (2020).

33. D'Souza, D. M. *et al.* Diet-induced obesity impairs muscle satellite cell activation and muscle repair through alterations in hepatocyte growth factor signaling. *Physiol. Rep.* 3, e12506 (2015).

34. Kohli, R. *et al.* High-Fructose, Medium Chain Trans Fat Diet Induces Liver Fibrosis and Elevates Plasma Coenzyme Q9 in a Novel Murine Model of Obesity and Nonalcoholic Steatohepatitis†. *Hepatology* 52, 934–944 (2010).

35. Donini, L. M. *et al.* Definition and Diagnostic Criteria for Sarcopenic Obesity: ESPEN and EASO Consensus Statement. *Obes. Facts* 15, 321–335 (2022).

36. Choi, K. M. Sarcopenia and sarcopenic obesity. *Korean J. Intern. Med.* 31, 1054–1060 (2016).

37. Axelrod, C. L., Dantas, W. S. & Kirwan, J. P. Sarcopenic obesity: emerging mechanisms and therapeutic potential. *Metabolism* 146, 155639 (2023).

38. Dalle, S., Rossmeislova, L. & Koppo, K. The Role of Inflammation in Age-Related Sarcopenia. *Front. Physiol.* 8, 1045 (2017).

39. Yin, L. *et al.* Skeletal muscle atrophy: From mechanisms to treatments. *Pharmacol. Res.* 172, 105807 (2021).

40. Zhang, H. *et al.* Oxidative stress: Roles in skeletal muscle atrophy. *Biochem. Pharmacol.* 214, 115664 (2023).

41. Reano, S., Graziani, A. & Filigheddu, N. Acylated and unacylated ghrelin administration to blunt muscle wasting: *Curr. Opin. Clin. Nutr. Metab. Care* 17, 236–240 (2014).

42. Frontera, W. R. & Ochala, J. Skeletal Muscle: A Brief Review of Structure and Function. *Calcif. Tissue Int.* 96, 183–195 (2015).

43. Düvel, K. *et al.* Activation of a Metabolic Gene Regulatory Network Downstream of mTOR Complex 1. *Mol. Cell* 39, 171–183 (2010).

44. Ong, P. S. *et al.* Judicious Toggling of mTOR Activity to Combat Insulin Resistance and Cancer: Current Evidence and Perspectives. *Front. Pharmacol.* 7, (2016).

45. Saxton, R. A. & Sabatini, D. M. mTOR Signaling in Growth, Metabolism, and Disease. *Cell* 168, 960–976 (2017).

46. Schiaffino, S., Dyar, K. A., Ciciliot, S., Blaauw, B. & Sandri, M. Mechanisms regulating skeletal muscle growth and atrophy. *FEBS J.* 280, 4294–4314 (2013).

47. Larsson, L. *et al.* Sarcopenia: Aging-Related Loss of Muscle Mass and Function. *Physiol. Rev.* 99, 427–511 (2019).

48. Jiao, J. & Demontis, F. Skeletal muscle autophagy and its role in sarcopenia and organismal aging. *Curr. Opin. Pharmacol.* 34, 1–6 (2017).

49. Tang, G. *et al.* Butyrate ameliorate skeletal muscle atrophy in Diabetic Nephropathy via enhancing gut barrier function and GPR43 mediated PI3K/AKT/mTOR signals. Preprint at https://doi.org/10.22541/au.160688559.90642598/v1 (2020).

50. Dalle, S., Rossmeislova, L. & Koppo, K. The Role of Inflammation in Age-Related Sarcopenia. *Front. Physiol.* 8, 1045 (2017).

51. Lee, M.-K. *et al.* Nutrients against Glucocorticoid-Induced Muscle Atrophy. *Foods* 11, 687 (2022).

52. Hood, D. A., Memme, J. M., Oliveira, A. N. & Triolo, M. Maintenance of Skeletal Muscle Mitochondria in Health, Exercise, and Aging. *Annu. Rev. Physiol.* 81, 19–41 (2019).

53. Tilokani, L., Nagashima, S., Paupe, V. & Prudent, J. Mitochondrial dynamics: overview of molecular mechanisms. *Essays Biochem.* 62, 341–360 (2018).

54. Rinonapoli, G. *et al.* Obesity and Bone: A Complex Relationship. *Int. J. Mol. Sci.* 22, 13662 (2021).

55. Hadjidakis, D. J. & Androulakis, I. I. Bone Remodeling. *Ann. N. Y. Acad. Sci.* 1092, 385–396 (2006).

56. Lorincz, C., Reimer, R. A., Boyd, S. K. & Zernicke, R. F. High-fat, sucrose diet impairs geometrical and mechanical properties of cortical bone in mice. *Br. J. Nutr.* 103, 1302–1308 (2010).

57. Hongliang, G. *et al.* Emerging role of liver-bone axis in osteoporosis. *J. Orthop. Transl.* 48, 217–231 (2024).

58. Viswanath, A., Fouda, S., Fernandez, C. J. & Pappachan, J. M. Metabolic-associated fatty liver disease and sarcopenia: A double whammy. *World J. Hepatol.* 16, 152–163 (2024).

59. Paintin, J., Cooper, C. & Dennison, E. Osteosarcopenia. *Br. J. Hosp. Med.* 79, 253–258 (2018).

60. Hirschfeld, H. P., Kinsella, R. & Duque, G. Osteosarcopenia: where bone, muscle, and fat collide. *Osteoporos. Int.* 28, 2781–2790 (2017).

61. Jafari Nasabian, P., Inglis, J., Kelly, O. & Ilich, J. Osteosarcopenic obesity in women: impact, prevalence, and management challenges. *Int. J. Womens Health* Volume 9, 33–42 (2017).

62. Saeki, C., Saito, M. & Tsubota, A. Association of chronic liver disease with bone diseases and muscle weakness. *J. Bone Miner. Metab.* 42, 399–412 (2024).

63. Christ, A., Lauterbach, M. & Latz, E. Western Diet and the Immune System: An Inflammatory Connection. *Immunity* 51, 794–811 (2019).

64. Kopp, W. How Western Diet And Lifestyle Drive The Pandemic Of Obesity And Civilization Diseases. *Diabetes Metab. Syndr. Obes. Targets Ther.* Volume 12, 2221–2236 (2019).

65. Nani, A., Murtaza, B., Sayed Khan, A., Khan, N. A. & Hichami, A. Antioxidant and Anti-Inflammatory Potential of Polyphenols Contained in Mediterranean Diet in Obesity: Molecular Mechanisms. *Molecules* 26, 985 (2021).

66. Monsanto, S. P. *et al.* The new total Western diet for rodents does not induce an overweight phenotype or alter parameters of metabolic syndrome in mice. *Nutr. Res.* 36, 1031–1044 (2016).

67. Tokarz, V. L., Mylvaganam, S. & Klip, A. Palmitate-induced insulin resistance causes actin filament stiffness and GLUT4 mis-sorting without altered Akt signalling. *J. Cell Sci.* 136, jcs261300 (2023).

68. Matsuba, I., Fujita, R. & Iida, K. Palmitic Acid Inhibits Myogenic Activity and Expression of Myosin Heavy Chain MHC IIb in Muscle Cells through Phosphorylation-Dependent MyoD Inactivation. *Int. J. Mol. Sci.* 24, 5847 (2023).

69. Yoon, H. J., Bang, M.-H., Kim, H. & Imm, J.-Y. Improvement of palmitate-induced insulin resistance in C2C12 skeletal muscle cells using Platycodon grandiflorum seed extracts. *Food Biosci.* 25, 61–67 (2018).

70. Malesza, I. J. *et al.* High-Fat, Western-Style Diet, Systemic Inflammation, and Gut Microbiota: A Narrative Review. *Cells* 10, 3164 (2021).

71. Manzel, A. *et al.* Role of "Western Diet" in Inflammatory Autoimmune Diseases. *Curr. Allergy Asthma Rep.* 14, 404 (2014).

72. Cremonese, C. *et al.* Short-Term Western Diet Aggravates Non-Alcoholic Fatty Liver Disease (NAFLD) With Portal Hypertension in TGR(mREN2)27 Rats. *Int. J. Mol. Sci.* 21, 3308 (2020).

73. Barrea, L. *et al.* Nutrition, inflammation and liver-spleen axis. *Crit. Rev. Food Sci. Nutr.* 58, 3141–3158 (2018).

74. Wei, S., Nguyen, T. T., Zhang, Y., Ryu, D. & Gariani, K. Sarcopenic obesity: epidemiology, pathophysiology, cardiovascular disease, mortality, and management. *Front. Endocrinol.* 14, 1185221 (2023).

75. Heo, J. *et al.* Differential effects of Western diet and traumatic muscle injury on skeletal muscle metabolic regulation in male and female mice. *J. Cachexia Sarcopenia Muscle* 14, 2835–2850 (2023).

76. McGowan, E. M., Ehrlicher, S. E., Stierwalt, H. D., Robinson, M. M. & Newsom, S. A. Impact of 4 weeks of western diet and aerobic exercise training on whole-body phenotype and skeletal muscle mitochondrial respiration in male and female mice. *Physiol. Rep.* 10, e15543 (2022).

77. Hosseini, Z., Whiting, S. J. & Vatanparast, H. Current evidence on the association of the metabolic syndrome and dietary patterns in a global perspective. *Nutr. Res. Rev.* 29, 152–162 (2016).

78. Trovato, F. M., Castrogiovanni, P., Szychlinska, M. A., Purrello, F. & Musumeci, G. Impact of Western and Mediterranean Diets and Vitamin D on Muscle Fibers of Sedentary Rats. *Nutrients* 10, 231 (2018).

79. Provera, A. *et al.* Vegetal oil-based ketogenic diet improves inflammation and fibrosis in experimental metabolic dysfunction-associated steatohepatitis. *Front. Immunol.* 16, 1518687 (2025).

80. Kalinkovich, A. & Livshits, G. Sarcopenic obesity or obese sarcopenia: A cross talk between age-associated adipose tissue and skeletal muscle inflammation as a main mechanism of the pathogenesis. *Ageing Res. Rev.* 35, 200–221 (2017).

81. Sishi, B. *et al.* Diet-induced obesity alters signalling pathways and induces atrophy and apoptosis in skeletal muscle in a prediabetic rat model. *Exp. Physiol.* 96, 179–193 (2011).

82. Sousa, L. G. O. D. *et al.* The effects of diet composition and chronic obesity on muscle growth and function. *J. Appl. Physiol.* 130, 124–138 (2021).

83. Bischoff-Ferrari, H. A. *et al.* Dietary Calcium and Serum 25-Hydroxyvitamin D Status in Relation to BMD Among U.S. Adults. *J. Bone Miner. Res.* 24, 935–942 (2009).

84. Van Driel, M. & Van Leeuwen, J. P. T. M. Vitamin D and Bone: A Story of Endocrine and Auto/Paracrine Action in Osteoblasts. *Nutrients* 15, 480 (2023).

85. J. Kelly, O., C. Gilman, J., Kim, Y. & Z. Ilich, J. Macronutrient Intake and Distribution in the Etiology, Prevention and Treatment of Osteosarcopenic Obesity. *Curr. Aging Sci.* 10, 83–105 (2017).

86. McGaugh, E. & Barthel, B. A Review of Ketogenic Diet and Lifestyle. *Mo. Med.* 119, 84–88 (2022).

87. Caprio, M. *et al.* Very-low-calorie ketogenic diet (VLCKD) in the management of metabolic diseases: systematic review and consensus statement from the Italian Society of Endocrinology (SIE). *J. Endocrinol. Invest.* 42, 1365–1386 (2019).

88. Muscogiuri, G. *et al.* European Guidelines for Obesity Management in Adults with a Very Low-Calorie Ketogenic Diet: A Systematic Review and Meta-Analysis. *Obes. Facts* 14, 222–245 (2021).

89. Garbow, J. R. *et al.* Hepatic steatosis, inflammation, and ER stress in mice maintained long term on a very low-carbohydrate ketogenic diet. *Am. J. Physiol.-Gastrointest. Liver Physiol.* 300, G956–G967 (2011).

90. Kessler, S. K., Gallagher, P. R., Shellhaas, R. A., Clancy, R. R. & Bergqvist, A. G. C. Early EEG improvement after ketogenic diet initiation. *Epilepsy Res.* 94, 94–101 (2011).

91. Huffman, J. & Kossoff, E. H. State of the ketogenic diet(s) in epilepsy. *Curr. Neurol. Neurosci. Rep.* 6, 332–340 (2006).

92. Ilyas, Z. *et al.* The Ketogenic Diet: Is It an Answer for Sarcopenic Obesity? *Nutrients* 14, 620 (2022).

93. Paoli, A., Cancellara, P., Pompei, P. & Moro, T. Ketogenic Diet and Skeletal Muscle Hypertrophy: a Frenemy Relationship? *J. Hum. Kinet.* 68, 233–247 (2019).

94. McGaugh, E. & Barthel, B. A Review of Ketogenic Diet and Lifestyle. *Mo. Med.* 119, 84–88 (2022).

95. Yurista, S. R. *et al.* Therapeutic Potential of Ketone Bodies for Patients With Cardiovascular Disease. *J. Am. Coll. Cardiol.* 77, 1660–1669 (2021).

96. Pirali, B. *et al.* LA DIETA CHETOGENICA NELL'OBESITÀ: (2022).

97. Jani, S., Da Eira, D., Stefanovic, M. & Ceddia, R. B. The ketogenic diet prevents steatosis and insulin resistance by reducing lipogenesis, diacylglycerol accumulation and protein kinase C activity in male rat liver. *J. Physiol.* 600, 4137–4151 (2022).

98. Li, R., Liu, Y., Liu, H. & Li, J. Ketogenic diets and protective mechanisms in epilepsy, metabolic disorders, cancer, neuronal loss, and muscle and nerve degeneration. *J. Food Biochem.* 44, (2020).

99. Xu, Y., Zheng, F., Zhong, Q. & Zhu, Y. Ketogenic Diet as a Promising Non-Drug Intervention for Alzheimer's Disease: Mechanisms and Clinical Implications. *J. Alzheimers Dis.* 92, 1173–1198 (2023).

100. Harvey, K. L., Holcomb, L. E. & Kolwicz, S. C. Ketogenic Diets and Exercise Performance. *Nutrients* 11, 2296 (2019).

101. Wallace, M. A. *et al.* The ketogenic diet preserves skeletal muscle with aging in mice. *Aging Cell* 20, e13322 (2021).

102. Ang, Q. Y. *et al.* Ketogenic Diets Alter the Gut Microbiome Resulting in Decreased Intestinal Th17 Cells. *Cell* 181, 1263-1275.e16 (2020).

103. Watanabe, M. *et al.* Beneficial effects of the ketogenic diet on nonalcoholic fatty liver disease: A comprehensive review of the literature. *Obes. Rev.* 21, e13024 (2020).

104. Nakao, R., Abe, T., Yamamoto, S. & Oishi, K. Ketogenic diet induces skeletal muscle atrophy via reducing muscle protein synthesis and possibly activating proteolysis in mice. *Sci. Rep.* 9, 19652 (2019).

105. Yakupova, E. I., Bocharnikov, A. D. & Plotnikov, E. Y. Effects of Ketogenic Diet on Muscle Metabolism in Health and Disease. *Nutrients* 14, 3842 (2022).

106. Choi, B. H., Hyun, S. & Koo, S.-H. The role of BCAA metabolism in metabolic health and disease. *Exp. Mol. Med.* 56, 1552–1559 (2024).

107. Zhu, X. *et al.* Effect of short-term fasting and glucocorticoids on KLF15 expression and branched-chain amino acids metabolism in Chinese perch. *Aquac. Rep.* 19, 100617 (2021).

108. Hirata, Y. *et al.* A Piezo1/KLF15/IL-6 axis mediates immobilization-induced muscle atrophy. *J. Clin. Invest.* 132, 1–13 (2022).

109. Clarke, B. A. *et al.* The E3 Ligase MuRF1 Degrades Myosin Heavy Chain Protein in Dexamethasone-Treated Skeletal Muscle. *Cell Metab.* 6, 376–385 (2007).

110. de Hart, N. M. *et al.* Palmitate-Induced Inflammation and Myotube Atrophy in C2C12 Cells Are Prevented by the Whey Bioactive Peptide, Glycomacropeptide. *J. Nutr.* 153, 2915–2928 (2023).

111. Lee, H., Lim, J.-Y. & Choi, S.-J. Oleate Prevents Palmitate-Induced Atrophy via Modulation of Mitochondrial ROS Production in Skeletal Myotubes. *Oxid. Med. Cell. Longev.* 2017, 2739721 (2017).

112. Plotkin, D. L. *et al.* Skeletal muscle myosin heavy chain fragmentation as a potential marker of protein degradation in response to resistance training and disuse atrophy. *Exp. Physiol.* 109, 1739–1754 (2024).

113. Hitachi, K. *et al.* Simultaneous loss of skeletal muscle myosin heavy chain IIx and IIb causes severe skeletal muscle hypoplasia in postnatal mice. *FASEB J. Off. Publ. Fed. Am. Soc. Exp. Biol.* 37, e22692 (2023).

114. Agarwal, M. *et al.* Myosin heavy chain-embryonic regulates skeletal muscle differentiation during mammalian development. *Dev. Camb. Engl.* 147, dev184507 (2020).

115. Li, Y. *et al.* Low-Carbohydrate Diet Modulates Glucose–Lipid Utilization in Skeletal Muscle of Diabetic Mice. *Nutrients* 15, 1513 (2023).

116. Baylie, T., Ayelgn, T., Tiruneh, M. & Tesfa, K. Effect of Ketogenic Diet on Obesity and Other Metabolic Disorders: Narrative Review. *Diabetes Metab. Syndr. Obes.* Volume 17, 1391–1401 (2024).

117. Paoli, A. Ketogenic Diet for Obesity: Friend or Foe? *Int. J. Environ. Res. Public. Health* 11, 2092–2107 (2014).

118. Wood, R. J. *et al.* Preservation of fat-free mass after two distinct weight loss diets with and without progressive resistance exercise. *Metab. Syndr. Relat. Disord.* 10, 167–174 (2012).

119. Heymsfield, S. B., Gonzalez, M. C. C., Shen, W., Redman, L. & Thomas, D. Weight loss composition is one-fourth fat-free mass: a critical review and critique of this widely cited rule. *Obes. Rev.* 15, 310–321 (2014).

120. Conte, C., Hall, K. D. & Klein, S. Is Weight Loss-Induced Muscle Mass Loss Clinically Relevant? *JAMA* 332, 9–10 (2024).

121. Koutnik, A. P. *et al.* Ketone Bodies Attenuate Wasting in Models of Atrophy. *J. Cachexia Sarcopenia Muscle* 11, 973–996 (2020).

122. Volek, J. S., Kackley, M. L. & Buga, A. Nutritional Considerations During Major Weight Loss Therapy: Focus on Optimal Protein and a Low-Carbohydrate Dietary Pattern. *Curr. Nutr. Rep.* 13, 422–443 (2024).

123. Athinarayanan, S. J. & Volek, J. S. Mitigating muscle loss during weight loss: can nutritional ketosis make a difference? A call for more research. *Obesity* 33, 431–434 (2025).

124. Antonio Paoli, A. *et al.* Effects of 30 days of ketogenic diet on body composition, muscle strength, muscle area, metabolism, and performance in semi-professional soccer players. *J. Int. Soc. Sports Nutr.* 18, 62 (2021).

125. Barrea, L. *et al.* Ketogenic nutritional therapy (KeNuT)—a multi-step dietary model with meal replacements for the management of obesity and its related metabolic disorders: a consensus statement from the working group of the Club of the Italian Society of Endocrinology (SIE)—diet therapies in endocrinology and metabolism. *J. Endocrinol. Invest.* 47, 487–500 (2024).

126. Park, S. B. & Yang, S. J. Ketogenic diet preserves muscle mass and strength in a mouse model of type 2 diabetes. *PLOS ONE* 19, e0296651 (2024).

127. Chaillou, T., Lee, J. D., England, J. H., Esser, K. A. & McCarthy, J. J. Time course of gene expression during mouse skeletal muscle hypertrophy. *J. Appl. Physiol.* 115, 1065–1074 (2013).

128. Wang, Y. *et al.* An 8-week ketogenic diet improves exercise endurance and liver antioxidant capacity after weight loss in obese mice. *Front. Nutr.* 10, (2023).

129. Zhang, J., Chen, B. & Zou, K. Effect of ketogenic diet on exercise tolerance and transcriptome of gastrocnemius in mice. *Open Life Sci.* 18, 20220570 (2023).

130. Li, L., Tan, J., Miao, Y., Lei, P. & Zhang, Q. ROS and Autophagy: Interactions and Molecular Regulatory Mechanisms. *Cell. Mol. Neurobiol.* 35, 615–621 (2015).

131. Sandri, M. Protein breakdown in muscle wasting: Role of autophagy-lysosome and ubiquitin-proteasome. *Int. J. Biochem. Cell Biol.* 45, 2121–2129 (2013).

132. Xia, Q. *et al.* The Role of Autophagy in Skeletal Muscle Diseases. *Front. Physiol.* 12, 638983 (2021).

133. Shimizu, N. *et al.* Crosstalk between Glucocorticoid Receptor and Nutritional Sensor mTOR in Skeletal Muscle. *Cell Metab.* 13, 170–182 (2011).

134. She, P. *et al.* Disruption of BCATm in mice leads to increased energy expenditure associated with the activation of a futile protein turnover cycle. *Cell Metab.* 6, 181–194 (2007).

135. Mann, G., Mora, S., Madu, G. & Adegoke, O. A. J. Branched-chain Amino Acids: Catabolism in Skeletal Muscle and Implications for Muscle and Whole-body Metabolism. *Front. Physiol.* 12, (2021).

136. Ding, Y. *et al.* Sodium Butyrate Induces Mitophagy and Apoptosis of Bovine Skeletal Muscle Satellite Cells through the Mammalian Target of Rapamycin Signaling Pathway. *Int. J. Mol. Sci.* 24, 13474 (2023).

137. Mikkelsen, K. H., Seifert, T., Secher, N. H., Grøndal, T. & van Hall, G. Systemic, cerebral and skeletal muscle ketone body and energy metabolism during acute hyper-D-β-hydroxybutyratemia in post-absorptive healthy males. *J. Clin. Endocrinol. Metab.* 100, 636–643 (2015).

138. Walsh, M. E. *et al.* The histone deacetylase inhibitor butyrate improves metabolism and reduces muscle atrophy during aging. *Aging Cell* 14, 957–970 (2015).

139. Khouri, H., Roberge, M., Ussher, J. R. & Aguer, C. Acetoacetate and d- and l-β-hydroxybutyrate have distinct effects on basal and insulin-stimulated glucose uptake in L6 skeletal muscle cells. *Am. J. Physiol. Cell Physiol.* 326, C1710–C1720 (2024).

140. Bonetto, A., Andersson, D. C. & Waning, D. L. Assessment of muscle mass and strength in mice. *BoneKEy Rep.* 4, 732 (2015).

141. Weaver, C. M. *et al.* The National Osteoporosis Foundation's position statement on peak bone mass development and lifestyle factors: a systematic review and implementation recommendations. *Osteoporos. Int.* 27, 1281–1386 (2016).

142. Zheng, H.-F. *et al.* WNT16 Influences Bone Mineral Density, Cortical Bone Thickness, Bone Strength, and Osteoporotic Fracture Risk. *PLoS Genet.* 8, e1002745 (2012).

143. Faienza, M. F. *et al.* Nutraceuticals and Functional Foods: A Comprehensive Review of Their Role in Bone Health. *Int. J. Mol. Sci.* 25, 5873 (2024).

144. Cashman, K. D. Diet, Nutrition, and Bone Health. *J. Nutr.* 137, 2507S-2512S (2007).

145. Natelson, D. M. *et al.* Leptin signaling and the intervertebral disc: Sex dependent effects of leptin receptor deficiency and Western diet on the spine in a type 2 diabetes mouse model. Preprint at https://doi.org/10.1101/2019.12.23.887018 (2019).

146. Peng, Y., Zhong, Z., Huang, C. & Wang, W. The effects of popular diets on bone health in the past decade: a narrative review. *Front. Endocrinol.* 14, (2024).